ABSTRACT

Title of the Thesis: HEALTH STATUS ASSESSMENT METHODOLOGY FOR ELECTRONIC HARDWARE

Sony Mathew, Master of Science, 2005

Thesis directed by: Professor Michael Pecht

Department of Mechanical Engineering

Remaining life assessment is the process of predicting the future operational life of a product, based on estimate of life consumed under its life cycle environmental conditions. Remaining life is typically an output of health monitoring and prognostics. In this thesis, a generic 'Health Status Assessment' methodology has been developed, that provides a guideline for conducting a remaining life assessment for electronic hardware already deployed in the field. The methodology presents the assessor with the possible techniques that can be used and the criteria for implementing each technique. A practical application of the new methodology is demonstrated by assessing the remaining life of an electronic circuit card subjected to shock and random vibration loads in its life cycle environment. During life testing, a mechanical support structure on the board was damaged. Analytical and finite element methods were employed to determine and explain the cause of failure.

HEALTH STATUS ASSESSMENT METHODOLOGY FOR ELECTRONIC HARDWARE

by

Sony Mathew

Thesis submitted to the Faculty of the Graduate School of the
University of Maryland, College Park, in partial fulfillment
of the requirements for the degree of
Master of Science
2005

Advisory Committee:

Professor Michael Pecht, Chair
Associate Professor Peter Sandborn
Associate Professor Patrick McCluskey
Dr. Michael Osterman
Dr. Diganta Das

DEDICATION

I dedicate this work to Lord Jesus Christ, my grandparents and my parents.

ACKNOWLEDGEMENTS

I thank Lord Jesus Christ for making, a Masters degree in Mechanical Engineering in the United States, a reality for me. I acknowledge His continuous guidance and grace in all that I have accomplished on this campus. I thank Him for the wisdom and intelligence that He has bestowed upon me. I thank Him for the doors that He has opened for me and His help during difficult times.

I thank the University of Maryland and the Department of Mechanical Engineering for providing me an opportunity to study here. I thank Dr. Michael Pecht for having faith in me and for financially supporting me for my studies. I thank him for guiding my thesis work. I thank Dr. Diganta Das and Dr. Michael Osterman for guiding me in my research work. I thank Dr. Peter Sandborn and Dr. Patrick McCluskey for serving on my thesis committee. I thank Dr. Balachandran for allowing me the use of his laboratory facilities and for his help and guidance. I also thank Dr. Cunniff, Dr. Dasgupta and Dr. Barker for their guidance. I thank Dr. Al-Bassyiouni for his help in the vibrations laboratory. I thank Richard Tersline for his help in the manufacturing the test fixture. I thank Dr. Azarian and Dr. Rodgers for their valuable advice and assistance in developing my thesis. I thank NASA for giving me an opportunity to do a project with them. I thank members of NASA (Robin Ferebee and Tim Milner), United Space Alliance (Gerry Margulies and Jim Lacassagne) and BD Systems, Inc., (Joseph Clayton, Scott Pollard, Bill Rooker and Emmette McDonald) for assistance with my project.

I thank all the staff members of Computer Aided Life Cycle Engineering, Electronics Products and Systems Center (CALCE EPSC) for their co-operation and

support. I thank the faculty members of the Mechanical Engineering Department for the knowledge that they have imparted to me. I thank Elyse Beaulieu-Lucey and Michelle Tan for their cheerful support and help. I also thank the staff members of the Mechanical Engineering Department for their help.

I thank my family for their prayers and support in my endeavour. I thank my fellow students in CALCE for the joy, happiness, encouragement and help they have given me during my tenure at CALCE. I thank all my friends for being an encouragement for me. I thank Mark and Sue Hoffman and members of the Chi Alpha Christian Fellowship for their love, prayers and friendship. I thank Brent Anderson for helping me tremendously during the past two years. I also thank the members of the Marthoma Church of Greater Washington and Cornerstone Church of Bowie for making me feel at home and encouraging me during my studies at the University of Maryland. Last but not the least I thank my housemates (past and present) for making my stay here in the US a pleasant experience.

TABLE OF CONTENTS

Chapter 1: INTRODUCTION... 1
Chapter 2: ENGINEERING HARDWARE ASSESSMENT METHODS............. 6
Chapter 3: HEALTH STATUS ASSESSMENT METHODOLOGY 15
3.1: Step 1: Life cycle environment profile 16
3.2: Step 2: Failure mechanisms, modes and effects analysis 16
3.3: Step 3: Virtual remaining life assessment.. 17
3.4: Step 4: Non-destructive physical analysis 20
3.5: Step 5: Testing 21
Chapter 4: REMAINING LIFE CASE STUDY- SOLID ROCKET BOOSTER 24
4.1: Background 24
4.2: Solid rocket booster 24
4.3: Integrated electronic assembly (IEA) 27
4.4: Why conduct a remaining life assessment? 28
4.5: Electronic hardware under review 28
4.6: Life cycle environment of IEA circuit cards.. 31
4.6.1: Vibration loads.. 31
4.6.2: Shock load... 34
4.6.3: Temperature conditions 35
Chapter 5: VIRTUAL REMAINING LIFE ASSESSMENT 38
5.1: Design capture 38
5.2: Load history characterization... 41
5.2.1: Vibration load simplification 42
5.2.2: Shock load simplification 43
5.2.3: Load transformation.. 45
5.3: Damage assessment 48
5.4: Ranking of potential failures.. 50
5.5: Calculating remaining life.. 50
Chapter 6: LIFE TESTING FOR REMAINING LIFE ASSESSMENT............. 52
6.1: Test loads 52
6.2: Test cycle and sequence... 55
6.3: Test duration 56
6.4: Test fixture 59
6.5: Test monitoring.. 60
6.6: Tests 62
6.7: Test results 64
Chapter 7: BRACKET FAILURE ASSESSMENT 68
7.1: Analytical estimation of natural frequency.. 68
7.2: Finite element modeling 70
7.3: Damage calculation.. 73
7.3.1: Random vibration load.. 74
7.3.2: Shock as harmonic vibration... 77
7.3.3: Total damage ratio 81
7.4: Summary 81
Chapter 8: CONCLUSION 82
Chapter 9: CONTRIBUTIONS.. 84

Chapter 10: FUTURE WORK 86
APPENDIX A: List of components and parts on the 3-ampere combination switch card. 87
APPENDIX B: CalcePWA modeling assumptions 89
APPENDIX C: Solid rocket booster flight segmentation 90
APPENDIX D: Life test fixture drawings 91
APPENDIX E: Grouping of SRB flight events for developing life test loads 93
APPENDIX F: Life test loads data 94
APPENDIX G: Life test procedure 98
APPENDIX H: Schematic of aluminum frame 102
APPENDIX I: Matlab program for calculation of bracket damage 103
REFERENCE 108

LIST OF TABLES

Table 1: Methodologies applied to estimate remaining life of engineering hardware. 11
Table 2: Life cycle load history 31
Table 3: Input data for virtual assessment 39
Table 4: Printed wiring board data... 40
Table 5: Loads per future mission 50
Table 6: Estimate of survivable missions 51
Table 7: Test cycle sections: corresponding loads and durations 58
Table 8: Test durations with 10 equivalent missions in each axis.......................... 59
Table 9: Resonance test results 65
Table 10: Material properties of 1100 H14 aluminum [86]...................................... 68
Table 12: Damage to the bracket due to random vibration loads 76
Table 12: Life test X-axis acceptance profile 94
Table 13: Life test Y-axis acceptance profile 94
Table 14: Life test Z-axis acceptance profile.. 94
Table 15: Life test X-axis low PSD profile 94
Table 16: Life test Y-axis low PSD profile 95
Table 17: Life test Z-axis low PSD profile.. 95
Table 18: Life test X-axis high PSD profile 95
Table 19: Life test Y-axis high PSD profile 95
Table 20: Life test Z-axis high PSD profile... 95
Table 21: X-axis shock profile.. 96
Table 22: Y-axis shock profile.. 96
Table 23: Z-axis shock profile 96
Table 24 X axis shock spectrum 96
Table 25 Y axis shock spectrum 97
Table 26 Z axis shock spectrum.. 97

LIST OF FIGURES

Figure 1: Health status assessment methodology 15
Figure 2: Exploded view of solid rocket booster [45] 25
Figure 3: Solid rocket booster separation [47]... 26
Figure 4: Solid rocket booster trajectory [46]... 26
Figure 5: Integrated electronic assembly box geometry schematic [48] 27
Figure 6: Front view of test article... 30
Figure 7: Back view of test article 30
Figure 8: Vibration time history for one flight 32
Figure 9: PSD profile of event 22 of vibration isolated flight 33
Figure 10: PSD profile of x-axis vibration acceptance test 34
Figure 11: Shock profile 35
Figure 12: Acceptance test thermal cycling profile 36
Figure 13: Axial through-hole lead architecture.. 40
Figure 14: Software model of test article... 41
Figure 15: Original and reduced PSD profile for event 22 for vibration isolated flight... 43
Figure 16: Harmonic approximation of shock data 44
Figure 17: Boundary conditions for the test article 46
Figure 18: Natural frequencies of test article... 47
Figure 19: Example of random displacement for test article.. 47
Figure 20: Vibration time history 53
Figure 21: Low PSD 54
Figure 22: One life test loading sequence.. 56
Figure 23: One equivalent mission 56
Figure 24: Accelerometer placement on the test article... 61
Figure 25: Strain gauge placement on the test article 62
Figure 26: Mock test set up.. 64
Figure 27: Fixture resonance 65
Figure 28: Experimental natural frequencies of the circuit card..................................... 66
Figure 29: Failed aluminum bracket... 67
Figure 30: Bracket Transformation side view 69
Figure 31: Bracket front view... 69
Figure 32: Model of simple aluminum bracket and transistor 71
Figure 33: ANSYS model of half section of aluminum frame and transistors 72
Figure 34: ANSYS model of full aluminum frame and transistors 72
Figure 35: Spectrum analysis result showing stress at the bend of the bracket 73
Figure 36: Life test vibration acceptance PSD profile... 76
Figure 37: Cantilever beam with uniformly distributed load... 78
Figure 38: Y axis shock data... 80
Figure 39: Fixture Design 91
Figure 40: Top view of interface plate.. 92
Figure 41: Side view of interface plate 92
Figure 42: Aluminum frame top view 102
Figure 43: Aluminum frame front view... 102

Chapter 1: INTRODUCTION

Electronic hardware can experience a range of load conditions during different phases of their lifetime, such as during manufacturing, assembly, testing, storage, handling, transportation and operation. Depending on the application and the environment in which the electronic hardware is used, the loads may vary from being a benign to destructive. Continuous application of such loads cause damage to the printed circuit board, electronic components and component to board interconnects. Over a period of time, damage during the lifecycle phases accumulates and affects the reliability of the electronic hardware [36]. The electronic hardware's reliability is defined as its ability to perform its intended functions for a specific period of time, in its life cycle application environment.

Traditional reliability prediction methods include methods based on field data, test data, stress and damage models and reliability handbooks. These reliability prediction methods generally do not accurately account for the life cycle environment of electronic hardware [38]. This arises from either fundamental flaws in the reliability assessment methodologies used [43] or uncertainties in the product life cycle [42]. The limitations of traditional reliability prediction methods can be overcome through the use of prognostics and health monitoring, which is a proactive approach of estimating the reliability of a product. Health monitoring is a process of observing and recording the extent of deviation or degradation from an expected normal operating condition [39]. Health monitoring techniques typically combine sensing, recording and interpretation of environmental, operational, usage and performance-related parameters indicative of the

products health [38]. Applications of health monitoring are typically classified as diagnostics, prognostics and life consumption monitoring.

Diagnostic systems monitor the current operating state of health of the product to identify the potential causes of failure [39] and can provide efficient fault detection and identification and maintain the effectiveness of the equipment through timely repair actions. Prognostic systems monitor the faults or precursors to failure, and predict the time or number of operational cycles to failure, induced by a monitored fault [39]. It provides real time reliability estimates for a product in its actual application conditions. Life consumption monitoring is a health monitoring method which quantifies the products degradation into the amount of its life consumed [41]. The life consumption monitoring process involves the continuous or periodic collection and interpretation of products life cycle environment. The remaining life estimate of the product is an output of the life consumption monitoring method.

Estimating the remaining life of electronic hardware that has been already deployed in the field presents a unique challenge. For such hardware, the life cycle data available is not the data obtained by a premeditated monitoring but through a routine general data collection event. In most such cases specific life cycle environmental data may not have been monitored. A remaining life assessment estimates the ability of the electronic hardware to meet the required performance specifications in its life cycle application environment for the remaining service life of the product [32]. Only a limited number of studies have been published on remaining life assessment methodologies for electronic hardware, and are first reviewed to identify the strategies used. From a review of the literature only three studies, Shetty *et. al.* [33], McCluskey *et. al.* [34] and

Valentine *et. al.* [32], have been found and are reviewed to identify the techniques used to estimate the remaining life.

Shetty *et. al* [33] conducted a remaining life assessment of four electronic circuit boards that had been deployed in the field for twenty years. The electronic circuit boards were from the space shuttle's shuttle remote manipulator system (SRMS) and had been used for fifteen space missions. The study used a combination of virtual remaining life assessment and physical analyses to estimate the remaining life of the electronic circuit boards. The virtual remaining life assessment was conducted using a physics of failure based software that utilized the life cycle loads, board and component geometry and material properties to estimate the damage till date to the component to board interconnects. Assuming the future loading conditions to be the same as its past conditions the damage due to one future mission was estimated. The number of future missions that the circuit board could experience without failure was estimated by dividing the value obtained by subtracting the damage to date from one by the damage per future mission. It was determined that the boards will be able to undertake twenty-five more missions in the next twenty years without failure. Thereafter, physical analyses were conducted wherein visual and optical inspection of two boards was conducted to identify any visible signs of degradation. The boards were cross sectioned to identify internal degradation. Component on the board were inspected and some critical components were cross sectioned to determine the level of degradation in them.

McCluskey *et. al* [34] conducted a remaining life assessment of twenty electronic circuit boards that had been deployed in the field, ten of which were in use for a period of six years and the remaining ten were in use for a period of three years. A three step

process was utilized to conduct the remaining life assessment. In the first step the probable degradations of the boards and the components were investigated. For the circuit board the following degradation mechanisms were studied: solder joint defects, non-wetting, dewetting, solder voids, pin holes, blow holes, bridging, solder joint fatigue and metallization corrosion. At the component level nondestructive examination of passive and active components were conducted and some active components were cross sectioned for further assessment. The degradation assessment process resulted in the identification of specific failure mechanisms. The second step involved the use of physics of failure models to calculate the acceleration factors for each dominant failure mechanism that were observed during the degradation assessment. The final step was testing of some of the printed circuit boards. Test conditions were developed using the acceleration factors such that it would provide maximum acceleration without including failure mechanisms that were not observed in actual operating environment. The study estimated that the circuit boards deployed in field for six years will survive for fourteen more years before any failure.

Valentine *et. al.* [32] conducted a remaining life assessment of a printed circuit board, which had been in service for fifteen years. The circuit board was part of the engine mounted control system in an aerospace engine. The study used the virtual remaining life assessment and qualification testing techniques to estimate the remaining life of the circuit card. Using the virtual remaining life assessment method the time to failure of the solder joint interconnects of each package on the circuit board was estimated. Based on the virtual assessment the critical integrated chip (IC) packages on the circuit board were identified. Accelerated qualification test was conducted on the IC

package that failed under virtual assessment. The virtual assessment and qualification test results were validated by comparing them to previously observed field failures. The study estimated that the circuit card will survive for seven more years before any failure due to solder joint fatigue.

From the above three studies ([32], [33] and [34]), it is observed that virtual remaining life assessment, physical analyses and testing techniques have been used to estimate the remaining life of electronic hardware. The studies however do not provide a basis for selection of the remaining life techniques used. None of the studies have presented a list of applicable techniques and the criteria for selection of these techniques during the remaining life assessment process. In this context this paper presents a methodology that provides a guideline for conducting a remaining life assessment of electronic hardware already deployed in the field. Given an electronic hardware already deployed in the field, the methodology will provide the assessor with the possible techniques that can be used and the criteria for implementing that technique.

To develop such a methodology a review of remaining life assessment studies for other engineering hardware was undertaken to compare strategies currently applied to them with those used for electronic hardware. The review also sought to identify the similarities in the techniques used for electronics and other hardware. The focus of the review was to determine the availability of a complete remaining life assessment methodology for other engineering hardware from which suitable strategies could be adopted for electronic hardware assessment.

Chapter 2: ENGINEERING HARDWARE ASSESSMENT METHODS

Excluding electronic assemblies, remaining life studies for engineering hardware that have been conducted include mechanical products and civil structures. Mechanical hardware include heavy equipments like gas and steam turbines, boilers, refinery heater tubes, industrial furnaces, pressure vessels, pressure vessel nozzles, components of petrochemical plants, liquid natural gas (LNG) plants, fossil power plants, power plants and ship turbines generators. The civil structures include reinforced concrete structures and bridges. Table 1 summarizes the techniques used by such studies to assess the remaining life of mechanical hardware and civil structures.

Remaining life assessment techniques for civil structures used by Liang *et. al.* [29] and Torres-Acosta *et. al.* [30] are described below. Liang *et. al* [29] conducted a remaining life assessment of a reinforced concrete bridge that had been in use for forty years. The assessment focused on the degradation of reinforced concrete structures due to chlorine ingress followed by corrosion of the steel reinforcement bars. A mathematical model based on chemical diffusion rate combined with previous laboratory tests and empirical results from other reinforced concrete structures was used for the estimation of the remaining life of the bridge. The mathematical model gives the value of the porous diffusion coefficient, which is a measure of the porosity of the concrete structure that has a significant effect on the absorption of chloride ions. The remaining life of reinforced concrete is divided into two stages: the initiation period, which is the time from exposure to chlorine to the time it reaches the inner steel bars and the propagation period, which is the time period during which the steel bar corrodes and reaches the critical limit of mechanical strength. Based on empirical data plots of diffusion coefficient versus time

for a particular extracted sample thickness and voltage potential were first generated. Then a concrete specimen of 5 centimeter thickness was extracted from the reinforced concrete bridge. The specimen was put into a chloride migration apparatus with accelerated electrical potential of 9 volts. After 208 hours the chloride concentration in the sample was found to be 0.003 times the critical concentration. From this result the time needed for the chloride to diffuse inwards and reach the steel was calculated using the mathematical model. It was estimated that the initiation period is 9.12 years and the propagation period is 10 years. Thus with the use of a mathematical model the remaining life of the bridge was estimated to be 19.12 years.

Torres-Acosta *et. al* [30] developed a method of estimating the remaining life of reinforced concrete structures in the marine environment. The focus of the study was linking the degree of degradation of a structure to the surface crack width. The study utilized data from six previous studies to develop an empirical relationship between the average corrosion penetration value and the surface crack width. An empirical relationship between the average corrosion penetration value and the load capacity ratio of the concrete structure was also developed. For verification twelve concrete slabs (9x19x31 cm) with 4 steel bars each were prepared. The slabs were contaminated with chlorides to accelerate the corrosion process and left in a high humidity environment for 700 days, after which the slabs were inspected for cracks. The position, width and length of each crack were measured. The steel bars from the concrete slabs were removed and after thorough cleansing the diameters of the bars were measured. From the results of the measurement the average corrosion penetration value is estimated. The load capacity ratio of the concrete structure was estimated from experimental values of structural stress

limits. An empirical relationship between the load capacity ratio of a reinforced concrete structure and the degree of steel bar radius loss by corrosion was developed. A second empirical relationship between the maximum surface crack and the average corrosion penetration was developed. By measuring the surface cracks of a reinforced concrete structure in a marine environment the load capacity of the structure can be estimated using the empirical relation. From the average corrosion penetration ratio the time for complete corrosion of the steel bars in the concrete structure can be calculated. This period is the remaining life of the concrete structure.

It was observed from the above two studies that Liang *et. al.,* used a mathematical model and sample testing method to determine the remaining life of the concrete structure while Torres-Acosta *et. al.,* used data from six previous studies to develop an empirical model for remaining life assessment of concrete structures and verified the model with accelerated testing. Other remaining life assessment studies for concrete structures are described briefly in Table 1.

Remaining life assessment techniques for mechanical hardware, used by Duvenhage and Wannenberg [18] and Cheruvu and Malmfeldt [14] are described below. Duvenhage and Wannenburg [18] conducted a remaining life assessment of a pressure vessel that had been in operation for twelve years. The pressure vessel was used to purify contaminated hydrogen-rich feed steam for power plant usage. The assessment methodology utilized data about the stresses on the pressure vessel, the material properties and the nondestructive examination results as inputs for fracture, fatigue, propagation and probabilistic analyses. The primary stresses caused by actual loading conditions were calculated by means of a finite element analysis. Secondary stresses

caused by welding were determined from empirical data. The material's stress- strain properties were used to generate a material specific failure assessment diagram. Toughness testing was conducted on samples taken from non critical welded bends and the results were adapted to accurately estimate the toughness properties of the weld material in the heat affected zones of the pressure vessel. The crack propagation rate was represented using a mathematical formulation and the constants for the equation were estimated from previous experimental data. Non-destructive examination was conducted to detect the crack locations and sizes. The samples taken from the bends were subjected to cyclic stresses and the test data obtained was compared to the S-N curves of the pressure vessel material. The minimum life before failure, obtained for any welded joint was 32.2 years. Using two industry methods (CEGB R6 and PD-6493) the critical defect size analyses were conducted. Since crack propagation analyses are dependent on the initial crack sizes a reverse calculation was conducted wherein the end size being known the initial crack size is estimated as a function of period of service. To incorporate the probabilistic nature of nondestructive examination methods, the crack size and number were modeled as a log normal distribution, for calculating the crack propagation rates. It was determined that the regular inspections scheduled after every 20 months would require all cracks longer than 25 millimeters be detected and sealed for failure free operation till the next scheduled inspection of the pressure vessel.

Cheruvu and Malmfeldt [14] conducted a remaining life assessment of a high pressure steam turbine rotor that had been in use for twenty-six years. The focus of the study was to estimate the remaining life of the rotor based on degradation of material properties due to prolonged exposure to very high temperatures. High temperatures cause

micro-structural changes in the material and depletion of alloying elements in the material thereby leading to degradation of yield, tensile and creep strengths of the material. This phenomenon of degradation of material properties due to temperature is called temper embrittlement and adversely affects the rotor life. For the assessment two material samples were drilled from the rotor: one from the region closer to the center where the temperature is comparatively low and another from a region towards the end of the rotor where the temperature is very high. These two samples are called cold and hot samples respectively. Another sample from an unused rotor was extracted for assessment. First micro-sections were taken from the samples for metallography. The sections were polished and etched and were observed under optical microscope to observe any differences in the microstructure. No significant differences in microstructures of the cold and hot specimen were observed. Tensile testing was conducted on the hot sample and it was observed that the tensile strength decreased by 3 to 4 % when compared to the sample from unused rotor. A Charpy V notch impact test was conducted on the cold sample and the sample from the unused rotor. There was a slight decrease in the impact properties in the cold sample but not significant enough to cause problems. Finally an accelerated creep rupture tests on the hot sample was conducted. The tests were accelerated by increasing the stress at the service temperature (isothermal) and raising the temperature at the service stresses (isostress). From the results of the tests two plots were generated: the stress versus rupture time plot and the temperature versus rupture time plot. A linear extrapolation of the stress versus rupture time plot estimated the time for crack initiation as 600 years while the temperature versus rupture time plot yielded a value of 68 years before crack initiation in the rotor. Due to the continued softening of

the material and temper embrittlement due to service conditions it was recommended that the rotor should be reevaluated for material properties after 10 more years of service.

It was observed that Duvenhage and Wannenberg used fracture mechanics based techniques to estimate the remaining life of the pressure vessel while Cheruvu and Malmfeldt used material degradation based techniques to estimate the remaining life of the high pressure steam turbine rotor. From the two above mentioned studies, it was observed that techniques like finite element analysis, empirical models, non-destructive examination, sample testing, accelerated testing, damage models and material degradation analyses are used to assess the remaining life of mechanical structures. Other remaining life assessment studies for mechanical hardware are described briefly in Table 1.

Table 1: Methodologies applied to estimate remaining life of engineering hardware.

Product	**Remaining Life Estimation Technique**	**Reference**
Mechanical hardware		
Turbine rotors	Ultrasonic detection technique to examine the cracks in turbine rotors. Based on the results stress and fracture analysis of the cracks were conducted to estimate the time to failure.	8, 1, 27
Refinery heater tubes, Steam turbine components	The creep properties of the product, obtained from non destructive testing, were utilized to calculate an acceleration rate and this value was compared to a database to estimate the remaining life.	11, 23
Furnace heater tubes	Ultrasonic wall thickness examination of furnace heater tubes was conducted and the	25

Product	Remaining Life Estimation Technique	Reference
	result was used to analytically estimate the remaining life.	
Turbine rotor, Fossil fuel power plant components, Industrial furnace tubes, Petrochemical plant components, Power plant components	Samples were extracted from the product and subjected to a variety of tests like creep test, impact test, hardness testing etc., and the results were compared to material properties to estimate the degradation and thereby predict the remaining life.	3, 4, 6, 15, 17
Boiler heater tubes	Non-destructive and destructive testing was conducted on boiler re-heater tubes to assess the damage and estimate the life. A virtual assessment was also conducted to estimate the life.	5
Pressure vessel nozzle, Furnace tubes, High pressure rotor, Super heater tubes	Sample of product was tested by subjecting it to cyclic stresses. Using characteristic curves of the material and comparing the cracks that developed the remaining life was estimated.	7, 12, 14, 24, 20
Pressure vessels, Gas turbine	A general approach for remaining life assessment of a product with emphasis on quantifying the system parameters and modeling the damage as a function of the parameters was developed.	2, 16
Service turbine generator of a ship, Power plant components	A finite element modeling and assessment method of estimating the remaining life was used.	9, 13
Pressure vessels	Non-destructive examination of the product was conducted and the results were used to develop a finite element model for evaluation.	10, 18

Product	Remaining Life Estimation Technique	Reference
	The results of the FEM were compared to a predetermined failure criterion to estimate the remaining life.	
Components of a liquefied natural gas (LNG) plant, Super-heater outlet header	The damage to the components of the product was modeled and was used to develop a finite element model to estimate the remaining life	21, 26
Civil structures		
Reinforced concrete bridge	A non-destructive chemical diffusivity evaluation in reinforced concrete structures was conducted and the result was used to analytically estimate the remaining life.	29
Reinforced concrete structures	An accelerated corrosion test was conducted on a reinforced concrete structure and the result was compared to empirical data to estimate the remaining life.	30
Reinforced concrete structures	Damage modeling technique was used to assess the degradation of reinforced concrete structure. This data was then studied by experts to provide initial estimate of the life. Then a mathematical technique was used to improve the estimate.	19
Reinforced concrete structures	Analytical calculations based on data available were used to estimate the remaining life of a bridge.	28, 31

Overall, the remaining life assessment techniques used for civil structures and mechanical products can be categorized into three main groups: physical analysis (non-

destructive and destructive), damage modeling (analytical and finite element) and testing. It was observed that most of the studies employed a combination of physical analysis, testing and damage modeling to determine the remaining life of the products. Many of the techniques used in the above studies can be applicable to electronic products deployed in the field. Some of these techniques are applicable (e.g., destructive testing of sample) only in cases where additional equivalent samples are available for possible destructive testing. Some are applicable (e.g., sample extraction) only on large mechanical systems where small samples harvested for testing does not impair the structural integrity of the system. These techniques were taken into consideration in developing a generic methodology for remaining life assessment of electronic hardware. The methodology is described in the following chapter.

Chapter 3: HEALTH STATUS ASSESSMENT METHODOLOGY

The process of determining the remaining life of a product already deployed in field is analogous to determining the status of the product's health at that given moment. Hence the new methodology is termed as 'Health Status Assessment Methodology' and is described below. Figure 1 shows the health status assessment methodology.

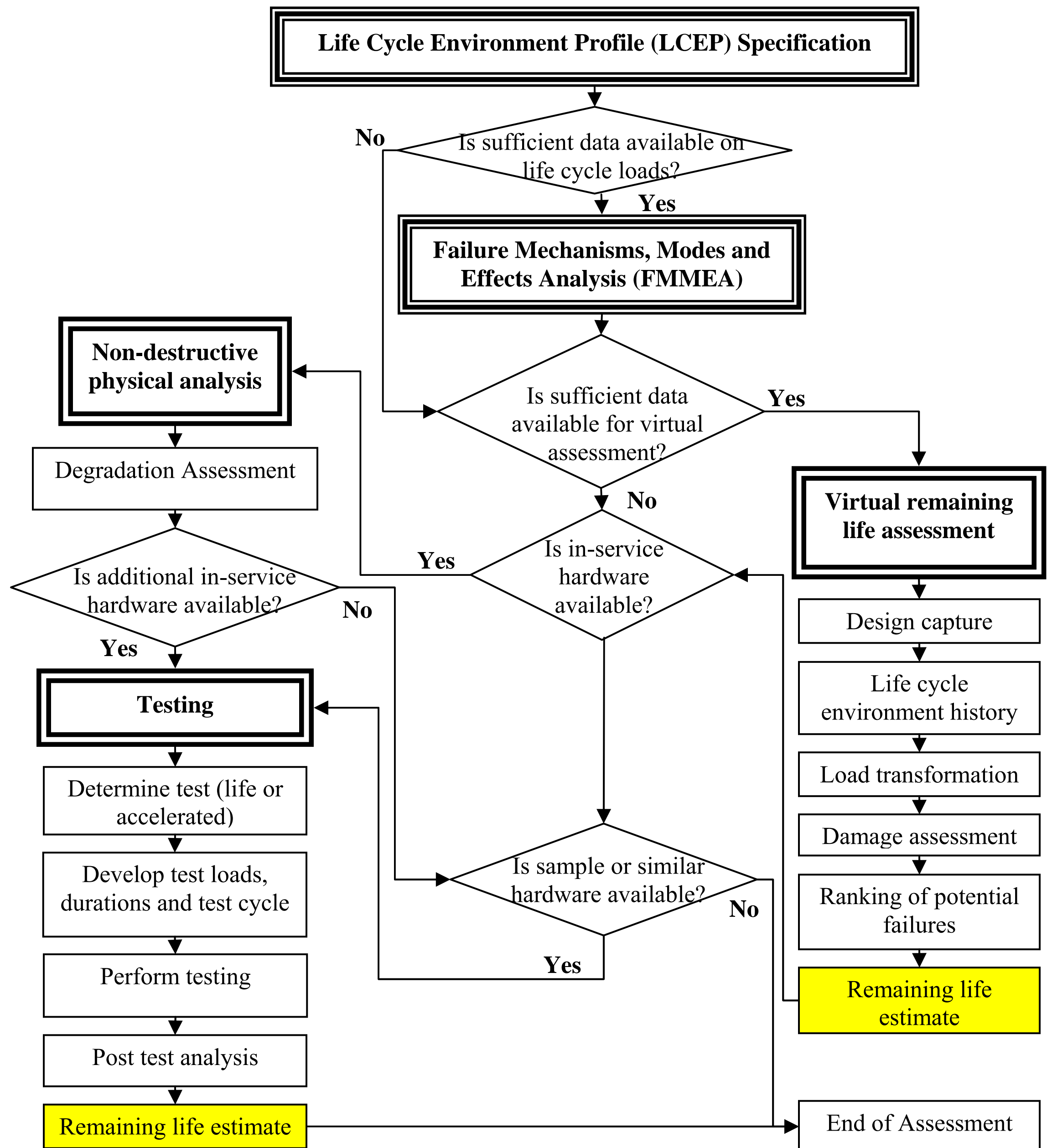

Figure 1: Health status assessment methodology

3.1: Step 1: Life cycle environment profile

For an electronic hardware with no in built monitoring system or for those for which there has been no predetermined data collection, the first step towards assessing its remaining life is to generate the life cycle environment profile (LCEP) of the hardware. LCEP involves the identification and quantification of the different operating and non operating load conditions of the hardware. The data to be collected involve the physical data, functional data and the life cycle environment data. Physical data includes information about the printed circuit board (length, width, thickness, number of layers, percent metallization, layer material etc.) and the components on the board (part types, dimensions, mounting styles, material, lead material, position of the component on the board etc.). The functional data includes the duty cycles, power cycles, duration of operation etc. The life cycle environment data includes the lifecycle loads, the life cycle phases, operating conditions, areas of application etc. A proper and complete collection of data is vital to the remaining life estimation. The more the data, more accurate the remaining life estimation will be.

After this step it is important to assess the sufficiency of the data generated for moving to the next step as shown in Figure 1. If the life cycle data is limited it will not be possible to proceed with the next step. In such a case the availability of an in-service hardware would help continue the remaining life assessment process.

3.2: Step 2: Failure mechanisms, modes and effects analysis

If there is enough data that has been generated in the LCEP step, then the second step of failure mechanisms, modes and effects analysis (FMMEA) for the hardware can be conducted. FMMEA is a process of identifying the failure mechanisms and models for

all potential failure modes and prioritizing them in order of potential damage impact. The process of prioritizing the failure mechanisms involves the use of information related to the application conditions, duration of application, active stresses and potential failure mechanisms. The first step in FMMEA is to define the hardware and the components on the hardware. This is followed by identifying the potential failure modes and causes. Next is the determination of the applicable failure mechanism to the identified potential failure mode and its probable cause. Next the appropriate failure models needed to evaluate the failure mechanism is defined. Finally the identified failure mechanisms are ranked in order of potential for highest impact under life cycle environment conditions. For estimating the remaining life of an electronic hardware the effect of the failure mechanisms and modes identified should be assessed in order of their priority ranking.

After the FMMEA if there is sufficient data about the material properties and geometry of the board and components the remaining life process moves on to the third step which is a virtual remaining life assessment. As shown in Figure 1 if the data is insufficient for virtual remaining life assessment, then a non-destructive physical analysis of an in-service hardware will help in estimating the hardware's remaining life. In case of non-availability of the in-service hardware, a sample or similar hardware can be tested to estimate the relative remaining life of the hardware under assessment.

3.3: Step 3: Virtual remaining life assessment

The virtual remaining life assessment is based on a physics-of-failure stress and damage accumulation analysis. This analysis involves using the material properties and geometry of the product and the measured life cycle loads to assess the dominant failure mechanisms. Based on a load-stress simulation, the physics-of-failure damage models

give an estimation of the accumulated damage for the product in its life cycle environment. The virtual remaining life process consists of the following steps: design capture, life cycle loading history characterization, load transformation, damage assessment, and ranking of potential failures for remaining life estimation.

Design capture involves identifying the components on the board, matching their respective part types, recording their dimensions and position on the board, recording the board dimensions and recording the board and component material properties into the software program. This includes part information (e.g., substrate material, encapsulants, underfills, leads and platings), interconnects (e.g., solder composition, conductive adhesives, socket materials), and the makeup of the printed wiring board (e.g., resin system, plating, embedded passives).

Life cycle load history characterization involves identifying and recording significant life cycle loads and simplifying them for assessment Examples of environmental loads needed for life cycle loading characteristics include temperature limits, average temperature, frequency of temperature cycles, vibration, shock and electrical loads. The level of these experienced loads should be accompanied with details of rate of change and duration of exposure. The life cycle loads profiles are converted into a form that can be used as input to the software program for modeling.

The load transformation process utilizes the characterized loading conditions to estimate the effect of these loads on the circuit card. In load transformation the software takes the environment and architecture input and produces the stress fields (e.g., temperature, displacement, and curvature). Thermal stresses are usually associated with

mechanical (structural) failures (e.g., ductile rupture, brittle fracture, creep, stress relaxation, thermal shock, stress, and corrosion).

The damage assessment is conducted using a failure model consisting of a stress model and a damage model. Stress models correlate the environmental and operational loads, package architecture, and material properties to stress, strain and energy distributions within the components and the solder joint interconnects. The damage models are used to determine the number of cycles to failure. In the damage assessment step, the damage for each part is defined in terms of damage ratio (DR), which is the ratio of the number of cycles applied to the number of cycles (or other equivalent units) it can survive.

Ranking of potential failures involves ranking the components in decreasing order of damage ratios. Once the failure potentials are listed in descending order of damage accumulation the remaining life of the component for which the damage ratio is highest is estimated. The remaining life is given by subtracting the damage ratio from the damage criterion (equal to 1) and dividing that value by damage ratio per future life cycle. The remaining life of the electronic hardware is equal to the remaining life of the component with the highest damage ratio.

If the in-service hardware is available for assessment then the remaining life assessment process moves on to the fourth step of non-destructive physical analysis. If the in-service hardware is not available then the availability of a similar circuit card that has been in use or a sample circuit card with similar construction but not used in the field, should be determined. As shown in Figure 1 if sample or similar circuit cards are not

available then the remaining life estimate obtained from the virtual remaining life assessment is the best possible estimate.

3.4: Step 4: Non-destructive physical analysis

The non-destructive physical analysis of the hardware involves the assessment of degradation to the printed circuit board, the components on the board, the solder joint interconnects and the metal traces on the board. Non-destructive analysis uses techniques such as optical inspection, ultrasonic testing, dye penetration test etc., to identify and investigate signs of degradation. Optical inspection of the components and the solder joint interconnections reveal visible signs of damage. Cracks and voids affect the reliability of the component which in turn affects the remaining life of the electronic circuit board. The components are inspected to determine the possible presence of visible physical damage to the components. The circuit board and the metal traces on the board are also inspected for any visible damage. Characterization of small solder samples taken from the solder joint interconnections and comparison of the results to virgin solder properties will indicate the amount of degradation at the solder joints. The degradation can be expressed in terms of percentage of characteristic or virgin properties or in terms of damage ratio. From the value of amount of degradation the remaining life of the hardware can be predicted.

After the non-destructive physical analysis if additional in-service hardware in available for assessment the remaining life assessment process moves to the fifth and final step of testing. In case additional in-service hardware is not available then a similar circuit card that has been in use or a sample circuit card with similar construction but not

used in the field, can be tested. As shown in Figure 1 if the similar or sample circuit card is also not available the remaining life assessment is terminated.

3.5: Step 5: Testing

The fifth and final step in the remaining life assessment process is testing. The objective of the testing is to subject the electronic hardware to continuous cycles of life cycle environment load until a failure occurs. Testing involves selection of test type, development of test loads, test durations, test cycles, actual testing and post test analysis.

Testing can be of two types: accelerated testing and life testing. Determination of the type of testing depends on the usage conditions of the hardware, at what stage in the designed life is the assessment being conducted and the practical feasibility of conducting the test activity. If an accelerated testing has to be conducted the proper acceleration factors for the test loads should be estimated so as to correlate the testing results to the expected results under normal conditions. For a life test the test loads should be representative of the actual loading conditions. Testing may require design and manufacture of a test fixture that approximately recreates the mounting conditions of the electronic hardware in the actual life cycle environment.

Next the test loads, test cycles and test durations are determined. The test loads are designed on the basis of the life cycle loads identified in the FMMEA. The load sequencing should consider the application of the load in actual life cycle environment. The duration of application of the test load should be estimated from the actual duration of the load in the life cycle environment. Sometimes time compression may be necessary in order to reduce the total testing time.

Actual testing involves affixing the electronic hardware in the test fixture, setting up the monitoring hardware and subjecting the assembly to the test loads, in the determined sequence, for the determined duration, in a particular axis. The criteria for stopping the life test have to be defined before the beginning of the testing. Functional and physical monitoring should be continuously conducted during the testing. If the hardware fails during test the total number of cycles from the beginning of the test to the cycle before the cycle in which it failed is considered to estimate the life of the hardware. For a life test the total number of such cycles is the life of the hardware while for accelerated tests the life is estimated using the acceleration factors.

Post test analysis of the results of the testing is conducted to adjust the remaining life prediction. The testing procedure and results are analyzed for correctness and compliance with expected norms. If there are any variations then they are analyzed using analytical or numerical techniques and the results of the analysis are factored into the remaining life prediction.

In case remaining life estimates from virtual remaining life assessment, non-destructive analysis and testing are available the result of the testing process should be selected for future course of action. The virtual remaining life assessment will provide accurate estimates only for the failure mechanisms that had been modeled. Non-destructive physical analysis will provide an estimate of the amount of degradation in a component or at a particular site. The amount and rate of future damage may vary depending on the future operating conditions. Testing usually provides the best remaining life estimate since the hardware is actually subjected to its life cycle loads till a failure

occurs. This result can be used as the basis for future operation and maintenance strategy for an electronic hardware unit similar to the hardware under review.

Chapter 4: REMAINING LIFE CASE STUDY- SOLID ROCKET BOOSTER

The remaining life assessment methodology described in the previous chapter has been implemented in this case study. This study was conducted in conjunction with the National Aeronautics and Space Administration (NASA). This chapter describes in brief the background and the electronic hardware under test.

4.1: Background

The National Aeronautics and Space Administration Agency (NASA), in its quest for developing a reusable space transportation system, conducted numerous feasibility tests in collaboration with the US Air Force. In July 1972, NASA awarded Rockwell International the contract for the design, development, test and evaluation of the space shuttle [44]. The first shuttle mission was successfully completed on April 12, 1981 when the Space Shuttle Columbia lifted off from the Kennedy Space Center, Florida [44]. The space shuttle program is formally known as Space Transportation System (STS) [44].

4.2: Solid rocket booster

Two solid rocket boosters (SRBs) are attached to the external tank and provide the bulk of the thrust at lift-off and during the first stage of ascent [44]. The SRBs also support the weight of the orbiter and the external tank. Each SRB weighs 1,300,000 pounds at launch and has a height of 149.16 feet and diameter of 12.17 feet. "Primary elements of each booster are the motor (including case, propellant, igniter and nozzle), structure, separation systems, operational flight instrumentation, recovery avionics, pyrotechnics, deceleration system, thrust vector control system and range safety destruct system."[44]. Figure 2 shows an exploded view of a solid rocket booster.

The SRBs are used to lift the shuttle up to an altitude of about 150,000 feet. After reaching an altitude of 150,000 feet the SRBs separate from the orbiter and the external tank. Figure 3 shows the separation of the solid rocket booster from the orbiter. It reaches its apogee at approximately 220,000 feet and falls into the ocean approximately 122 nautical miles from the launch site. Figure 4 shows the flight trajectory of the solid rocket booster.

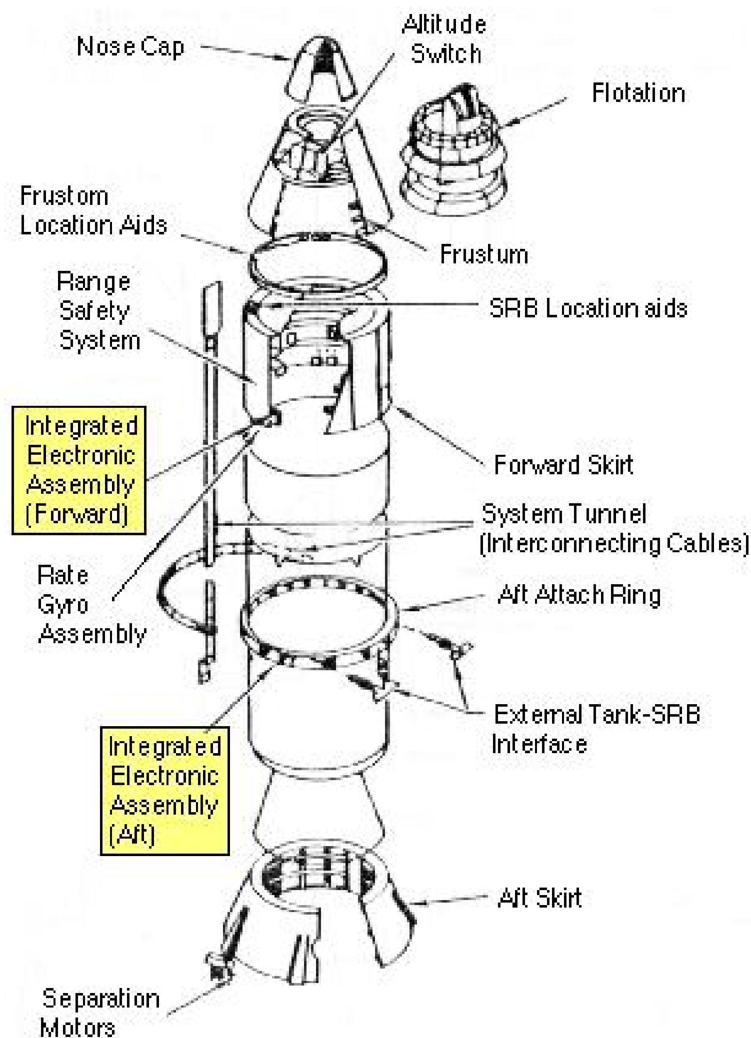

Figure 2: Exploded view of solid rocket booster [45]

Figure 3: Solid rocket booster separation [47]

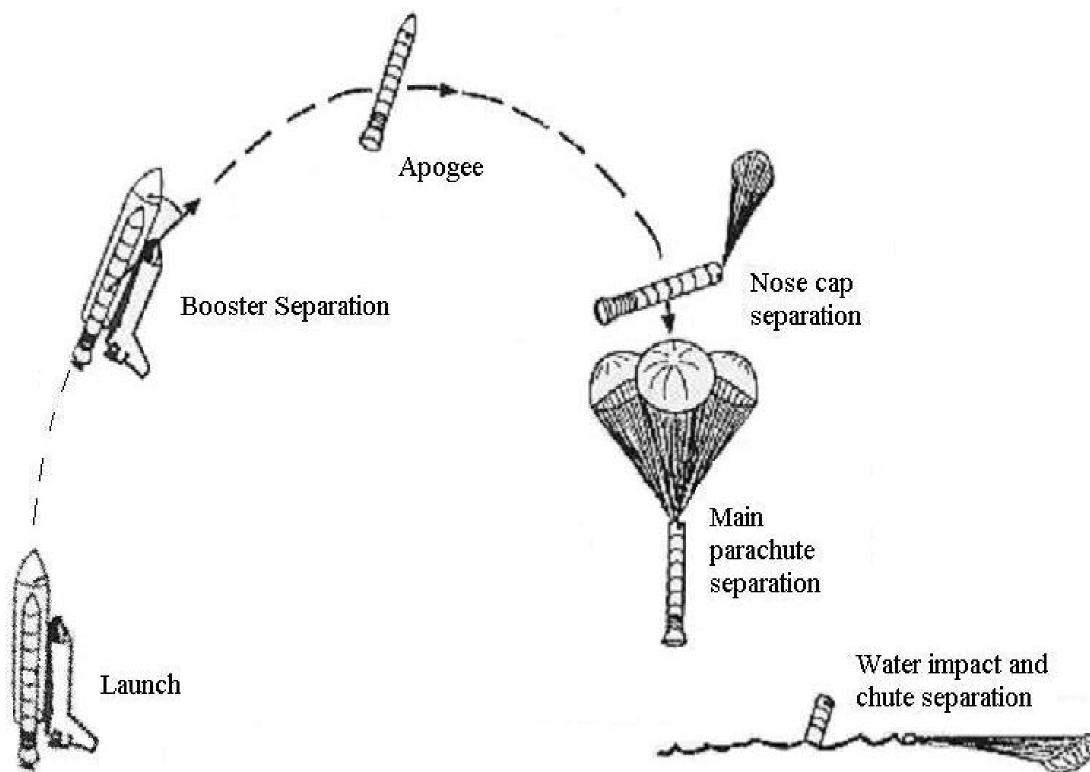

Figure 4: Solid rocket booster trajectory [46]

4.3: Integrated electronic assembly (IEA)

The Solid Rocket Booster Integrated Electronics Assembly is the primary communications link between the SRB and the Shuttle's Orbiter. The IEA provides the control electronics for the SRB during the launch, ascent, separation, reentry and recovery phases of the mission. Each solid rocket booster contains two integrated electronic assembly (IEA) boxes: the forward and the aft assembly boxes. The integrated assembly box contains a number of electronic printed wiring boards. The IEAs receive and execute SRB separation and range safety commands [44]. Figure 5 shows the wire frame of the IEA and circuit cards.

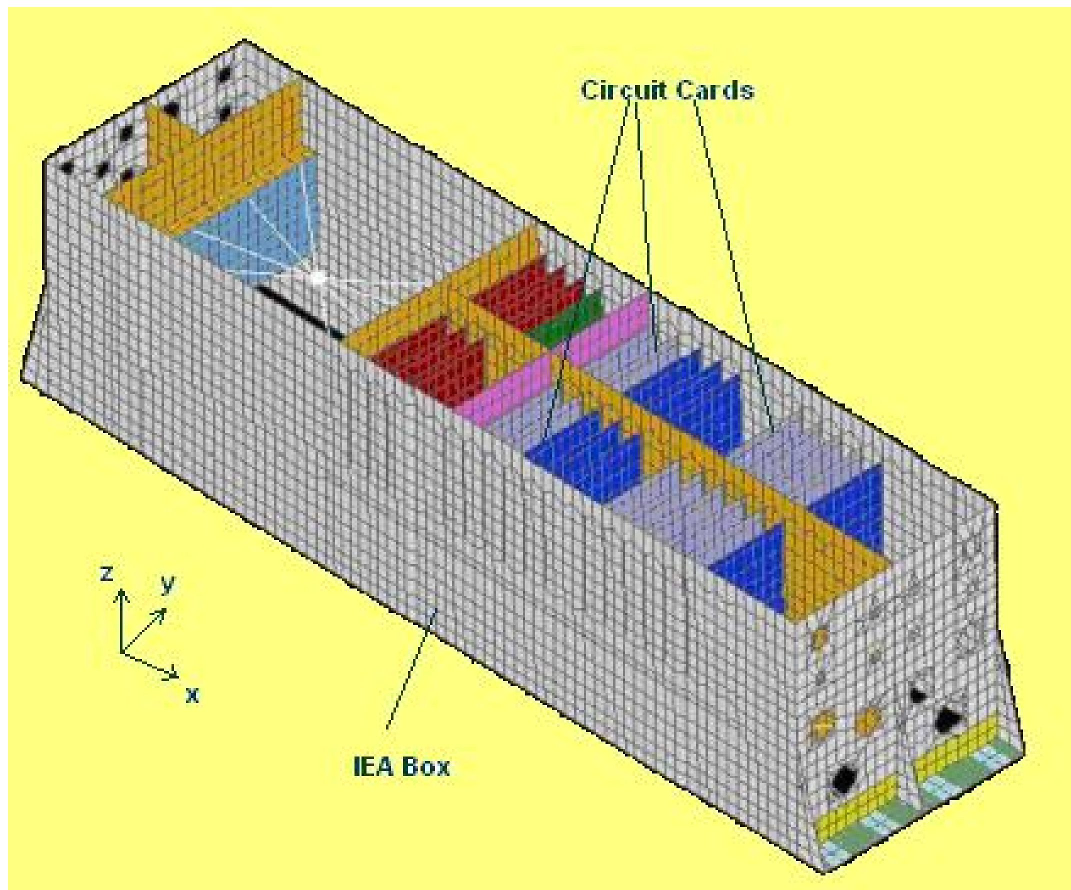

Figure 5: Integrated electronic assembly box geometry schematic [48]

4.4: Why conduct a remaining life assessment?

NASA's Reusable Launch Vehicle (RLV) that is to replace the present Space Shuttle fleet is not expected to be ready before 2020 and hence NASA hopes to extend the usage of the Space Shuttles up to the year 2020. NASA also needs to make necessary engineering decisions to ensure that all shuttle components are capable of life extension till that time. Over the years NASA has observed some component failures in the Solid Rocket Booster's Integrated Electronic Assembly circuit cards after their recovery from the sea. The Solid Rocket Booster experiences random vibrations along its trajectory from its take off to water impact. The Integrated Electronic Assembly is also subjected to the same random vibrations. The multiple random vibration loads during flight and the shock during water impact have an effect of causing damage to the booster's electronic hardware. A remaining life assessment is instrumental in estimating the number of future missions the boosters can undertake under the known flight conditions before failure in the IEA electronic hardware. The results of the remaining life assessment will also serve as an input to decisions on the upgrade, repair, rework and testing method changes for this hardware.

4.5: Electronic hardware under review

It was decided to assess the remaining life of an electronic circuit card from the aft IEA box since the circuit cards in the aft box experiences higher stresses and severe environment than those in the forward box. From the available circuit cards in the integrated electronic assembly, one 3-ampere combination switch card henceforth called test article, was selected to be assessed for its remaining life. This card was selected on

the availability of an identical engineering (sample) circuit card and the general similarity of the circuit card to the other circuit cards in the IEA box.

The test article is a rectangular, single layered circuit card with epoxy-F substrate. The length is approximately 157 millimeters, the width is approximately 109 millimeters and the layer thickness is approximately 2.25 millimeters. The board is split into 4 identical quadrants. There are a total of 121 components on the circuit card. These components belong to the following types of parts: resistors, capacitors, diodes, transistors, transformer assembly, connector, and optocoupler. A list of the components and parts on the test article is given in Appendix A.

All the components except the four transistors and two transformers are insertion mount components. Four transistors are screwed on to aluminum brackets that are part of the aluminum wedge frame riveted to the printed wiring board (PWB). The two transformers are directly screwed onto the center of the board. The vias through which the leads of the through hole components pass are not plated through holes. The leads of the through hole components are bent on the other side of the PWB and are then soldered to the interconnect traces. The C shaped aluminum frame on the circuit card is used to slide the circuit card into the birtcher guides in the IEA box. Figure 6 and Figure 7 show the front and back of the test article respectively.

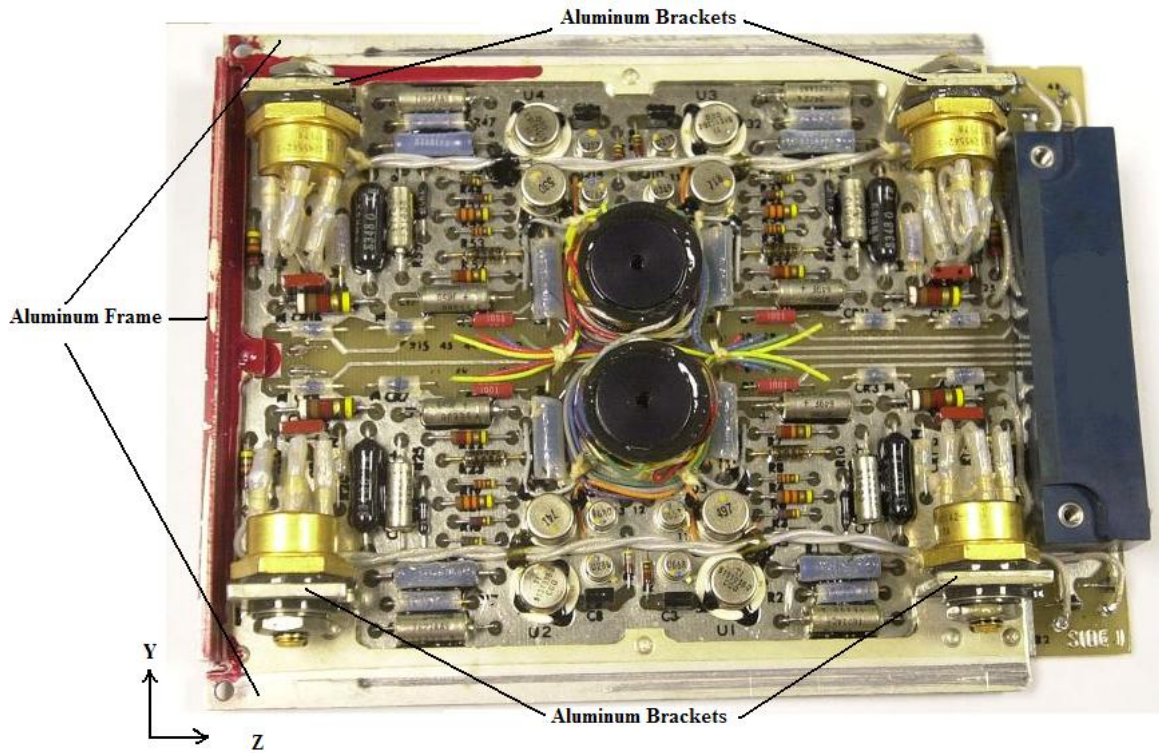

Figure 6: Front view of test article

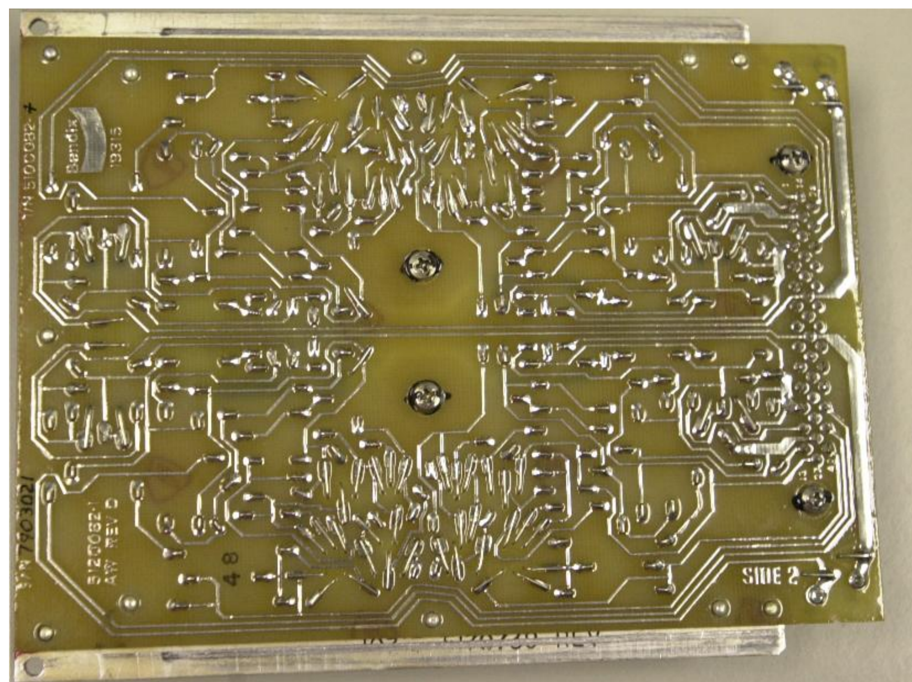

Figure 7: Back view of test article

4.6: Life cycle environment of IEA circuit cards

The test article has been used for eight space missions. During the first flight vibration isolation was not provided for the IEA box while for the next seven flights vibration isolation was provided. Before each flight the IEA is subjected to thermal and vibration acceptance tests. During flight the circuit cards experience random vibrations and experience shock upon water impact. During the preflight acceptance tests the IEA is subjected to random vibration and temperature cycling loads. The circuit cards experience insignificant loading during storage, transportation and recovery phases of its life cycle. Table 2 shows the circuit card's life cycle exposures and the loads experienced.

Table 2: Life cycle load history

Life Cycle Environment	Load Type	Exposures to Date
Vibration Acceptance Test	Random Vibrations	15
Thermal Acceptance Test	Temperature Cycling	27
Flight (Vibration Non-Isolated)	Random Vibration and Shock	1
Flight (Vibration Isolated)	Random Vibration and Shock	7

4.6.1: Vibration loads

The test article is subjected to random vibrations in its life cycle. The phases where it experiences vibrations are during flight, acceptance tests and transportation to and from storage site.

4.6.1.1: Flight

The test article experiences varying intensity of random vibration during the SRB's entire flight sequence. It experiences the most random vibrations during its re-entry phase starting from it reaching its trajectory apogee to its splash down in the sea.

The motion of the entire booster is random and thereby the vibrations are stochastic in nature. Figure 8 show the vibration time history of one flight of the SRB. The SRB flight has been divided into thirty-two (32) different events. The even numbered sections indicate the major events. The transition events are odd numbered and are not indicated in the figure. The major events are lift-off, booster separation, apogee, re-entry, drogue chute deployment, main parachute deployment and water impact. A list of the thirty-two events, the load during each event and the duration of each event is given in Appendix C.

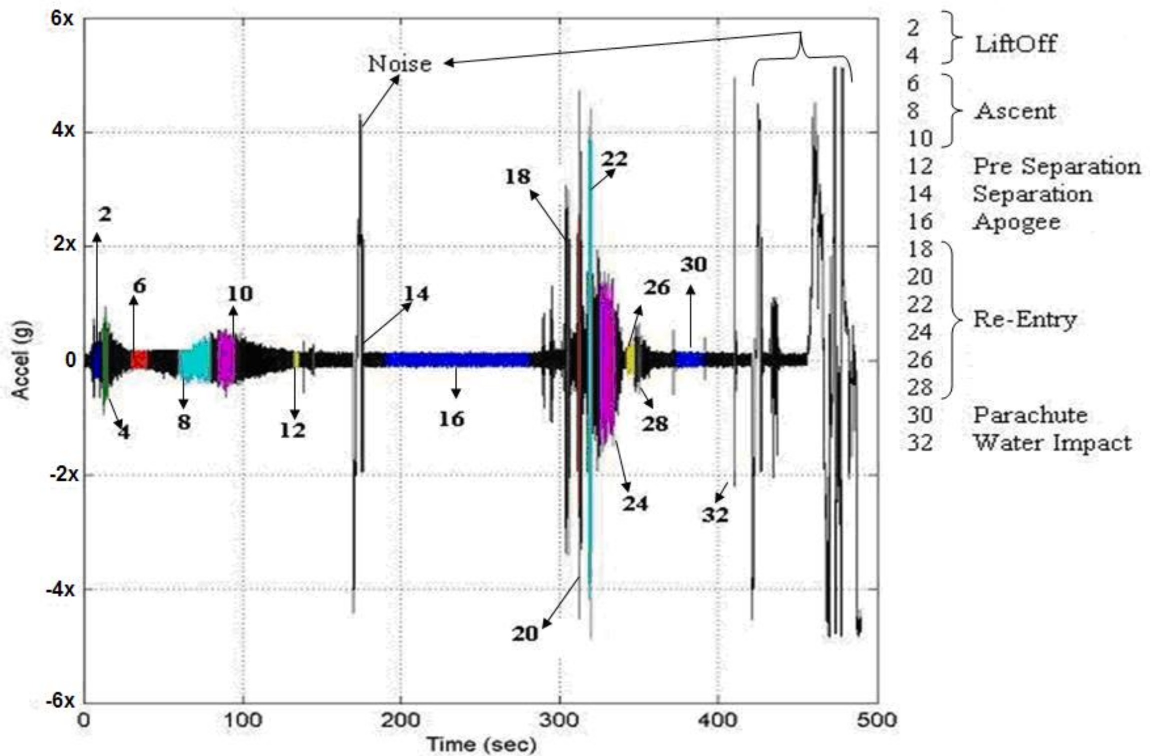

Figure 8: Vibration time history for one flight

The vibration profile was recorded by an accelerometer fixed on the casing of an IEA. BD Systems Inc., contractors for NASA, used finite element modeling and transfer functions to transform the field data into Power Spectral Density (PSD) profiles for each of the thirty-two (32) events for the circuit card. The PSD data for both the flight

conditions that is with vibration isolators and without vibration isolators and the acceptance test has been provided in the above-mentioned form. For each individual event of a flight the data is further bifurcated to PSD data for each of the x, y and z reference axis. Figure 9 shows an example of the PSD profile for event 22 of the vibration isolated flight.

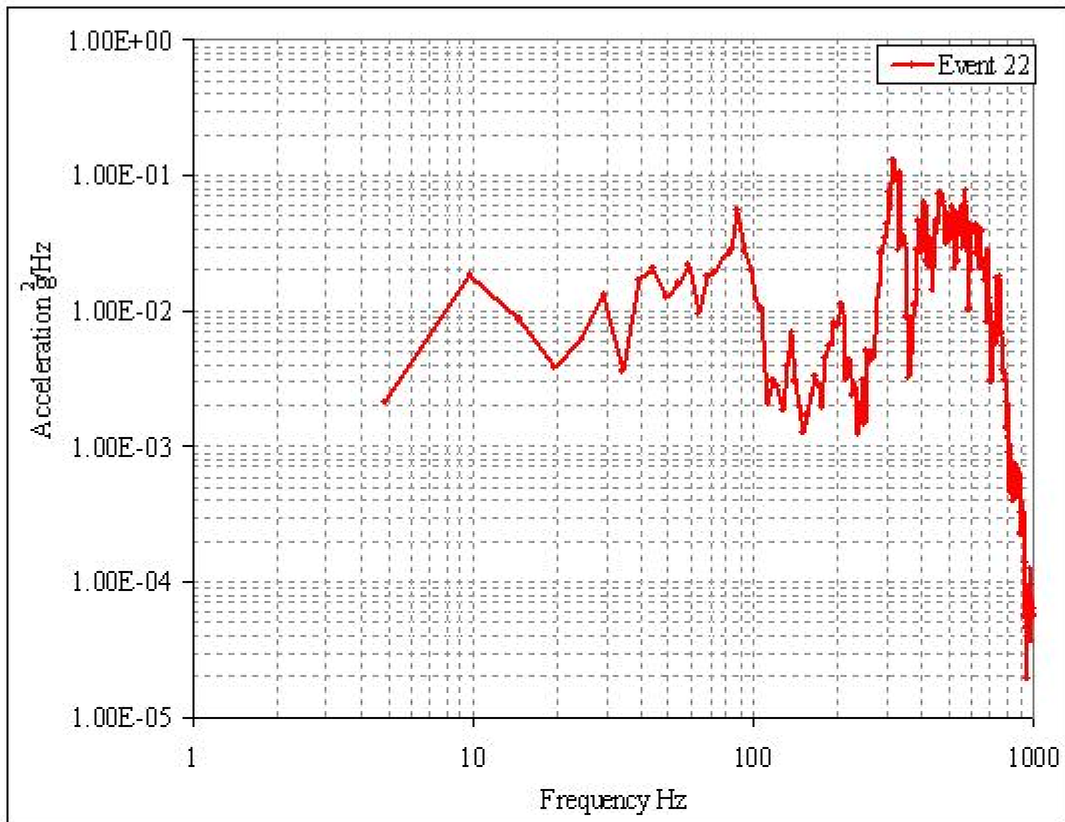

Figure 9: PSD profile of event 22 of vibration isolated flight

4.6.1.2: Acceptance test

The test article is subjected to mechanically generated vibrations during the vibration acceptance-testing phase before each flight of the SRB. These tests are conducted in all three axis of the circuit card. NASA provided the vibration profile for the test article during the acceptance test. The total time the test article has experienced

acceptance test vibration profile is 900 seconds. Each acceptance test is conducted for 60 seconds. Figure 10 shows the x-axis vibration acceptance PSD profile.

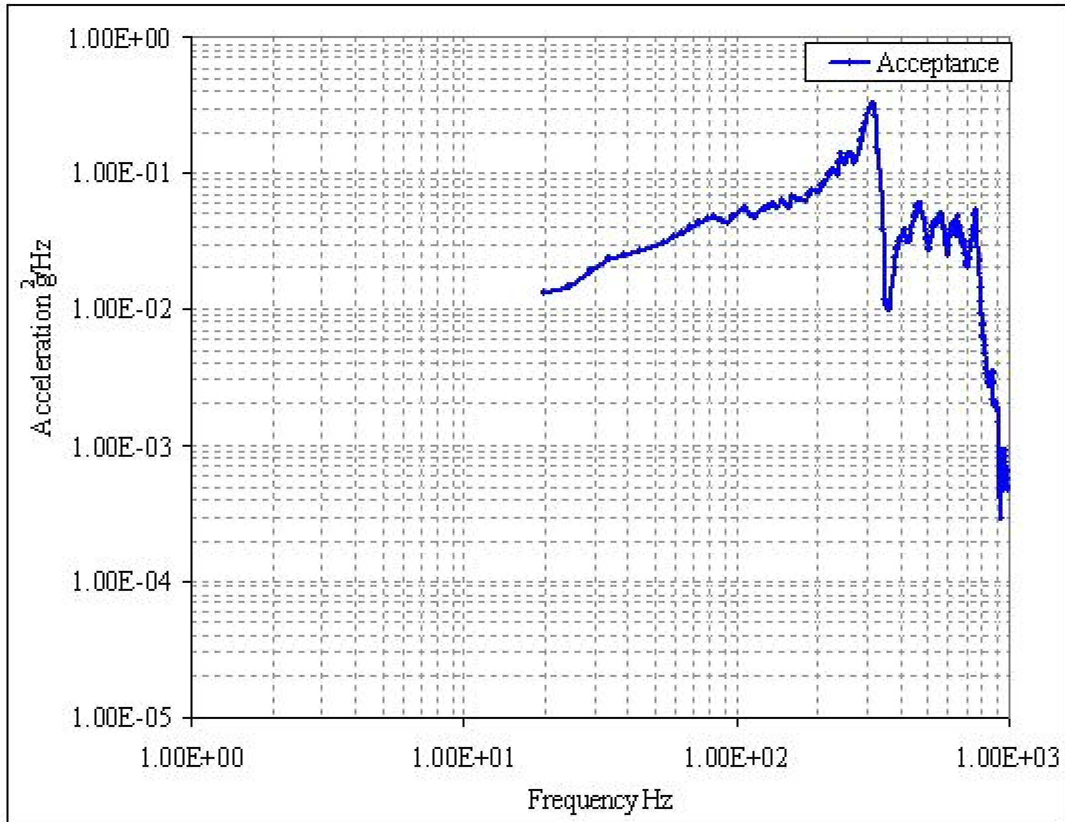

Figure 10: PSD profile of x-axis vibration acceptance test

4.6.1.3: Transportation

The IEA box is transported from storage site to the launch preparation site by road. During transportation the IEA box is placed on vibration and shock absorbers. The vibration to the circuit card is insignificant.

4.6.2: Shock load

On its way down to splash down in the sea the SRBs are considerably slowed down by the opening of the boosters drogue chute and later the main parachutes. Even with this slowing down the SRB experiences a large shock upon water impact. The

shock information provided for the circuit card was available in the form of a plot of acceleration 'g' along the vertical axis and time in the horizontal axis. BD Systems Inc., used finite element modeling software to transform field data into shock profile for the test article. This data was provided for flight STS 26. During this flight the IEA box was provided vibration isolation. The thirty-second event of the SRB flight is the water impact or shock event. The PSD profile for this event was also provided. Figure 11 shows the shock data representation in acceleration versus time.

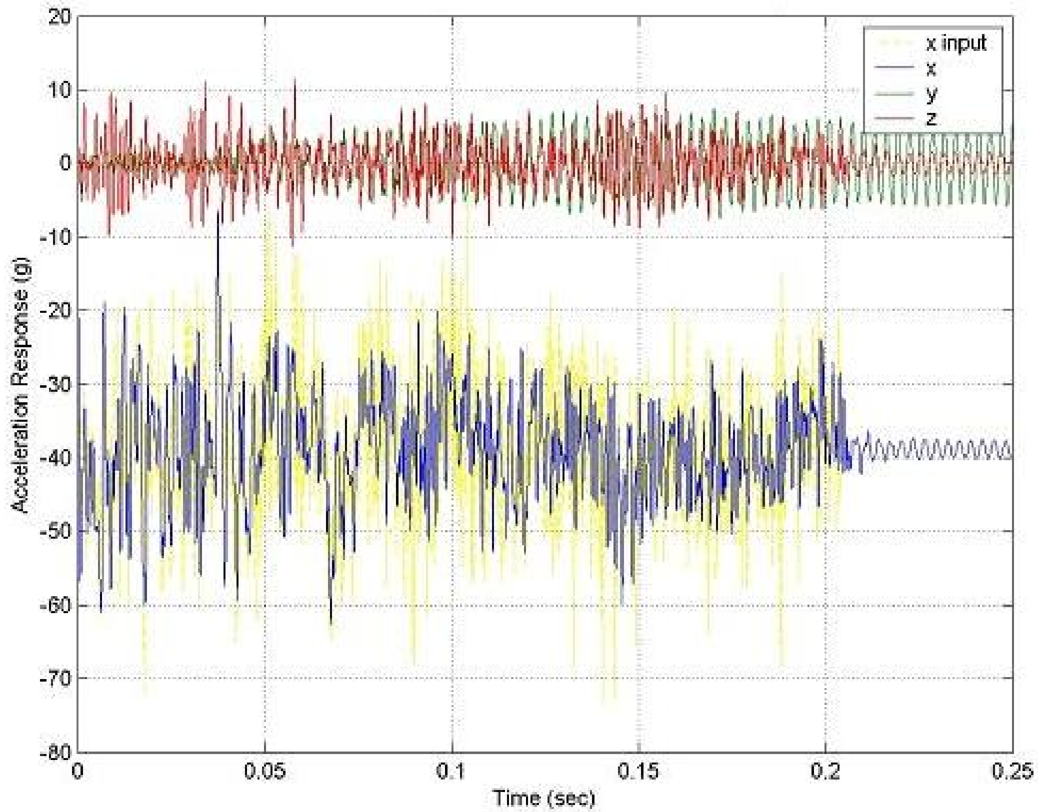

Figure 11: Shock profile

4.6.3: Temperature conditions

The circuit card experiences thermal conditions during pre-launch standby, flight, acceptance tests, recovery and storage.

4.6.3.1: Pre-launch and flight

The pre-launch thermal environment is close to the ambient temperature. The huge mass of the SRB contributes in keeping the temperature close to ambient during the pre-launch operations. The In-Flight temperature rise of the IEA is small. The recorded temperature values show less than 1°C rise in the IEA temperature. During the six minutes of flight the operating temperature of the circuit card is close to 33°C.

4.6.3.2: Acceptance test

Two types of test are conducted on the SRB per flight. They are the ATP or acceptance test and the MCO or burn in test. The "burn in" test is a test with a 5 hour soak time at each set point after which a 4 hour power on functional test is conducted at the ambient, cold, hot, cold, hot and ambient conditions. For the ATP test the soak time at each set point is again 5 hour after which a 4-hour power on functional test is conducted at ambient, cold, hot and ambient conditions. Figure 12 show the temperature cycling profile.

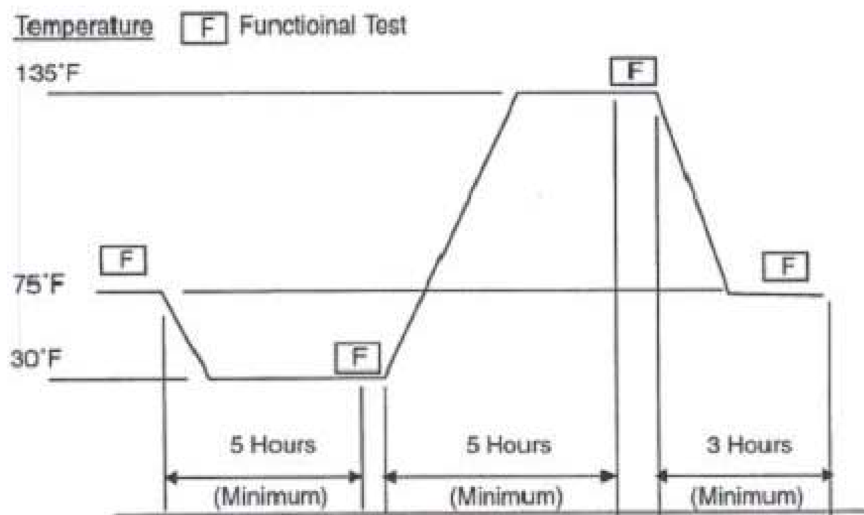

Figure 12: Acceptance test thermal cycling profile

4.6.3.3: Recovery and storage

The SRB is dragged by tow boats from the site of splash down to the port facilities of the launch site. The temperature variation of the IEA during this period is insignificant. The IEA is usually stored indoors and the general temperature ranges between 15.5^{o}C to 26.6^{o}C. The temperature fluctuations are not very significant.

Chapter 5: VIRTUAL REMAINING LIFE ASSESSMENT

A virtual remaining life assessment of the test article was conducted to estimate the number of future missions for which it can be used without failure. The virtual remaining life assessment process consists of the following steps: design capture i.e. generating a software model of the circuit card using the geometry and material data of the board and components, load history characterization i.e. selection of significant life cycle loads and their simplification for analysis, load transformation i.e. application of characterized loads to the software model to obtain suitable responses, damage assessment i.e. estimating the damage to solder joint interconnections of each component, ranking of potential failures i.e. ranking components in descending order of damage accumulation to their solder joint interconnects, and calculation of remaining life of the circuit card. The CalcePWA software was used to calculate the damage accumulated in the solder joint interconnects of the components on the circuit card.

5.1: Design capture

In the design capture step the physical dimensions, functionality, and constitutive elements (e.g., material properties) details of the board and all the components on the board are gathered and documented. This involves identifying the components on the board, matching their respective part types, recording their dimensions and position on the board, recording the board dimensions and recording the board and component material properties into the software program. This data is used by the software to generate a model of the circuit card. For the hardware under study there were a total of 121 components belonging to 7 part types. All components are modeled as insertion

mounted. The board is rectangular, single sided and made of FR4 material. The aluminum frame is modeled as 4 discrete mechanical components attached to the board.

Table 3 shows excerpts of information input for three sample parts. Table 4 shows the input data for the printed wiring board. Figure 13 shows the lead architecture of an axial through-hole component. With this information a software model of the board was generated. Figure 14 shows the software model of the circuit card. The assumptions and simplifications made for the software modeling are detailed in Appendix B.

Table 3: Input data for virtual assessment

BD Systems Part Identification Number	R1	C1	CR1
Data			
Description	Resistor	Capacitor	Diode
Length (mm)	14.2	13.7	6.0
Width (mm)	4.5	4.8	3.4
Thickness (mm)	4.5	4.8	3.4
Material	Composite	Composite	Composite
Weight in grams	0.94	1.14	0.14
Number of I/O	2	2	2
Lead material	Copper	Copper	Copper
Lead length L3 (mm)	3.1	2.95	3.46
Lead radius at first bend (mm)	2	2	2
Lead length L2 (mm)	5.1	5	4.5
Wire Diameter (mm)	0.889	0.6069	0.6069
Location x-center (mm)	102.108	102.108	117.348
Location y-center (mm)	15.494	6.858	33.782

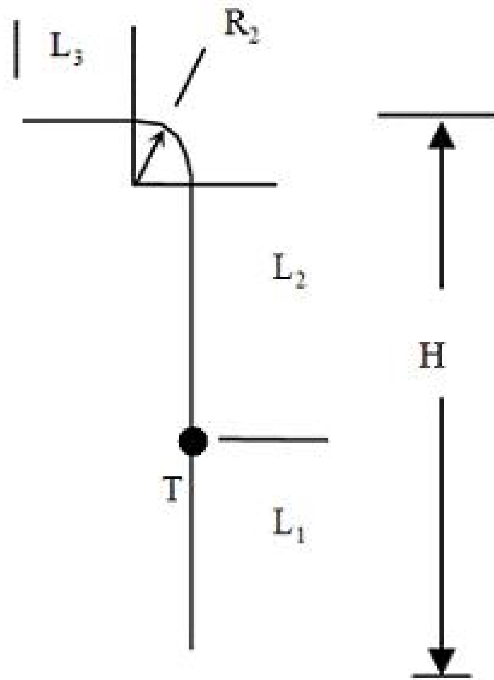

Figure 13: Axial through-hole lead architecture

Table 4: Printed wiring board data

Number of layers	1
Material	FR4
Length (mm)	158.0
Width (mm)	109.3
Thickness (mm)	2.3
Metallization material	Copper
Percent metallization	10

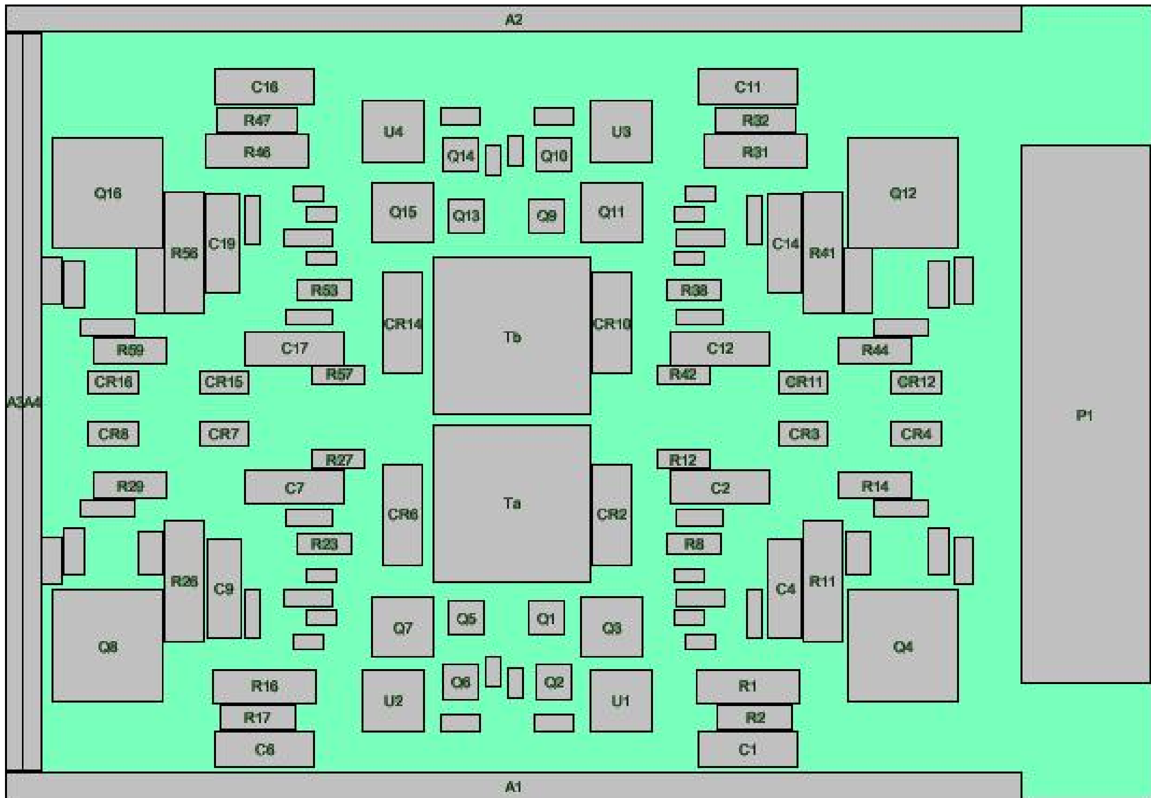

Figure 14: Software model of test article

5.2: Load history characterization

Life cycle load history characterization involves identifying and recording significant life cycle loads and simplifying them for assessment. Field data can not be used as direct inputs to the damage models because of its complexity and hence have to be transformed into a simpler form based on damage models and the capability of the assessment tool. The most significant loads for the hardware under study consists of the vibration acceptance load, the random vibration experienced during flight, the shock upon water impact and the thermal loads during acceptance test. The thermal loads during the pre-flight operations, flight, recover and storage and the vibrations during transportation are minimal and hence not considered for the virtual remaining life assessment. A printed circuit board experiences maximum deflections in its out-of- plane

axis compared to the in-plane axes and therefore only the out-of-plane vibration and shock is considered for virtual remaining life assessment. For the hardware under study the out-of-plane axis is the X-axis.

5.2.1: Vibration load simplification

The entire flight trajectory of the SRB has been divided into thirty-two events. The random vibration data for each event was provided in the form of curve plots with power spectral density, in units of G^2/Hz along the vertical axis and the frequency, in units of Hz along the horizontal axis. There are 206 data points in each curve. Each PSD profile was simplified by selecting a set of PSD data points that covered the acceleration peaks of the original PSD profile thereby accounting for the magnitudes of the accelerations at the resonant frequencies [33]. The total energy of the random vibration is related its root mean square (RMS) value which can be estimated from the area under the curve. This is given by the equation,

$$\sqrt{Area} = \sqrt{G^2 / Hz * Hz} = \sqrt{G^2} = G_{RMS} \quad (1)$$

For the software used to conduct this assessment though the first mode natural frequency is much more important than the RMS value, it is seen that the simplified PSD profile has a higher RMS value than the original profile. The RMS value of the original curve is 4.4 where as the RMS value of the simplified curve is 7.4. Figure 15 shows an original PSD curve and the reduced PSD curve for event 22 of the flight.

This simplification process was conducted for the thirty-one PSD curves for the flight with vibration isolation and the flight without vibration isolation. This same process was used to simplify the preflight vibration acceptance test PSD profile.

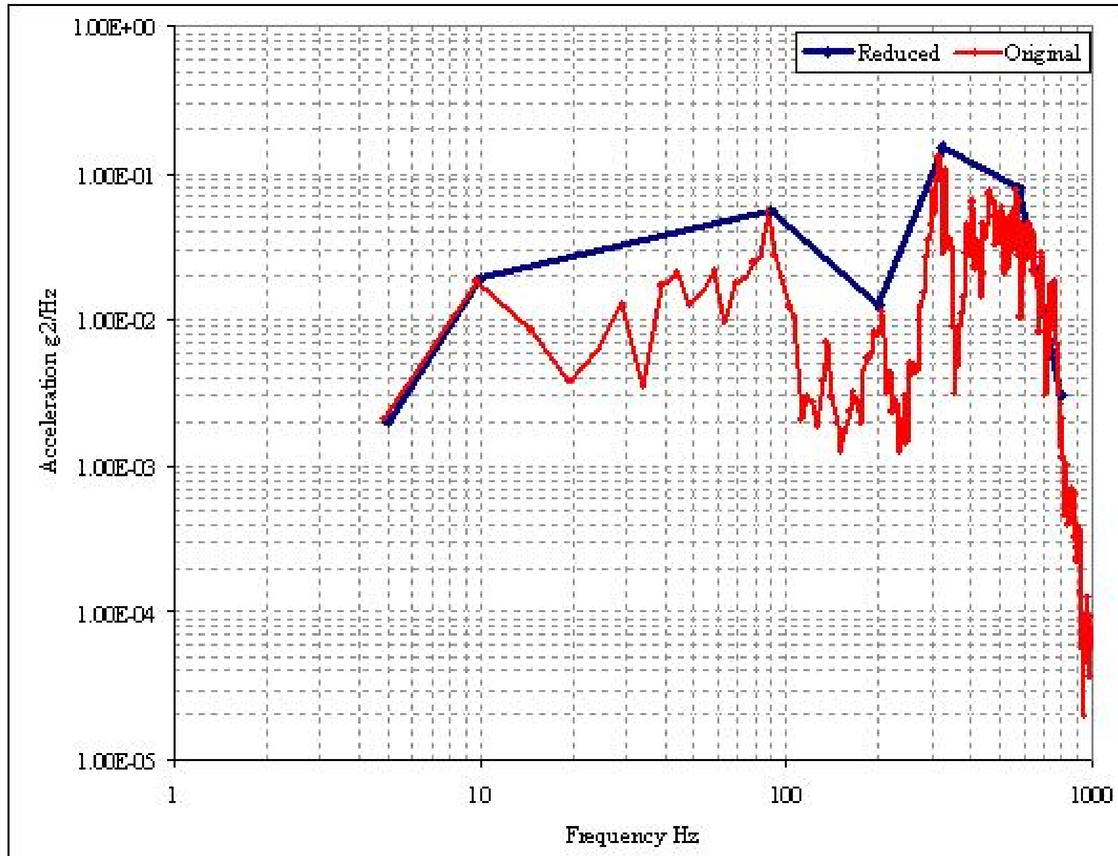

Figure 15: Original and reduced PSD profile for event 22 for vibration isolated flight.

5.2.2: Shock load simplification

The thirty-second (32) event of the SRB flight is the water impact or shock event. The shock data is presented in the form of a plot of acceleration along the vertical axis and time in the horizontal axis. The PSD profile for this event is also available and for analysis the original profile is simplified as mentioned above. The PSD data was not used for modeling the shock since the G_{rms} value of a PSD curve is just a representation of the total energy during a particular random vibration event. It is collection of all the possible frequencies that could be excited during the random vibration event. The shock is an event where a high g load is applied to the printed circuit board. The G_{rms} value of the

PSD is far less than the high g load seen by the board. The shock load was first modeled as an overstress load to estimate whether the components on the circuit card would survive the shock. The components survived the overstress shock load. It is however, understood that the shock event did cause damage to the component interconnects and there is need to estimate that damage and include that in the damage accumulation model. In order to account for the damage caused by the shock during the water impact event the shock load was modeled as a sinusoidal harmonic load. Figure 16 shows the simplification of the shock data.

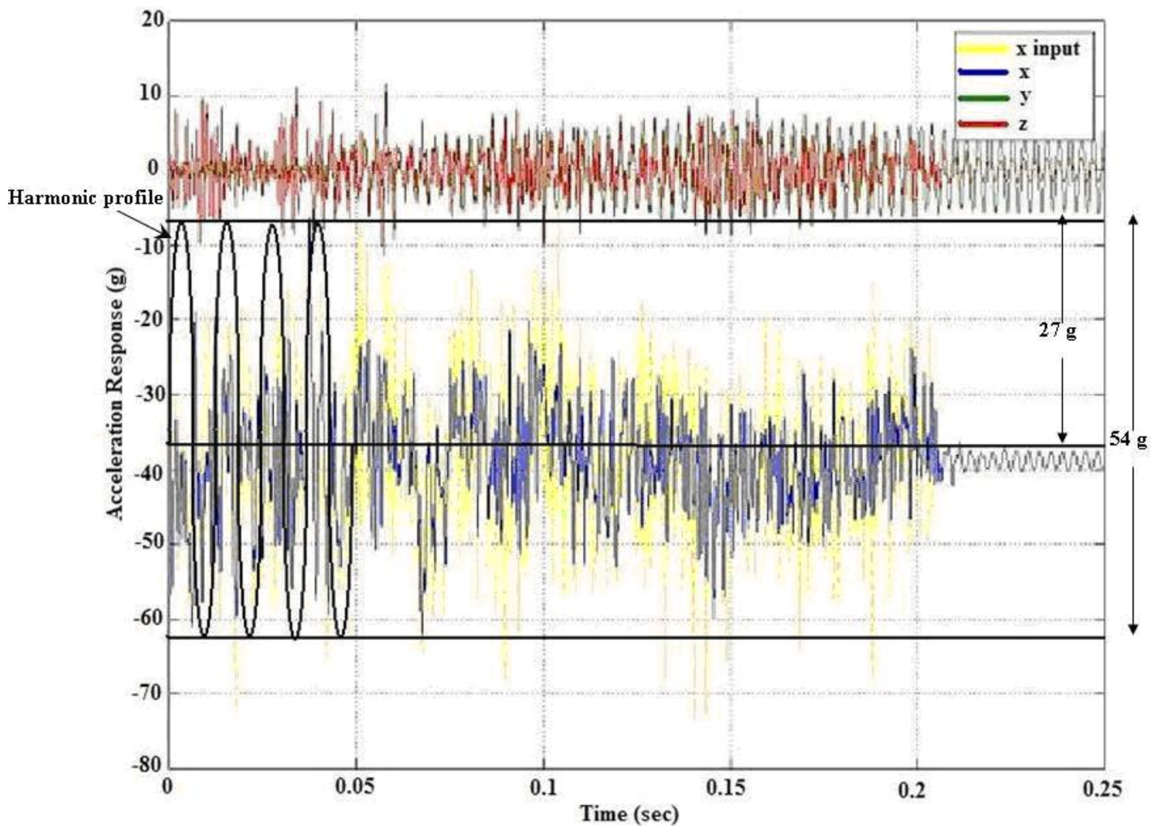

Figure 16: Harmonic approximation of shock data

The maximum and minimum value of the shock load response was extracted from the time history data. The highest peak to peak value was 54 g. A bound was

created on either side of the mean with the limit being 27 g. As a worst-case condition, the shock load due to water impact was approximated as harmonic vibration load with 27g peak acceleration. This harmonic load duration for each flight was 0.2 seconds with a frequency equal to the natural frequency of the test article.

5.2.3: Load transformation

The load transformation step takes life cycle load history and circuit card architecture as input and produces the stress fields (e.g., temperature, displacement, and curvature). The load transformation process utilizes the characterized loading conditions to estimate the effect of these loads on the circuit card. The random vibrations and the shock that the circuit card may experience may cause the displacement of the components on the board or cause the solder joints to fail. Using the software the board curvature due to the vibration and shock loading conditions are estimated.

The fundamental step in calculating the vibration fatigue life of the components mounted on a printed wiring board is the determination of the natural frequencies and the corresponding mode shapes of the board. The dynamic board displacements are inversely proportional to the natural frequencies of the board a slight increase in the natural frequency of the board can reduce the maximum amplitude of the displacements. The vibration, shock and thermal analyses are dependent on the method of mounting the printed circuit board in its casing.

The circuit card was assumed to be wedge locked on three sides along the aluminum frame and simply supported on the fourth side. Figure 17 shows the boundary conditions for the test article. After fixing the mounting conditions of the software model,

the simplified random vibration loading profiles are used as input to the software. The software created a finite element model of the circuit card and on running the vibration analysis gave its natural frequencies and the component and board displacements. The displacement values for each of the thirty one (31) random vibration profiles are calculated. The first natural frequency of the circuit card estimated by the software is 270 Hertz. Figure 18 shows the natural frequencies of the board calculated by the software. Figure 19 shows an example of the board displacement calculated for a random vibration load.

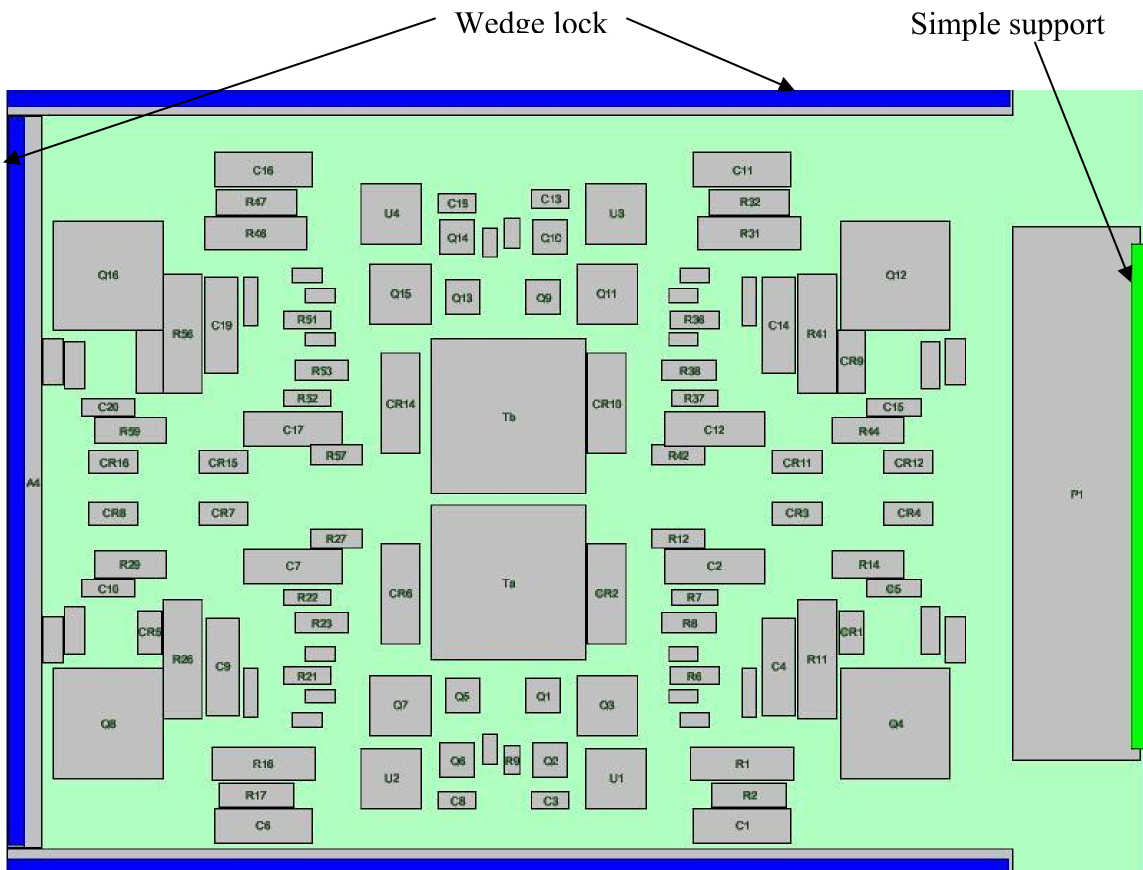

Figure 17: Boundary conditions for the test article

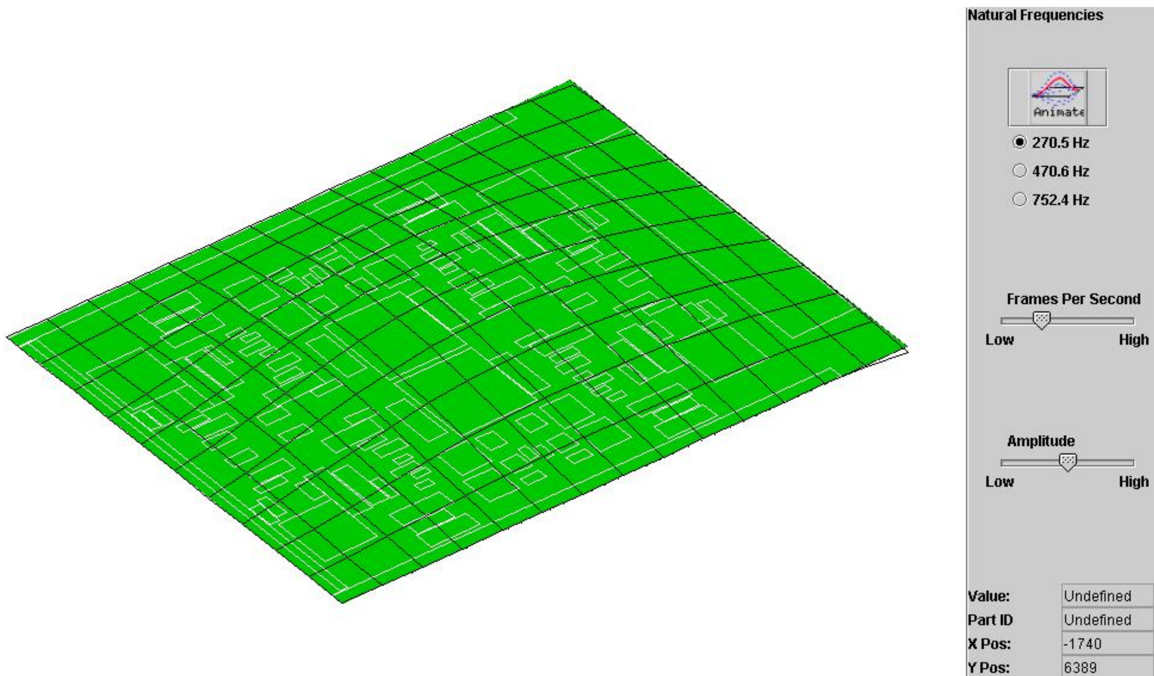

Figure 18: Natural frequencies of test article

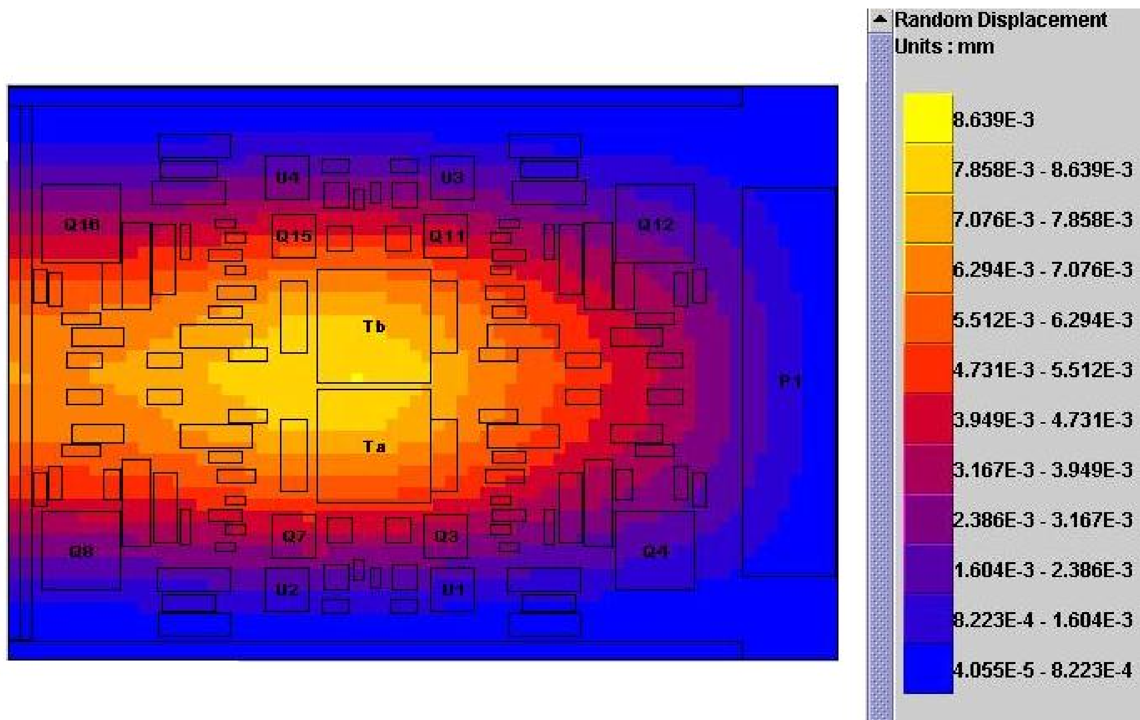

Figure 19: Example of random displacement for test article

The shock loading mechanism considered is fatigue failure due to wear out. The failure model considered is for the interconnect failure due to repeated stress reversals under harmonic load. The shock being considered was modeled as a 27g harmonic vibration load. A finite element model generated by the software was used to estimate the board and component displacements due to the harmonic load.

The thermal acceptance test temperature cycling profile was input to the software generated finite element model to determine the effect of the temperature cycling on the circuit card. The software calculated the damage ratio at each solder joint interconnect due to the temperature cycling load.

5.3: Damage assessment

The damage assessment for the component solder joint interconnect is conducted using the failure analysis feature of the software. The failure analysis module uses a failure model consisting of a stress model and a damage model. Stress models correlate the environmental and operational loads, package architecture, and material properties to stress, strain and energy distributions within the interconnects. A damage model roughly determines the number of cycles to failure. Under vibration loading, the fatigue failure is termed high cycle (greater than 1million cycles) and is modeled by a Basquin high cycle fatigue relation. The model is defined life in terms of cycles to failure as

$$N_f = C(\Delta\sigma)^b \qquad (2)$$

where C and b are material constants and $\Delta\sigma$ is a stress metric that represents the worst case stress in the package to board interconnect due the vibration loading condition. For the assessment of life under temperature excursions, the expected life is expressed in

cycles for failure and is characterized as a low cycle fatigue. In this assessment, a Manson-Coffin relation is assumed.

$$N_f = \frac{1}{2}\left(\frac{\Delta\gamma}{2\varepsilon_f}\right)^{\frac{1}{c}} \tag{3}$$

where c and ε_f are material properties and $\Delta\gamma$ is the stress metric for the interconnect due to the defined temperature cycle. In the damage assessment step, the damage for each part is defined in terms of damage ratio (DR), which is the ratio of the number of cycles applied to the number of cycles it can survive.

$$D_i = \frac{N_i^{applied}}{N_i^{available}} \tag{4}$$

When considering multiple stress segments, the total damage index is defined using the Miner's rule.

$$D_{total} = \sum_i \frac{N_i^{applied}}{N_i^{available}} \tag{5}$$

For the test article the damage ratio for each component's interconnects due to each random vibration load, shock load and temperature cycling load was estimated. The total damage ratio for each component's interconnects is the sum of the damage ratios due to random vibration, shock and temperature cycling. This total damage ratio due to the past life cycle loads is termed as damage to date (D_{TD}). Table 2 shows the summary of the past loading history. It was assumed that one future life cycle would consist of one vibration isolated flight, two exposures to the acceptance level vibration, and three

temperature acceptance tests. The load profiles were assumed to be same as the past load profiles. Re-applying the random vibration, shock and temperature cycling loads to software model for one future life cycle the expected total damage per mission (D_M) was estimated. Table 5 shows the assumed future loading per mission.

Table 5: Loads per future mission

Life Cycle Environment	Load Type	Exposure per mission
Flight (Vibration Isolated)	Random vibration and Shock	1
Vibration Acceptance Test	Random vibration	2
Thermal Acceptance Test	Temperature cycling	3

5.4: Ranking of potential failures

The software calculates the total damage ratio for each component's solder joint interconnects. The components are ranked based on the damage to their interconnects. The component with highest damage to its interconnects is ranked number 1 and the component with least damage is ranked the last. This helps in identifying the potential failure spots on the printed circuit board under life cycle loads. The 121 components of the test article were also ranked based on the respective damage ratios.

5.5: Calculating remaining life

The failure criterion (D_f) for a solder joint interconnect is a total damage ratio equal to 1. The remaining life of a printed circuit board is determined by finding the time under the applied life cycle load conditions at which the worst-case damage ratio for any interconnect becomes equal to 1. From the damage to date and the expected damage per future life cycle the remaining life of the printed circuit board is estimated. For the circuit

card the number of survivable missions (N_M) is estimated from the damage to date, the failure criteria, and the expected damage per mission, as:

$$N_M = \frac{(D_f - D_{TD})}{D_M} \tag{6}$$

The estimate of survivable missions for the circuit card's top ten components with the worst-case damage ratio is presented in Table 6.

Table 6: Estimate of survivable missions

Failure Site	D_{TD}	D_M	N_M
P1 (Connector)-interconnect-open	0.25	3.18E-02	22
CR14 (Diode)-interconnect-open	0.16	2.08E-02	40
CR6 (Diode)-interconnect-open	0.13	1.64E-02	52
CR10 (Diode)-interconnect-open	0.12	1.52E-02	57
Tb (Transformer)-interconnect-open	0.10	1.31E-02	68
CR2 (Diode)-interconnect-open	0.09	1.20E-02	75
Ta (Transformer)-interconnect-open	0.09	1.18E-02	76
Q15 (Transistor)-interconnect-open	0.014	1.59E-03	619
Q11 (Transistor)-interconnect-open	0.014	1.58E-03	621
Q3 (Transistor)-interconnect-open	0.014	1.58E-03	623

The connector on the test article is secured to the board with screws on both ends. Therefore the connector failure was ignored and the diode survivable missions' value was used as a baseline for predicting the remaining life of the test article. It was estimated that the test article could survive forty (40) more launch missions.

Chapter 6: LIFE TESTING FOR REMAINING LIFE ASSESSMENT

Based on the virtual remaining life assessment a life test was planned. It was determined that the random vibrations during pre flight acceptance test and during the actual flight and the shock on water impact were the most damaging loading conditions that the test article experiences. The temperature changes during flight and during storage, transportation and acceptance test were determined to cause insignificant damage to the components on the test article. Thus, for this life testing, the test article was subjected to only random vibration and shock loads.

6.1: Test loads

The life test involved simulating the vibration and shock loads representative of the actual operating conditions of the test article. Figure 20 shows the vibration time history recorded during one flight of the SRB. The vibration time history was modeled as thirty-two (32) discrete events from pre launch stage to the splash down into the sea and the Power Spectral Density (PSD) profile representing the vibration load for each event was generated. The even numbered sections indicate the major events. The transition events are odd numbered and are not indicated in the figure. The vibration history was grouped into three categories. The low PSD segments (events 1-17 and 26-31) encompass the launch vibrations, separation shock, post separation vibration, initial re-entry vibrations, parachute deployment shock and post parachute deployment vibrations. The high PSD segments (event 18-25) comprise o the vibrations experienced during the re-entry phase of the flight. The thirty-second (32) event is the shock due to water impact.

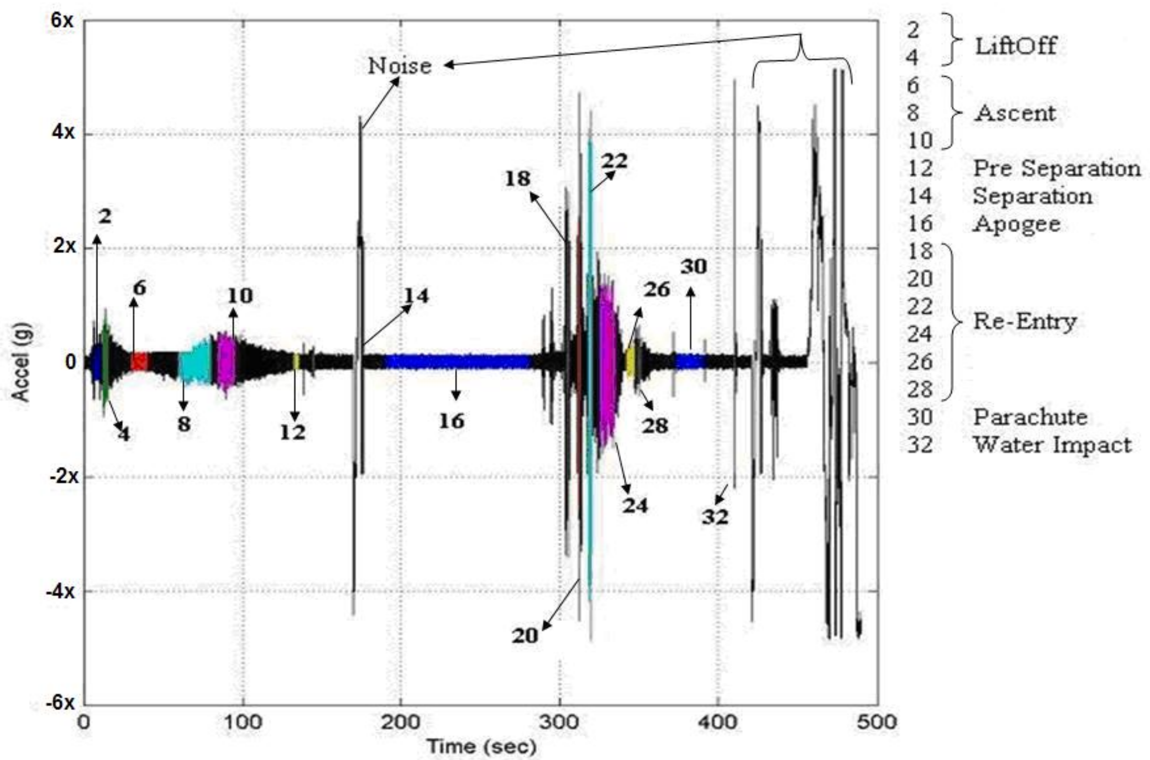

Figure 20: Vibration time history

The low PSD section profile was estimated by calculating the time weighted average PSD value at each frequency point for the low PSD events. A plot of the time averaged PSD versus the frequency was developed and a profile enveloping the time-averaged profile was generated such that the profile could be reproduced on the vibration table. The life test low PSD profiles for the X, Y and Z-axis vibration were generated using this process. Figure 21 shows the estimated life test low PSD profile X-axis input to the vibration table.

Frequencies where the PSD value peaked were used to calculate the high PSD profile. The high PSD section profile was estimated by selecting the maximum PSD value at each frequency point for the first thirty-one (31) events. The thirty-second event is the shock event and hence excluded from the calculation. By combining all the

maximum PSD values at each frequency a PSD profile was generated. The high PSD profile thus generated was simplified for the vibration table input, by selecting a set of PSD data points that covered the acceleration peaks of the profile [33].

The shock spectrum profile generated by NASA was used as the shock load during life testing. The vibration acceptance load profile provided by NASA was simplified by selecting a set of PSD data points that covered the acceleration peaks of the profile around the actual PSD profile and this simplified profile was used as input to the vibration table. The low PSD, high PSD, shock profile and the vibration acceptance PSD profile were developed for the X, Y and Z axis of the test article.

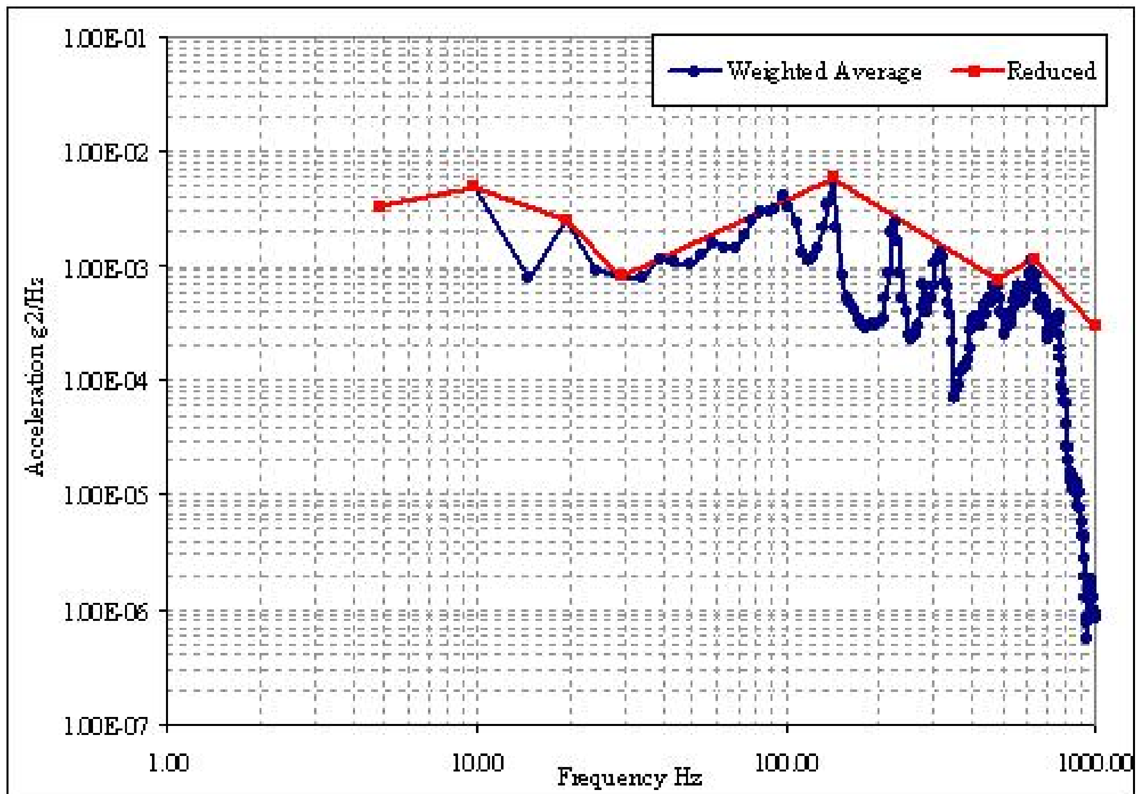

Figure 21: Low PSD

6.2: Test cycle and sequence

In an actual mission cycle of the test article, it experiences damaging loads due to random vibrations during the acceptance test and flight and due to shock upon water impact. To conduct a life test it is necessary to simulate the actual operating conditions. Practically it is difficult to continuously simulate the thirty-one random vibration conditions on a vibration machine. This is because of the ramp up time and the ramp down time involved in generating the programmed profile and because the machine has to be reprogrammed to generate the next vibration profile. In order to overcome this difficulty it was decided to generate a single power spectral density (PSD) profile from the thirty-one different PSD profiles. First the events for which the PSD levels are low were identified and grouped together. Then the high PSD events were grouped together. A table of the low and high PSD events is given in Appendix E.

To recreate the most damaging environmental conditions for the test article during the life test, it was to be subjected to low vibration, high vibration, shock and acceptance test vibration loads. The sequence of loads was acceptance test vibration, low vibration, high vibration and then shock load. This sequence of loading was to be conducted in all three axis of motion. The one complete test cycle was defined as: a test sequence in the x (out of plane) axis, followed by one in the y (in plane) axis, followed by one in the z (second in plane) axis. One complete test cycle is equivalent to one flight mission of the test article. Figure 22 shows the schematic of the test loading sequence. Figure 23 shows a schematic of one test cycle or one equivalent mission.

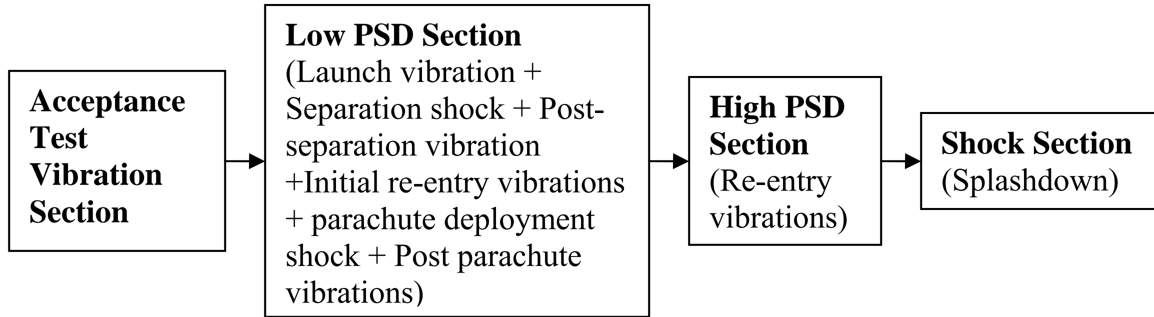

Figure 22: One life test loading sequence

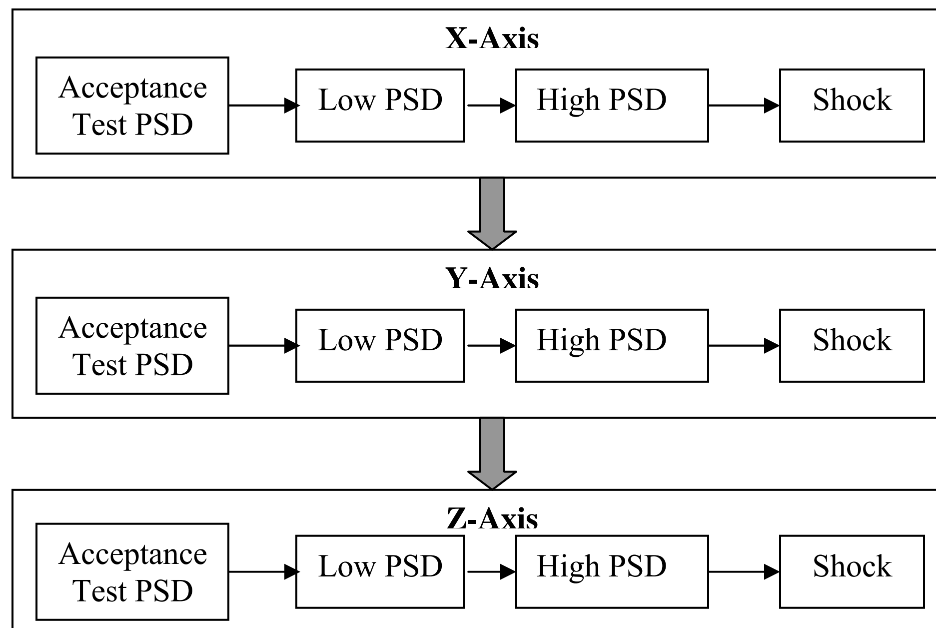

Figure 23: One equivalent mission

6.3: Test duration

Each of the above mentioned life test loading sequence was executed for a specific period of time. In normal operation the pre flight acceptance test is conducted for 60 seconds. During an actual flight the combined duration of the low PSD level events is 400.9 seconds and the combined duration for the high PSD level events of the flight is 32.3 seconds. The shock event occurs for 0.2 sec. For the life test the high vibration loading levels was estimated by taking the maximum PSD value for each frequency level

for thirty-one events. The time duration for the life test high vibration sequence cannot be the same as the total flight time. The application time for the high vibration life test segments was determined by equating the damage induced by the proposed test levels to the damage sustained in use [66]. The mathematical equation for relating the test times is based on the assumption that the time to failure of the system can be modeled as a power law [56]. Specifically,

$$N = C(\Delta\sigma)^b \tag{7}$$

For vibration-induced damage it is generally assumed that the stress at the failure site is directly proportional to the square root of PSD level at the natural frequency of the system. Therefore,

$$\frac{N_{test}}{N_{use}} = \left(\frac{\Delta\sigma_{test}}{\Delta\sigma_{use}}\right)^b = \left(\frac{PSD_{test}}{PSD_{use}}\right)^{b/2} = \frac{t_{test}}{t_{use}} \tag{8}$$

For vibration, b has been reported to be between -4 to -6.4 [82]

Using the equation 8, the duration for which the high PSD section is to be applied during the life testing was estimated. The vibration acceptance test section was applied for the same duration as in the actual operation. Since the high vibration levels were estimated from the maximum PSD values at each frequency using equation 8, the life test time duration was reduced. Using a value of b = -6.4 and summing over all thirty-one events the total equivalent test time for the High PSD level is approximately 0.5 sec. For the low vibration level since the profile was generated by time averaging the PSD valued of the low vibration events the life test time duration was kept similar to that in actual

operation. The life test shock loading duration was kept similar to that during actual operation. Table 7 shows the equivalent times for the life test for each section.

Table 7: Test cycle sections: corresponding loads and durations

Test cycle section	**Load condition**	**Actual Time (sec)**	**Test Time (seconds)**
Acceptance test vibration	Random vibration (acceptance test PSD levels)	60	60
Low PSD	Time averaged PSD levels	400.9	400
High PSD	High PSD levels	32.3	0.5
Shock	Shock spectrum	0.2	0.2

During the life test the test article will be affixed in a fixture and the fixture is bolted on top of a vibration shaker table, which generates the random vibration loads for testing. Taking into consideration the approximate time for bolting and unbolting the fixture assembly and the approximate time for cycling PSD levels, the time for testing the circuit card for one mission cycle would be approximately 1 hour. This translates in to 40 hours or 5 days of testing to achieve 40 missions. This time does not include the optical inspection every 20 missions and the time for the electrical and mechanical set up after each optical test. Also not included is the time required for conducting the fixture test, the time for analyzing the data collected during the test, and time required for modification of loading levels if necessary. Considering all the abovementioned durations, the life test would take approximately 8 days to be completed. In order to save testing time, it was decided to apply an equivalent of ten (10) missions on each axis before rotation. It is assumed that linear superposition is valid. Appling the equivalent of 10 equivalent

missions would reduce the testing time considerably to approximately two days. Table 8 shows the test times with ten equivalent missions.

Table 8: Test durations with 10 equivalent missions in each axis

Test cycle section	**Load condition**	**Actual Use time (sec)**	**Test Time (sec)**	**Number of Equivalent Missions**	**Test Time (sec)**
Acceptance test vibration	Random vibration (acceptance test PSD levels)	60	60	10	300
Low PSD	Time averaged PSD levels	400.9	400	10	2000
High PSD	High PSD levels	32.3	0.5 to 1	10	10
Shock	Shock spectrum	0.2	0.2	10	2

6.4: Test fixture

The IEA box is a rectangular metal box partitioned longitudinally into two by a metal wall. Circuit cards are placed vertically downward on either side of the partition. Each circuit card is held in place inside the IEA box by sliding it through a pair of birtcher guides. The card connector mates with a pin connector attached to the IEA box on one of the vertical end. A metal covering covers the other side of the IEA box. For life testing the test fixture was designed such that the boundary conditions of the circuit card are replicated during the testing.

The test set up had two parts: the fixture and the interface plate. The fixture is made out of a 7 inch X 6 inch X 3 inch block of 6061 grade aluminum. It has a 2-inch depth cut 0.5 inch inside along the length and 0.22 inch inside along one of the sides.

Four 3/8-inch holes with center-to-center distance of 3 inches were drilled in the bottom of the fixture. The interface plate was designed with a multiple use perspective. This interface plate was designed to fit the hole pattern of the vibration machines at University of Maryland and the NASA's testing facility. The interface plate was made from a 10-inch X 10 inch X 2 inch 6061 grade aluminum plate. In this plate 4 holes of ½ inch diameter with 8.5 inch center-to-center spacing were drilled. Next four 3/8-inch holes with center-to-center spacing of 3 inch were drilled, to a depth of 1 inch. Steel sinks were inserted in to theses holes. These holes were then tapped for 3/8-inch threads. Figure 39, Figure 40 and Figure 41 in Appendix D show the schematic diagrams of the test fixture and the interface plate.

For the experiment, the interface plate was first affixed on to the adapter plate of the vibration machine using ½ inch bolts. The ½ inch holes with 8.5 inches center-to-center spacing was used for this purpose. The fixture is secured on top of the interface plate using 3/8-inch bolts. The aluminum birtcher guides were secured on to the fixture using small screws. The connector with the electrical wires was pulled in through the opening in the third side of the fixture and screwed to the fixture on that side. Finally the test article is slid in to position through the aluminum guides.

6.5: Test monitoring

During the life tests the vibration and shock input were monitored with accelerometers and strain gauges. Two three-directional (3D) accelerometers were be used for measuring the accelerations experienced by the test article. One of the accelerometers was glued to the board surface and the other was glued onto the top of the connector. Prior to gluing the accelerometer onto the board the conformal coating and the

solder mask was removed. A two-step process of initial rough cleaning and then a fine cleaning was necessary for preparing the gluing site. The two accelerometers fixed on to the circuit card measured its dynamic response. The outputs of these accelerometers were matched with the input to estimate the corrections to be done to the inputs. Figure 24 shows the placement of accelerometers on the test article.

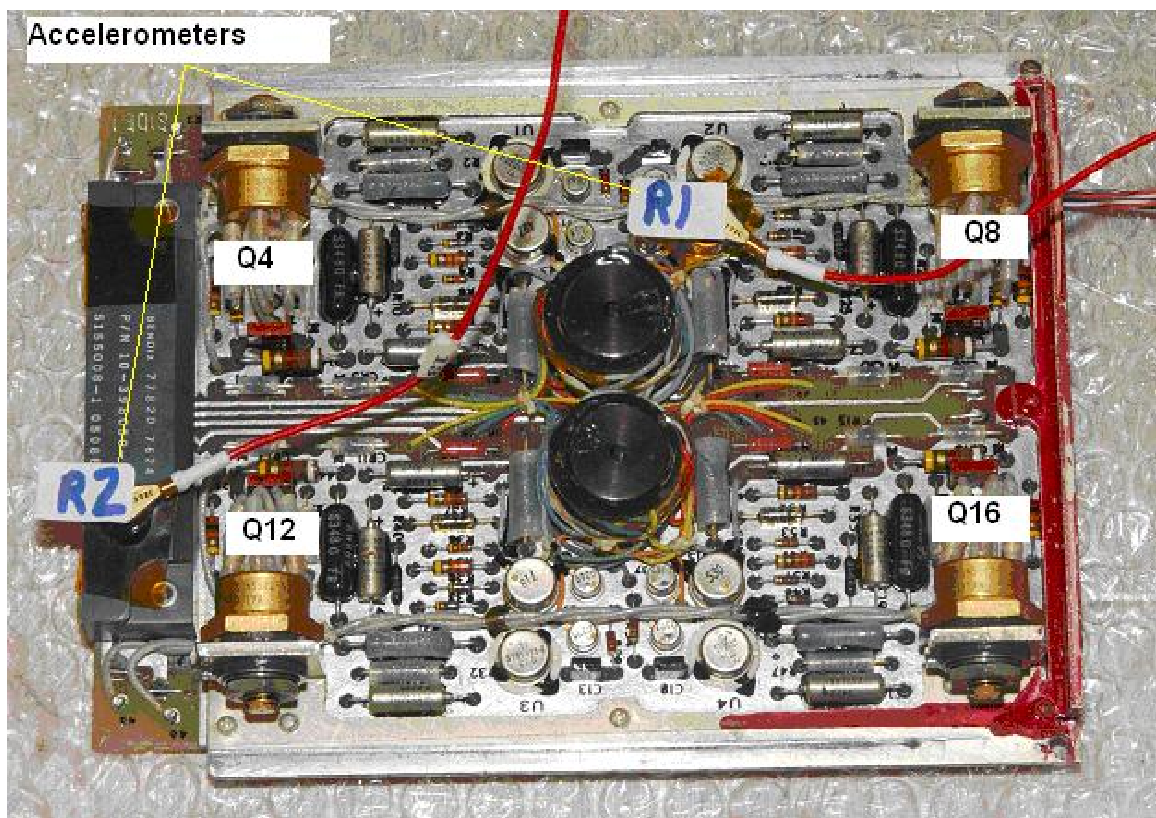

Figure 24: Accelerometer placement on the test article

Piezoelectric strain gauges were used to measure the card curvature. The gauges were place on the backside of the test article. These were connected to a data logger for data recording. Figure 25 shows the placement of the strain gauges on the test article. Personnel from one of NASA's contractors implemented the electrical set up for monitoring the test article during mechanical testing. The electrical input was provided

through the card connector which mates with the corresponding connector on the test article. The test article was powered up and a stimulus was applied to the 5 VDC and 28VDC control inputs. The stimulus was a low frequency square wave to simulate continuous switching commands. By continuously commanding the switches on and off all aspects of the cards electrical operation could be seen and monitored.

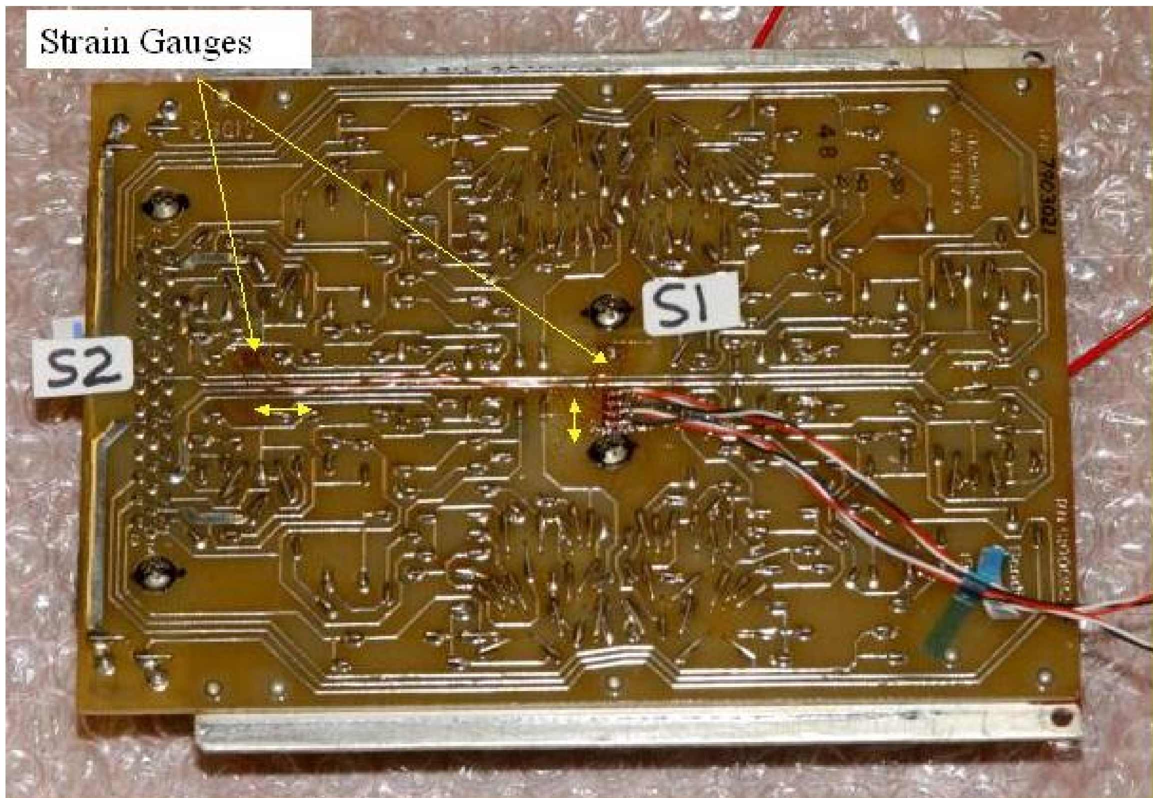

Figure 25: Strain gauge placement on the test article

6.6: Tests

The life test for assessing the remaining life of the test article was planned to have four stages. The first stage was the characterization of the test fixture. Initial fixture characterization was to assess the goodness of fit of the fixture and interface plate. The

ruggedness of the assembly and the resonance frequencies of the fixture assembly were verified.

The second stage was a validation of the testing loads to be used. The objective of this phase was to observe how the test article would react under actual testing. A sample engineering card, which is physically and functionally identical to the test article, was used for testing the appropriateness of the random vibration PSD levels and the shock levels specified for the life test and to check whether the card will sustain the loading conditions.

The third stage of testing was optical inspection of the test article. Before the beginning of the life test the test article was subjected to optical inspection to document the initial condition of the card before entering the test. The optical inspection was to be continued simultaneously with the life test.

The fourth stage of the life test involved the actual testing of the test article. In this stage, the test article was subjected to a series of vibration and shock load levels as defined in the previous subsection. The test article was connected to a power source and fully functional during the test.

Two accelerometers were attached to the front surface of the test article to monitor the dynamic its response to the input vibrations. Two strain gauges were affixed on the backside of the test article to measure the board curvature. For the life testing, the interface plate was first affixed on to the adapter plate of the vibration machine. The fixture was secured on top of the interface plate. The aluminum birtcher guides were secured on to the fixture. The connector with the electrical wires is affixed on the third

side of the fixture. Finally the test article was slid in to position through the aluminum guides. The test article was then subjected to the predetermined test loads for a predetermined duration in the predetermined sequence. Detailed procedure for each life test stage is listed in Appendix G. Figure 26 shows the mock test set up.

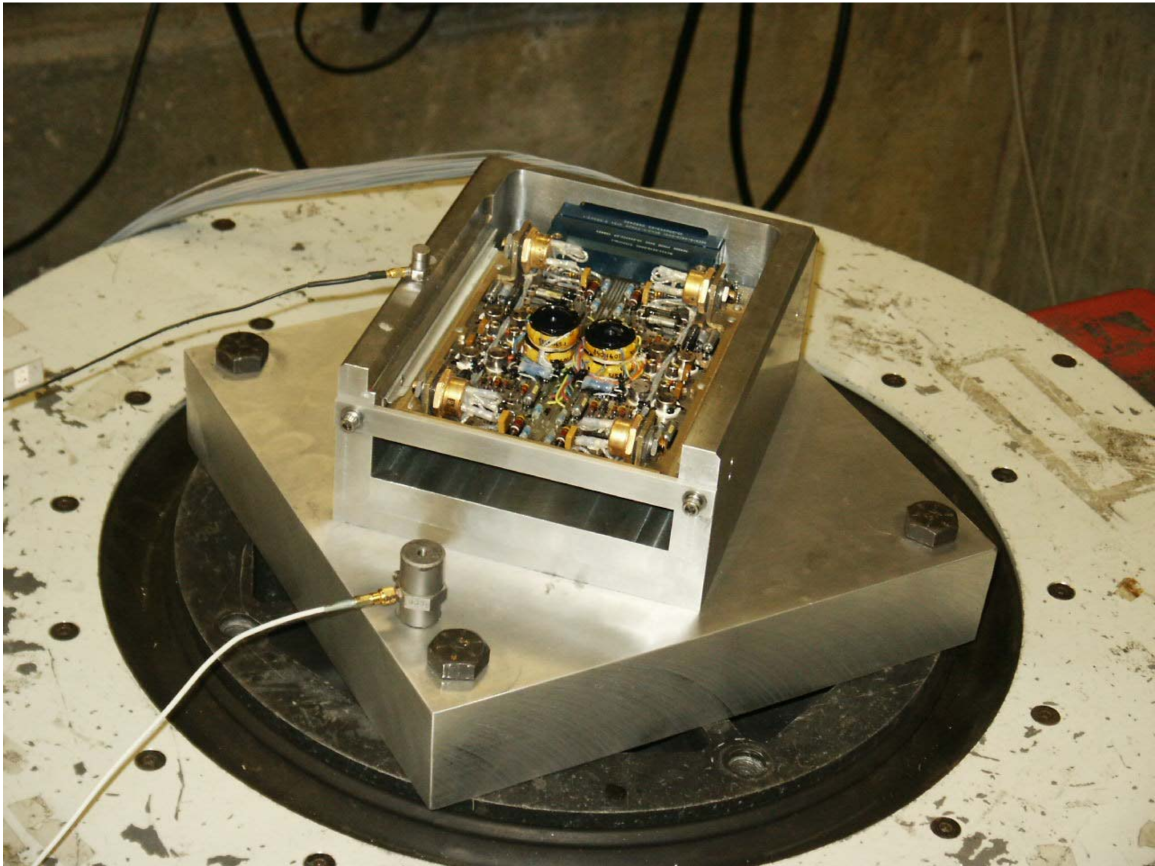

Figure 26: Mock test set up

6.7: Test results

The fixture characterization test conducted in the vibrations laboratory at the University of Maryland yielded the experimental values of natural frequency of the fixture and the test article. The lowest resonance of the fixture and interface plate assembly was observed as 2160 Hz. Figure 27 shows the graphical representation output of the signal analyzer for the fixture. The resonance of the circuit card was also estimated

during this test. The test article's first three resonances were observed in the range of 260 Hz, 480 Hz and 820 Hz. Table 9 gives the results of the resonance test. Figure 28 shows the graphical representation output of the signal analyzer for the test article. With the ruggedness test the fixture was found to be able to securely hold the flight and engineering cards. Vibration tests on the fixture demonstrated its ruggedness and suitability for the planned tests.

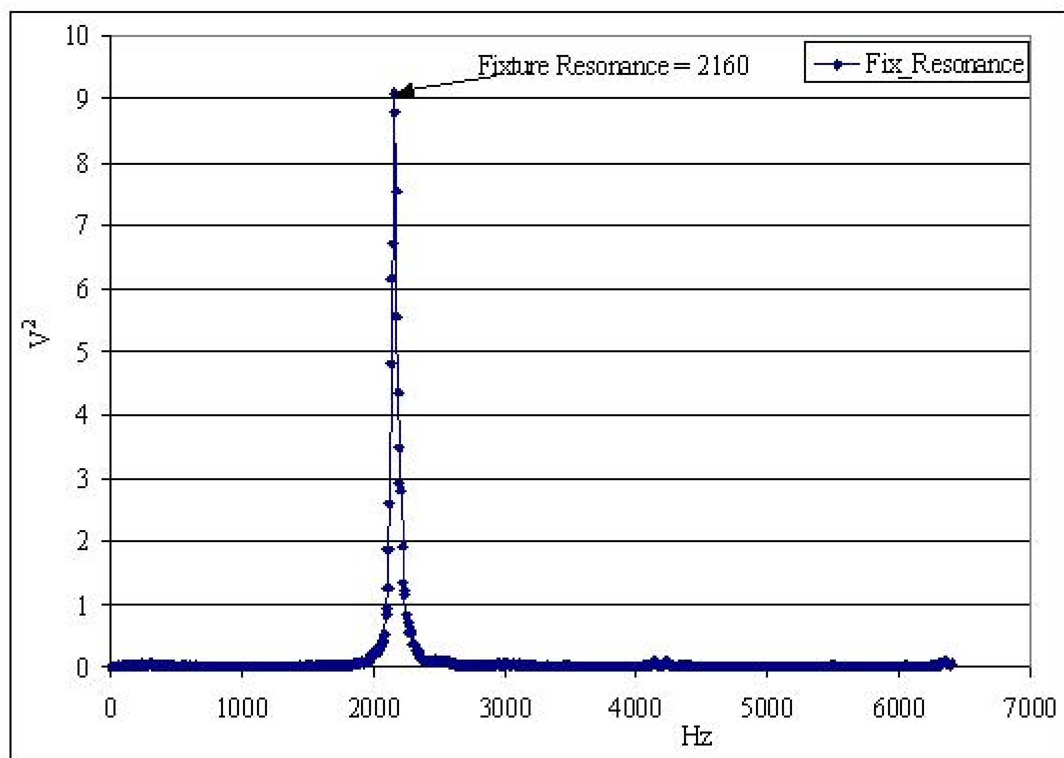

Figure 27: Fixture resonance

Table 9: Resonance test results

Item	**Natural frequency**
Fixture and Interface plate assembly	2160 Hz
Engineering card	260 Hz (1st NF)
Engineering card	480Hz (2nd NF)
Engineering card	820 Hz (3rd NF)

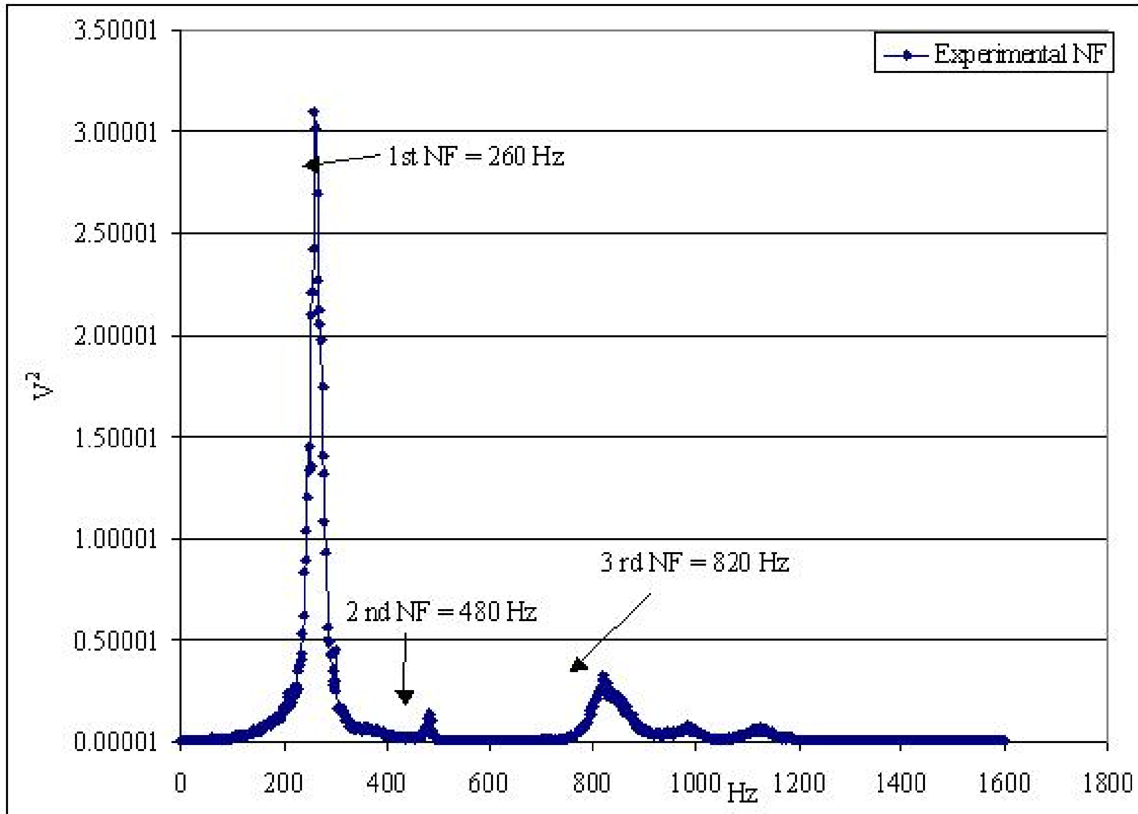

Figure 28: Experimental natural frequencies of the circuit card

For the second stage of testing as a reference point, the card resonance test was re-run in the Vibration Laboratory at Marshall Space Flight Center (MSFC), Huntsville, AL, using the fixture and the sample engineering card with a swept sine input in the out-of-plane direction. Under these conditions, the card resonance frequencies were determined to be 310, 500, 665, 831, 1003, and 1098 Hz, which are within 20% of those measured at UMD. Because the card frequency varies as a function of load amplitude and since these resonances were measured using a slowly varying sine input the natural frequencies observed are ok. In the third stage the test article was inspected visually for signs of cracking at the solder joint interconnects and on the component leads. No cracks were found in either site.

The test article functioned to specifications when subjected to 10 test load sequences in the out-of-plane (X) axis. During the sixth (6) acceptance test vibration level loading sequence, in the Y-axis, an aluminum bracket structure, on which a transistor was mounted, broke off from the aluminum frame affixed on the test article. Figure 29 shows the broken bracket. Two of the remaining three brackets developed cracks while the third one did not show any signs of damage. The electrical functioning of the test article was not impeded by the bracket failure. At this stage the life test was stopped. Experimentally the first mode frequency of the unbroken bracket was determined as 600Hz and that of a cracked bracket was 400Hz.

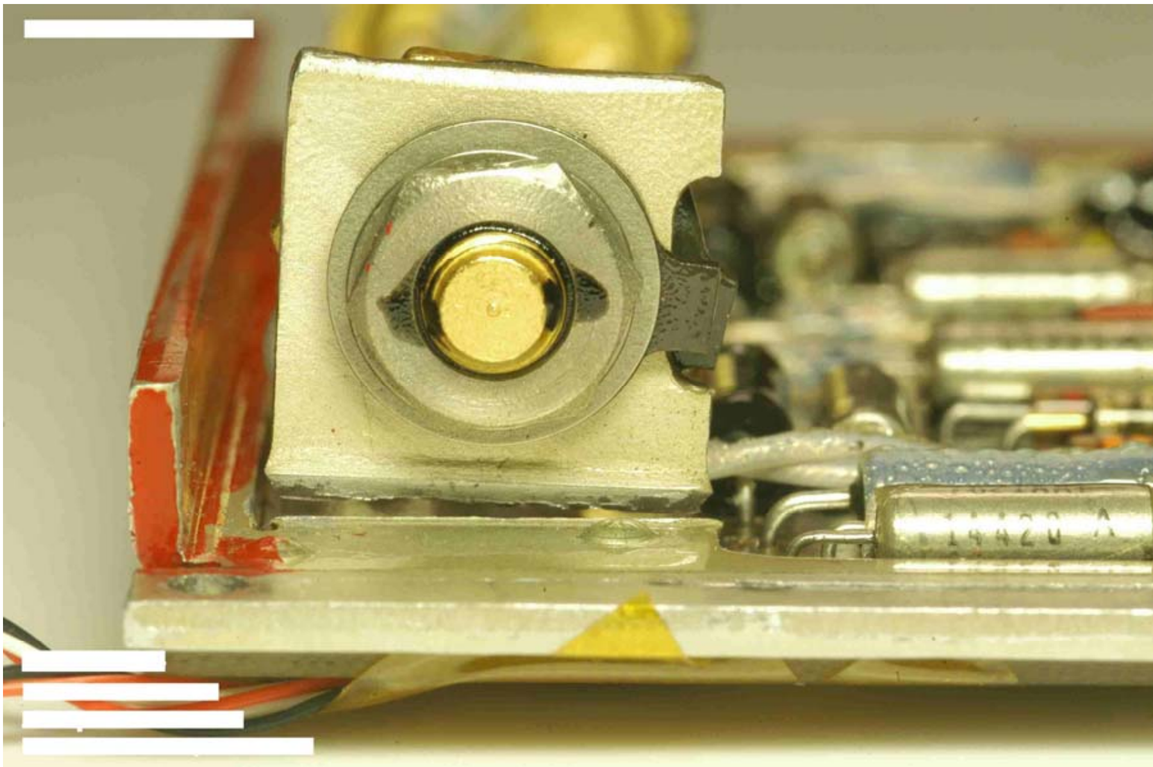

Figure 29: Failed aluminum bracket

Chapter 7: BRACKET FAILURE ASSESSMENT

Appendix H shows the schematic diagram of the one-piece aluminum frame affixed on the circuit card. The aluminum frame is riveted to the circuit card at 11 locations. The frame material is 1100 H14 aluminum. The structure is a one-piece C shaped cast, aluminum frame that is bent at four locations to form the bracket support for the four transistors. The transistors are mounted approximately at the center of the section perpendicular to the board. The transistors are screwed on to the brackets. The weight of each transistor is 13 grams. Table 10 gives the material properties of 1100 H14 aluminum

Table 10: Material properties of 1100 H14 aluminum [86]

Material Property	Value
Ultimate tensile strength (Pa)	1.24×10^{8}
Yield strength (Pa)	1.17×10^{8}
Ultimate shearing strength (Pa)	7.58×10^{7}
Endurance limit (Pa)	4.83×10^{7}
Modulus of elasticity (Pa)	6.89×10^{10}
Density (kg/m^3)	2700

7.1: Analytical estimation of natural frequency

The fracture occurred at the location where the aluminum frame is bent 90° to form the bracket. The individual bracket has been considered as a cantilever beam with a fixed base and a uniform load, for calculating the natural frequency of the bracket. Figure 30 shows the side view of the simple bracket. Figure 31 shows the front view.

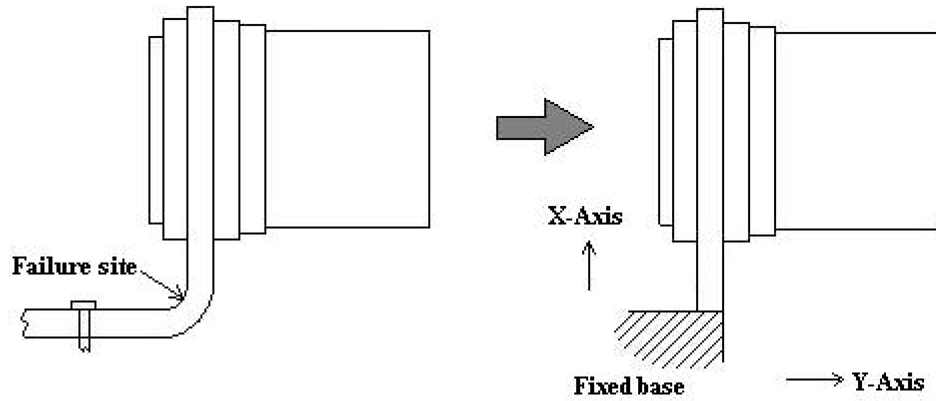

Figure 30: Bracket Transformation side view

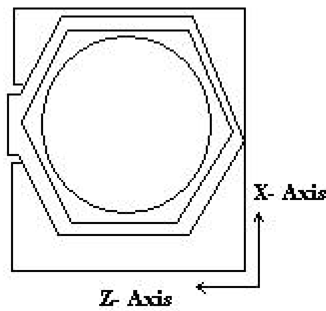

Figure 31: Bracket front view

The area moment of inertia *I*, for the bracket is calculated as:

$$I = \frac{BT^3}{12} \tag{9}$$

where *B* = width of the bracket, *T* = thickness of the bracket.

To find out the natural frequency of the bracket and transistor assembly the Dunkerley's formula [83] is used which considers the system as a cantilever beam with some non-negligible mass having an end mass at its tip. For calculation the length L has been considered from the base to the center of mass of the beam. For Dunkerley's formula there are two parts that are required, one to account for the uniformly loaded

beam by itself and the other to account for the mass attached to the beam. The two formulas are given as:

$$f_1^2 = 3.55^2 \left(\frac{EI}{m_1 L^3} \right) \quad \text{for uniformly loaded beam.} \tag{10}$$

$$f_2^2 = 3.00 \left(\frac{EI}{m_2 L^3} \right) \quad \text{for concentrated mass attached to the beam} \tag{11}$$

where E= modulus of elasticity of 1100 H14 aluminum, I = moment of inertia, m_1= mass of the beam, m_2= mass attached to the beam, L = length to the center of mass of the bracket. Substituting the above equations in the Dunkerley's formula we get the natural frequency f:

$$f = \sqrt{\frac{f_1^2 f_2^2}{f_1^2 + f_2^2}} \tag{12}$$

Using the Dunkerley's formula the first mode natural frequency was estimated to be approximately 900 Hertz. This value does not match the value of natural frequency obtained after testing.

7.2: Finite element modeling

A simple model of the bracket and transistor was generated using ANSYS software. The objective of the finite element modeling was to obtain the natural frequency of the bracket and to determine the area of maximum stress. Figure 32 shows the ANSYS model of the bracket. The dimensions of the bracket are same as the actual bracket. To represent the riveted joints to the test article board, the bracket was

considered as fixed, in all degrees of freedom, at two points at the bottom. To represent the clamping effect of the birtcher guides two points on the right edge of the bracket were considered as fixed in all degrees of freedom. A modal analysis of the bracket was conducted. From the modal analysis the natural frequency of the simple bracket was obtained as 930 hertz.

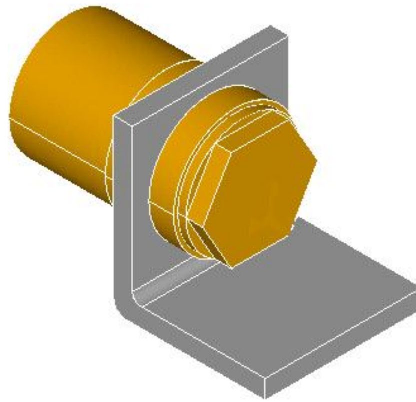

Figure 32: Model of simple aluminum bracket and transistor

Further two models: a half model and a full model of the aluminum frame were developed using the software. Figure 33 shows the half frame. Figure 34 shows the full frame. The boundary conditions were kept the same except that the points where the aluminum frame is fixed at the bottom are 5 for the half frame and 11 for the full frame. Seven points along the edges for the half frame are fixed and 20 points along the edges for full frame are fixed. Modal analyses conducted for the half frame and the full frame gave values of natural frequency as 990 hertz and 1050 hertz. The values of natural frequency obtained for the ANSYS models are very different from those obtained after testing, but are close to the numerical calculation value of 900 hertz.

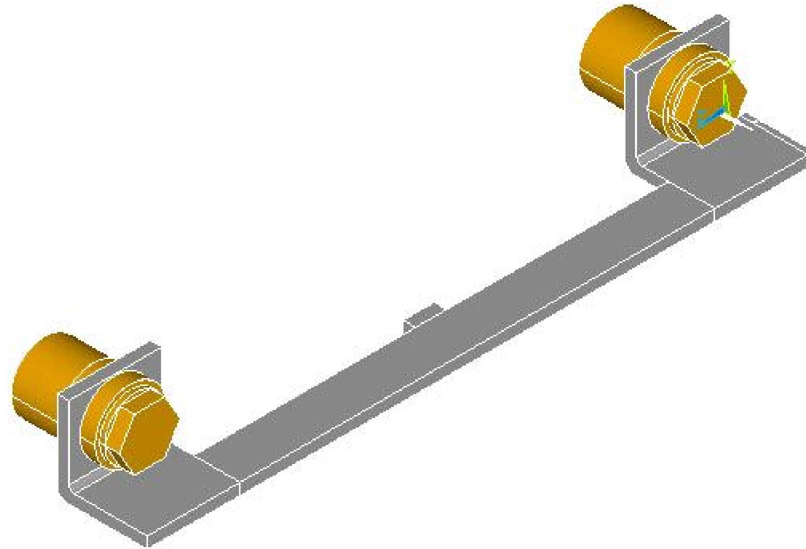

Figure 33: ANSYS model of half section of aluminum frame and transistors

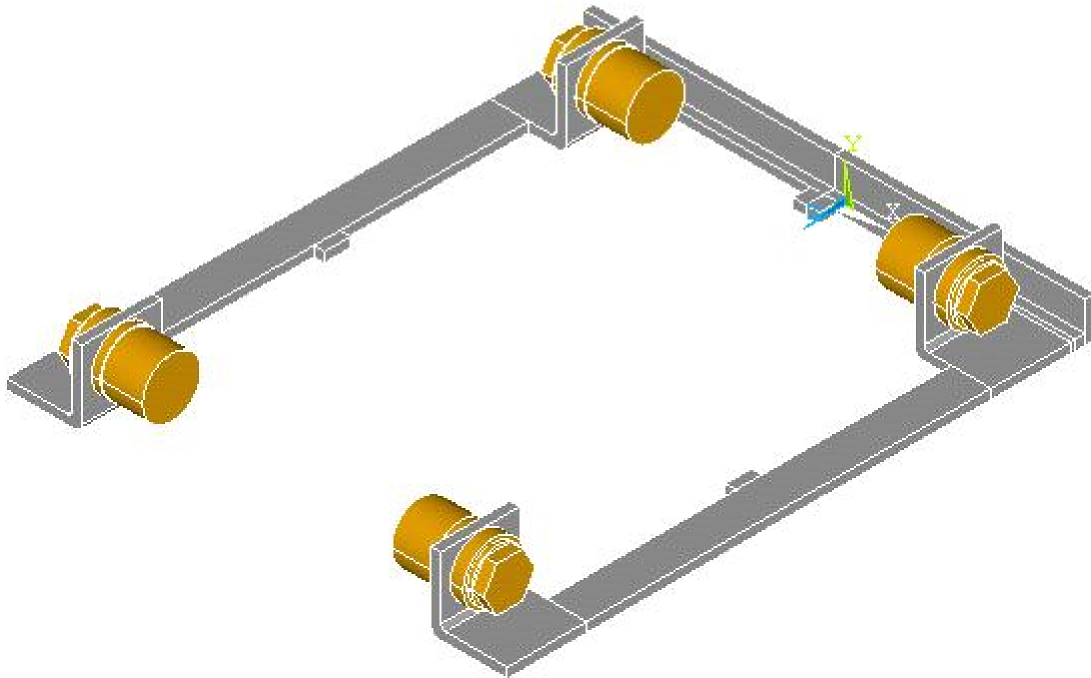

Figure 34: ANSYS model of full aluminum frame and transistors

Next a spectrum analysis of the simple bracket model was conducted using the ANSYS software for one random vibration profile of the operation cycle. Figure 35 shows the results of the spectrum analysis. It shows that the maximum stresses will be at the area of the bend in the aluminum bracket. Based on this result, for calculating the

damage ratio due to the random vibration and shock loads, the bracket was considered as a vertical cantilever beam, fixed at the base, with uniformly distributed load at some distance from the free end of the beam.

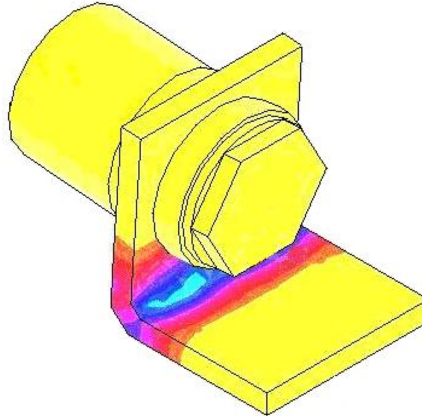

Figure 35: Spectrum analysis result showing stress at the bend of the bracket

7.3: Damage calculation

From the finite element modeling it is seen that the maximum stress due to vibration is at the bend of the bracket. Since the stresses are concentrated at the bend of the bracket repeated stress reversals will cause the material around the bend to dislocate and cause cracks. Further stress reversals will widen the cracks and finally will cause the bracket to break at this bend. For damage calculation analysis the bracket is considered as a vertical cantilever beam fixed at the base, with uniform loading. During the life test the test article was not excited above 1000 hertz. For damage assessment the natural frequency of the bracket was assumed as 950 hertz. This value is the mean of the lowest estimated natural frequency value and the highest possibly excited frequency. The effects of the random vibration and shock loads at the fixed based of the cantilever beam were analyzed separately. The following sections detail the damage calculations for random vibration load and shock as a harmonic load.

7.3.1: Random vibration load

The damage ratio due to the random vibration loads is estimated using the natural frequency of 950Hz obtained by finite element analysis. The transmissibility function *Q* represents the ratio of the maximum output force to the maximum input force. This is expressed as [82]:

$$Q = \sqrt{f} \tag{13}$$

Knowing the input PSD value in g2/Hz at the first mode frequency the G RMS acceleration response can be estimated using the following formula:

$$G = 9.81\sqrt{\frac{\pi P f Q}{2}} \tag{14}$$

For numerical analysis of random vibration effects, the three-band technique is commonly used. This technique is based on the Gaussian distribution wherein the instantaneous accelerations between +1σ and -1σ are assumed to act at the 1σ level 68.3% of the time. Like wise the instantaneous accelerations between +2 σ and -2 σ are assumed to act 27.1% times and those between +3 σ and -3 σ act 4.33% of the times [82]. For this technique first the RMS bending stress S_b has to be estimated using the formula:

$$S_b = \frac{Mc}{I} \tag{15}$$

where M is the RMS bending moment given by M = m2 GL, and c = Thickness/2. The stress concentration factor K, for aluminum, is assumed as equal to 2 [82]. The number of stress cycles required to produce fatigue failure 'N', using the 3-band method is given by

$$N = N_2 \left(\frac{S_2}{S_b} \right)^b \tag{16}$$

where N_2= 1000, S_2 = 1.24 x10^8 Pa and b = 6.4 [82]. The actual number of cycles 'n', applied during the operation, is estimated by multiplying the time period, the first mode frequency and the percentage of times corresponding to each sigma band.

$$n_1 = f * t * 0.683, \qquad n_2 = f * t * 0.271, \qquad n_3 = f * t * 0.0433 \tag{17}$$

where n_1, n_2, n_3 are the actual number of cycles in the 1σ, 2σ and 3σ bands and t is the time. The corresponding cycles to failure for the 1σ, 2σ and 3σ bands are given by N_{11}, N_{12}, and N_{13} which are calculated as:

$$N_{11} = N_2 \left(\frac{S_2}{S_b} \right)^b, \qquad N_{12} = N_2 \left(\frac{S_2}{2S_b} \right)^b, \qquad N_{13} = N_2 \left(\frac{S_2}{3S_b} \right)^b \tag{18}$$

From the values of N and n the damage ratio can be calculated using the formula:

$$D = \left(\frac{n_1}{N_1} \right) + \left(\frac{n_2}{N_2} \right) + \left(\frac{n_3}{N_3} \right) \tag{19}$$

The above procedure can be performed for each load type that the test article and the aluminum bracket have experienced. Analysis for the different loading conditions generates the individual damage ratios for each segment. The total damage ratio is the sum of all the individual damage ratios. The life test random vibration profiles were approximated from the actual life cycle data provided by NASA. Figure 36 shows the life test vibration acceptance section PSD profile along with the original data. The G_{rms} value

of the original PSD profile is 12 and that of the life test profile is 32. The life test profile is more conservative than the original profile. For the aluminum bracket the damages caused due to the different life cycle usage conditions are detailed in Table 11. The total damage ratio due to all the random vibration loads was 0.095.

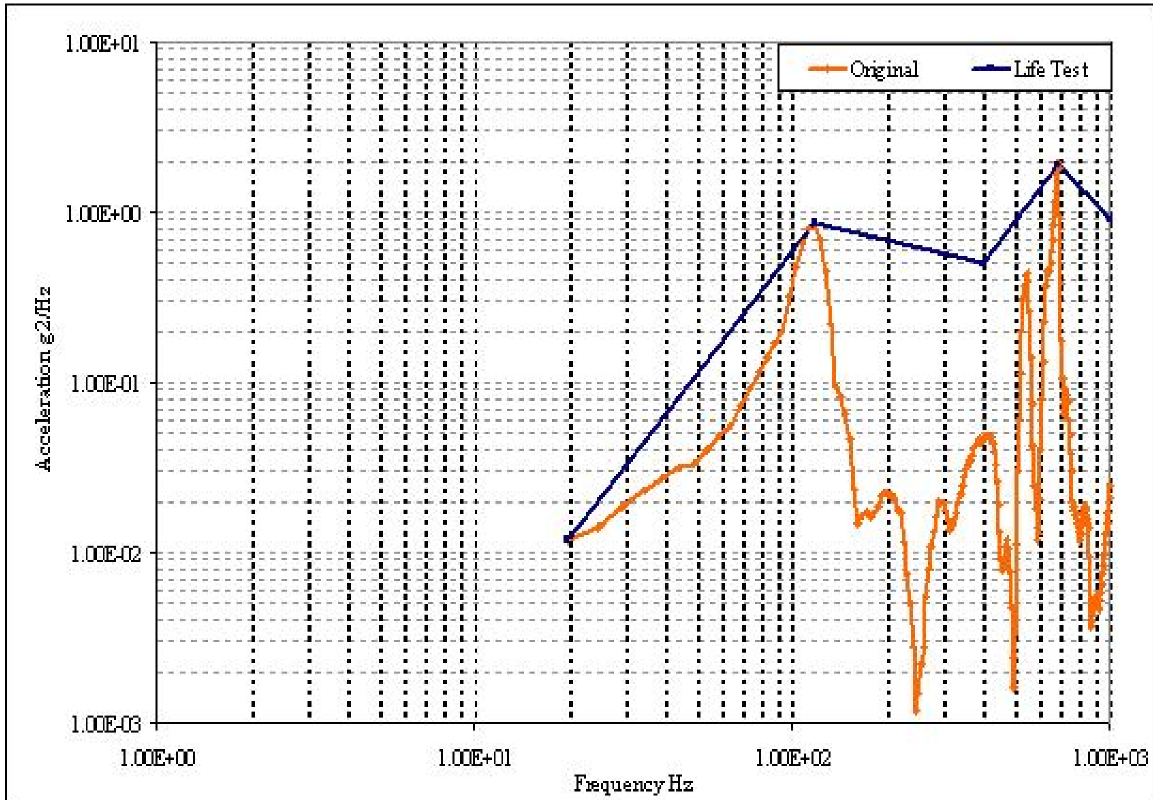

Figure 36: Life test vibration acceptance PSD profile

Table 11: Damage to the bracket due to random vibration loads

Usage Condition	**Exposures**	**Total Duration (sec)**	**Damage ratio**
Non vibration isolated flight	1	410.8	1.25×10^{-8}
Vibration isolated flight	7	3032.4	4.51×10^{-11}
Vibration acceptance test	15	900	8.25×10^{-7}
Life test vibration acceptance section	6	360	0.095
Total			**0.095**

7.3.2: Shock as harmonic vibration

The test article has experienced a total of eight shock events. The shock has been modeled as a harmonic vibration [91] for analyzing the damage caused in the bracket. For a sinusoidal harmonic load the displacement of the bracket Z is estimated using the following formula

$$Z = \frac{9.8 G_{in} Q}{4\pi^2 f^2} \tag{20}$$

where G_{in} is the peak input acceleration, Q is the transmissibility and f is the forcing frequency of the harmonic. In the case of the bracket the harmonic shock load is transmitted to the aluminum bracket from the printed circuit board. The value of Q is based on the frequency ratio R_{Ω}.

$$R_{\Omega} = \frac{f}{f_n} \tag{21}$$

where f_n is the natural frequency of the bracket. Knowing the frequency ratio the transmissibility is estimated as:

$$Q = \frac{1}{\left(1 - R_{\Omega}^2\right)} \tag{22}$$

The calculated value of displacement is now equated to the static deflection of the cantilever beam. From this the dynamic load on the beam can be estimated. The bracket is considered as a cantilever beam with uniformly distributed mass from a distance say

'*a*', from the fixed end, through to the free end of the beam. Figure 37 shows the simplified model of the bracket.

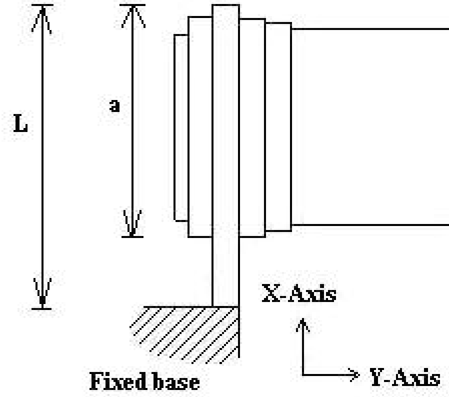

Figure 37: Cantilever beam with uniformly distributed load

The equation for static deflection, '*d*', of such a cantilever beam is written as:

$$d = \frac{wL^4}{8EI} - \left[\frac{w(L-a)^4}{8EI} - \frac{wa(L-a)^3}{6EI} \right] [85] \qquad (23)$$

where *w* is the total mass, *E* is the modulus of elasticity of the beam material and *I* is the area moment of inertia of the beam.

Equating the deflection *Z* with equation 23 and given the values of *E*, *I*, *a* and *L*, the dynamic load w_d can be estimated. The bending moment for the cantilever beam can be estimated using the following formula:

$$M = w_d a \left(L - \frac{a}{2} \right) \quad [85] \qquad (24)$$

The bending stress S_b is calculated using the formula:

$$S_b = \frac{Mc}{I}$$

where M is the bending moment, I is the area moment of inertia and c is the distance to the neutral axis. The vale of c is equal to half the bracket thickness. The stress concentration factor K, for aluminum, is assumed as equal to 2 [82]. The value of stress obtained is used in the equation below for estimating the cycles to failure for the cantilever beam.

$$N = N_2 \left(\frac{S_2}{S_b} \right)^b$$

where N_2= 1000, S_2 = 1.24 x10^8 Pa and b = 6.4 [82]

The values of cycles to failure and the actual number of cycles, n that the board has experienced are use to estimate the damage ratio D, for the bracket due to shock using the following formula:

$$D = \frac{n}{N} \tag{25}$$

Measured shock data was provided in the form of acceleration versus time plots. The assumption is that the shock experienced by the printed circuit board is transmitted to the aluminum bracket, since the bracket is riveted to the test article. The shock was modeled as a sinusoidal harmonic vibration load in order to account for the damage accumulated in the bracket due to each occurrence of the shock event. From the shock

data available, the forcing frequency of the harmonic vibration was assumed as 110 hertz. Figure 38 shows the Y axis shock data.

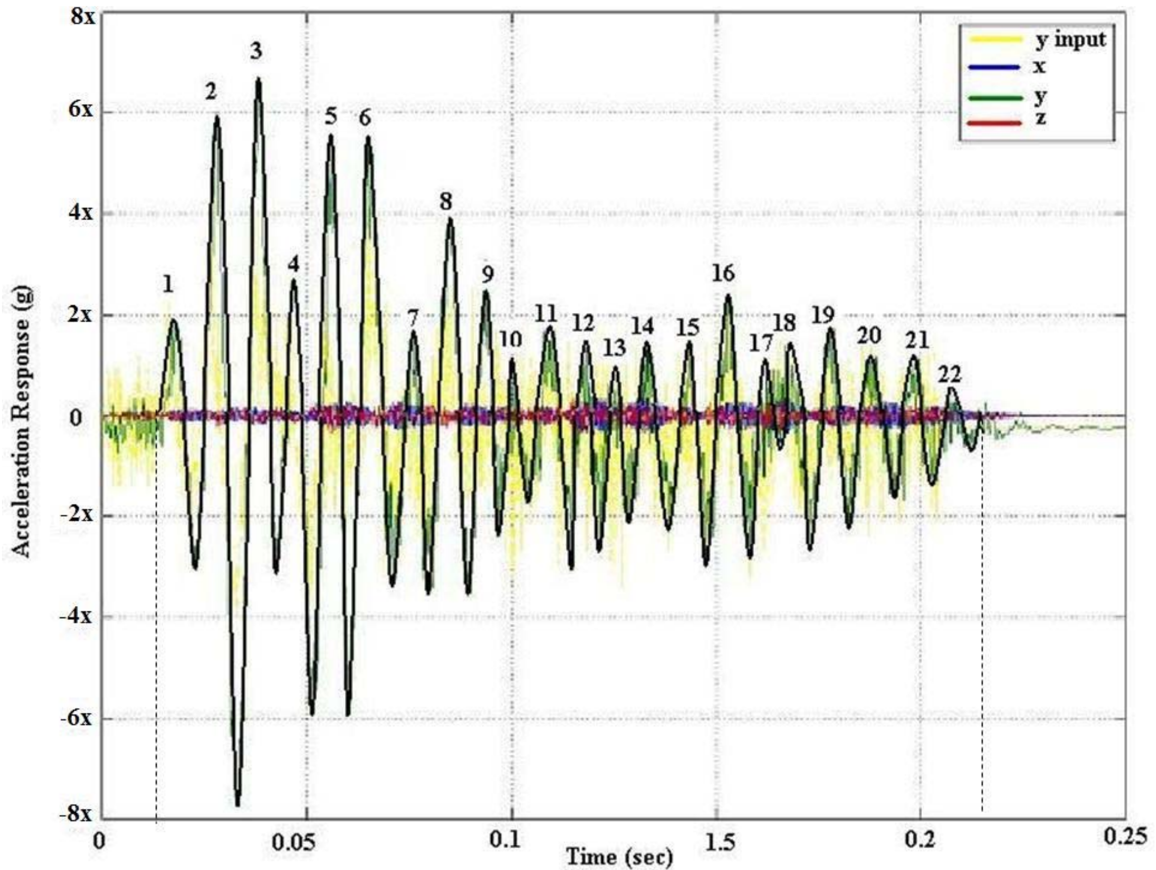

Figure 38: Y axis shock data

The shock event lasts for 0.2 seconds. There are a total of 22 significant sinusoidal harmonic waves of different amplitudes. The effect of each sinusoidal wave was individually analyzed. The mean amplitude for each harmonic wave was estimated and used as the input *G* value. The damage due to each harmonic load was estimated, then summed together to get the total damage due to the one shock event. This value multiplied by eight gives the total damage to date in the bracket after the 8 flights. The total damage in the aluminum bracket caused due to the shock conditions at water impact after 8 flights was 0.698.

7.3.3: Total damage ratio

The total damage to the aluminum bracket due to all the random vibration loads during its life cycle and during the life test was 0.095. The damage due to all the shock loads during the life cycle was 0.698. The total damage to the bracket to date is the sum of the damage due to random vibration and the shock loads. Hence the total damage ratio of the bracket was approximately 0.8.

7.4: Summary

Numerically the first mode natural frequency of the aluminum bracket was estimated as 900 Hertz. The value of natural frequency obtained by the finite element modeling is in the range from 930 hertz to 1050 hertz. The measured value was 600 Hertz. The measured natural frequency is different since it was captured after cracks developed in the aluminum frame during testing. The numerical calculation of damage to the aluminum bracket due to the life cycle random vibration loadings is 8.38×10^{-7}. This value is negligible. The damage to the bracket due to the shock events from the 8 flights it has experienced is substantial. The damage ratio due to the 8 shock events is 0.698. The damage due to the 6 life test vibration acceptance section profile is 0.095. It is seen that the life test vibration acceptance section profile contributes to the damage ratio. It is observed that the input PSD value at 950 Hertz is high as compared to NASA's actual input profile of the vibration acceptance test.

Chapter 8: CONCLUSION

This thesis presents a 'Health Status Assessment' methodology that provides a guideline for conducting a remaining life assessment of electronic hardware already deployed in the field. Given an electronic hardware already deployed in the field, the methodology will provide the assessor with the possible techniques that can be used and the criteria for implementing that technique. A combination of physical analysis, virtual assessment and testing can generate useful information regarding the remaining life of an electronic hardware. This information can be utilized for logistic decision making with respect to the electronic hardware. A virtual assessment provides an approximate estimate of the remaining life of the electronic hardware, provided the inputs to the simulation tool represent the actual conditions accurately. Utilizing a correct representation of the actual environmental loading condition information in the virtual assessment is vital in determining the damage to the hardware to date. The total damage accumulated at a particular site can be estimated by the addition of the damages due to each load applied individually. Knowing the damage to date and the damage per future operation, the remaining life of the electronic hardware can be estimated.

Testing of hardware, guided by the results of the virtual assessment provides additional input to the remaining life estimate. This testing can also help validate or iteratively improve the quality of virtual assessment. Testing will give a more accurate remaining life estimate than the virtual assessment. This is true provided the test loading conditions can recreate the actual life cycle environmental conditions.

A complete failure mechanisms, modes and effects analysis (FMMEA) should be conducted before proceeding with the remaining life assessment. From the analysis of the

failure on the circuit card, it is concluded that a FMMEA would have helped identify the bracket structure as an item of interest and would have forced an assessment of the bracket before designing the life test. FMMEA is an important step in assessment of the remaining life of an electronic hardware and should not be ignored under any circumstances.

Based on the assessment of the failed aluminum brackets of the test article, it is concluded that there was heavy damage accumulation at the bend of the brackets, due to the life cycle shock events, before entering into testing. It is also concluded that though the life test vibration acceptance section PSD profile was over specified the bracket would have still survived 40 such events in the Y axis, if there was no damage due to the shock events during the operational use of the circuit card. The life test vibration acceptance section random vibration load added to the existing damage and caused the bracket to fail during the life testing.

It is concluded that assessment of the in plane loads can not be ignored especially if there are structures and components mounted in the in plane axis. Mechanical mounting and support structures can potentially suffer high damage, sometimes more that the damage to the electronic components on the board. For the printed circuit boards in the integrated electronic assembly of the space shuttle's solid rocket booster, it is concluded that the probability of failure of aluminum brackets on the circuit card are high. It is suggested that NASA conduct a detailed assessment of the aluminum frame on the circuit card. Such an assessment is essential in identifying possible failure mechanisms and modes and in preventing any catastrophic failure in future.

Chapter 9: CONTRIBUTIONS

1. I developed a 'Health Status Assessment' methodology for remaining life assessment of electronic hardwares that are already deployed in the field.

I conducted a literature review of the methodologies used for assessing the remaining life of engineering hardware other than electronic products and identified the possible techniques that can be used for assessing electronic products. I identified the categories into which the methodologies used can be classified. Based on the knowledge gained from my study I developed a methodology suitable for assessing the remaining life of electronic hardware already deployed in the field. I further demonstrated the application of the methodology by assessing the remaining life of a printed circuit board using the methodology developed by me.

2. I demonstrated a method of modeling the shock load as a harmonic vibration load.

For conducting a virtual assessment of the printed circuit board, for estimating its remaining life, it was necessary to model the shock load that the hardware experienced during actual operation. For estimating the damage caused due to the shock load, the shock was first modeled as an overstress load. Since the components on the printed circuit board survived the overstress load, I modeled the shock load as a harmonic vibration load. Using this approach, of modeling the shock, the total damage accumulated in the component to board solder joint interconnects could be estimated. This approach was also used to conduct the post test analysis of the failed aluminum support structure on the printed circuit board.

3. I demonstrated through the design, implementation, and post-test analysis, the importance of testing and FMMEA in remaining life assessment.

I developed a test plan for conducting a life test for the printed circuit board. The life test simulated the random vibration and shock loading conditions experienced by the printed circuit board in the operational phase and the random vibration load in the acceptance testing phase of its life cycle. I developed the life test random vibration profiles and the shock profile from the life cycle loading data collected in the first step of the remaining life assessment methodology. I developed the test cycles, the test durations and the test procedures to be used for life testing. I also designed the test fixture and test set up assembly. Through the life test I demonstrated that for critical hardware, to get a good estimate of the remaining life it is necessary to perform testing and importantly an FMMEA before going into testing.

4. I demonstrated the use of a combination of finite element modeling and analytical analysis to identify the cause of the unanticipated failure during life testing of the printed circuit board.

I used the analytical method to estimate the natural frequency of the structure that failed during testing. I then used finite element modeling method to validate my analytical estimate of natural frequency of the structure. I then calculated the damage to the structure due to the life cycle random vibration and shock load. Form this estimation I was able to identify the load that contributed most to the failure of the structure.

Chapter 10: FUTURE WORK

Based on the application of the developed remaining life assessment methodology it is observed that the following aspects should be considered for future work:

1. The rapid assessment simulation tool used for this study needs to incorporate the ability to assess the in plane loads on a circuit card.
2. A virtual assessment tool that can simulate a combination of thermal, vibration and shock loads on a circuit card is essential to assess the combined effect of these loads on the remaining life of the circuit card.
3. A technique of assessing the effect of life cycle loads on individual components on the circuit card needs to be developed for a more accurate remaining life assessment.
4. A knowledge based system for electronic hardwares that can generate a rough estimate of degradation using the life cycle operational data, if developed will be helpful in determining the depth of the assessment to be conducted to get a satisfactory remaining life estimate.

APPENDIX A: List of components and parts on the 3-ampere combination switch card.

Sr. No.	Component	Part Type	Part Description	Sr. No.	Component	Part Type	Part Description
1	C1	Cap1	Capacitor	62	R9	Res6	Resistor
2	C2	Cap5	Capacitor	63	R10	Res1	Resistor
3	C3	Cap4	Capacitor	64	R11	Res7	Resistor
4	C4	Cap3	Capacitor	65	R12	Res3	Resistor
5	C5	Cap2	Capacitor	66	R13	Res17	Resistor
6	C6	Cap1	Capacitor	67	R14	Res4	Resistor
7	C7	Cap5	Capacitor	68	R15	Res15	Resistor
8	C8	Cap4	Capacitor	69	R16	Res2	Resistor
9	C9	Cap3	Capacitor	70	R17	Res14	Resistor
10	C10	Cap2	Capacitor	71	R18	Res13	Resistor
11	C11	Cap1	Capacitor	72	R19	Res10	Resistor
12	C12	Cap5	Capacitor	73	R20	Res9	Resistor
13	C13	Cap4	Capacitor	74	R21	Res5	Resistor
14	C14	Cap3	Capacitor	75	R22	Res8	Resistor
15	C15	Cap2	Capacitor	76	R23	Res16	Resistor
16	C16	Cap1	Capacitor	77	R24	Res6	Resistor
17	C17	Cap5	Capacitor	78	R25	Res1	Resistor
18	C18	Cap4	Capacitor	79	R26	Res7	Resistor
19	C19	Cap3	Capacitor	80	R27	Res3	Resistor
20	C20	Cap2	Capacitor	81	R28	Res17	Resistor
21	CR1	Diode4	Diode	82	R29	Res4	Resistor
22	CR2	Diode3	Diode	83	R30	Res15	Resistor
23	CR3	Diode2	Diode	84	R31	Res12	Resistor
24	CR4	Diode2	Diode	85	R32	Res11	Resistor
25	CR5	Diode4	Diode	86	R33	Res13	Resistor
26	CR6	Diode3	Diode	87	R34	Res10	Resistor
27	CR7	Diode2	Diode	88	R35	Res9	Resistor
28	CR8	Diode2	Diode	89	R36	Res5	Resistor
29	CR9	Diode1	Diode	90	R37	Res8	Resistor
30	CR10	Diode3	Diode	91	R38	Res16	Resistor
31	CR11	Diode2	Diode	92	R39	Res6	Resistor
32	CR12	Diode2	Diode	93	R40	Res1	Resistor
33	CR13	Diode1	Diode	94	R41	Res7	Resistor
34	CR14	Diode3	Diode	95	R42	Res3	Resistor
35	CR15	Diode2	Diode	96	R43	Res17	Resistor
36	CR16	Diode2	Diode	97	R44	Res4	Resistor
37	P1	Connector	Connector	98	R45	Res15	Resistor
38	Q1	Transistor2	Transistor	99	R46	Res12	Resistor
39	Q2	Transistor2	Transistor	100	R47	Res11	Resistor
40	Q3	Transistor3	Transistor	101	R48	Res13	Resistor

Sr. No.	Component	Part Type	Part Description	Sr. No.	Component	Part Type	Part Description
41	Q4	Transistor1	Transistor	102	R49	Res10	Resistor
42	Q5	Transistor2	Transistor	103	R50	Res9	Resistor
43	Q6	Transistor2	Transistor	104	R51	Res5	Resistor
44	Q7	Transistor3	Transistor	105	R52	Res8	Resistor
45	Q8	Transistor1	Transistor	106	R53	Res16	Resistor
46	Q9	Transistor2	Transistor	107	R54	Res6	Resistor
47	Q10	Transistor2	Transistor	108	R55	Res1	Resistor
48	Q11	Transistor3	Transistor	109	R56	Res7	Resistor
49	Q12	Transistor1	Transistor	110	R57	Res3	Resistor
50	Q13	Transistor2	Transistor	111	R58	Res17	Resistor
51	Q14	Transistor2	Transistor	112	R59	Res4	Resistor
52	Q15	Transistor3	Transistor	113	R60	Res15	Resistor
53	Q16	Transistor1	Transistor	114	T1	TAssy	Transformer Assembly
54	R1	Res2	Resistor	115	T2	TAssy	Transformer Assembly
55	R2	Res14	Resistor	116	T3	TAssy	Transformer Assembly
56	R3	Res13	Resistor	117	T4	TAssy	Transformer Assembly
57	R4	Res10	Resistor	118	U1	Opt_C	Opto Coupler
58	R5	Res9	Resistor	119	U2	Opt_C	Opto Coupler
59	R6	Res5	Resistor	120	U3	Opt_C	Opto Coupler
60	R7	Res8	Resistor	121	U4	Opt_C	Opto Coupler
61	R8	Res16	Resistor				

APPENDIX B: CalcePWA modeling assumptions

To model the 3 Amp combination switch card using the CalcePWA software some simplifying assumptions were made. The following are examples of assumptions made for modeling using CalcePWA software:

1. We assumed that the board being custom built the actual components were all right within the tolerance limit as indicated in the drawing.
2. All components on the board have been modeled as through hole components.
3. Some of the components like the transistors, opto couplers and the transformer assemblies on the board are cylindrical, but they are modeled as rectangular components.
4. For some of the components for which we did not have datasheets we assumed the component material based on similar components of different dimensions and also based on the general type available in the market.
5. The aluminum wedge used for sliding the circuit card into the IEA box is a one-piece component riveted to three sides of the card. For our modeling we have broken it down to 4 pieces, one each along the length of the card and two small strips at the rear end of the card. This has been done so as to incorporate the weight of the aluminum wedge on the card. This will in no way affect the outcome of our analysis.
6. The transformers T1 and T2 are stacked on top of each other on the board. For modeling purpose, a composite transformer Ta is used. The same approach is used for transformers T3 and T4.
7. The leads of the components are assumed as copper.

APPENDIX C: Solid rocket booster flight segmentation

Event Number	Event Name	Load	Time of Occurrence
			(Seconds)
Event 01	Transition	Random Vibration	0
Event 02	LiftOff1	Random Vibration	7.5
Event 03	Transition	Random Vibration	10
Event 04	LiftOff2 Peak	Random Vibration	11.5
Event 05	Transition	Random Vibration	14
Event 06	Ascent	Random Vibration	25
Event 07	Transition	Random Vibration	38
Event 08	High Q1	Random Vibration	54
Event 09	Transition	Random Vibration	63
Event 10	High Q2 Peak	Random Vibration	85
Event 11	Transition	Random Vibration	105
Event 12	Pre-Separation	Random Vibration	133
Event 13	Transition	Random Vibration	136
Event 14	Separation B	Random Vibration	141.5
Event 15	Transition	Random Vibration	143.5
Event 16	Apogee	Random Vibration	150
Event 17	Transition	Random Vibration	310
Event 18	Re-Entry 1	Random Vibration	327.7
Event 19	Transition	Random Vibration	329.2
Event 20	Re-Entry 2	Random Vibration	331.9
Event 21	Transition	Random Vibration	332.3
Event 22	Re-Entry 3	Random Vibration	334.5
Event 23	Transition	Random Vibration	336
Event 24	Re-Entry 4	Random Vibration	345
Event 25	Transition	Random Vibration	353.5
Event 26	Re-Entry 5	Random Vibration	360
Event 27	Transition	Random Vibration	362.5
Event 28	Re-Entry 6	Random Vibration	367
Event 29	Transition	Random Vibration	370
Event 30	Parachute	Random Vibration	374
Event 31	Transition	Random Vibration	382
Event 32	Water Impact B	Shock	433.2

APPENDIX D: Life test fixture drawings

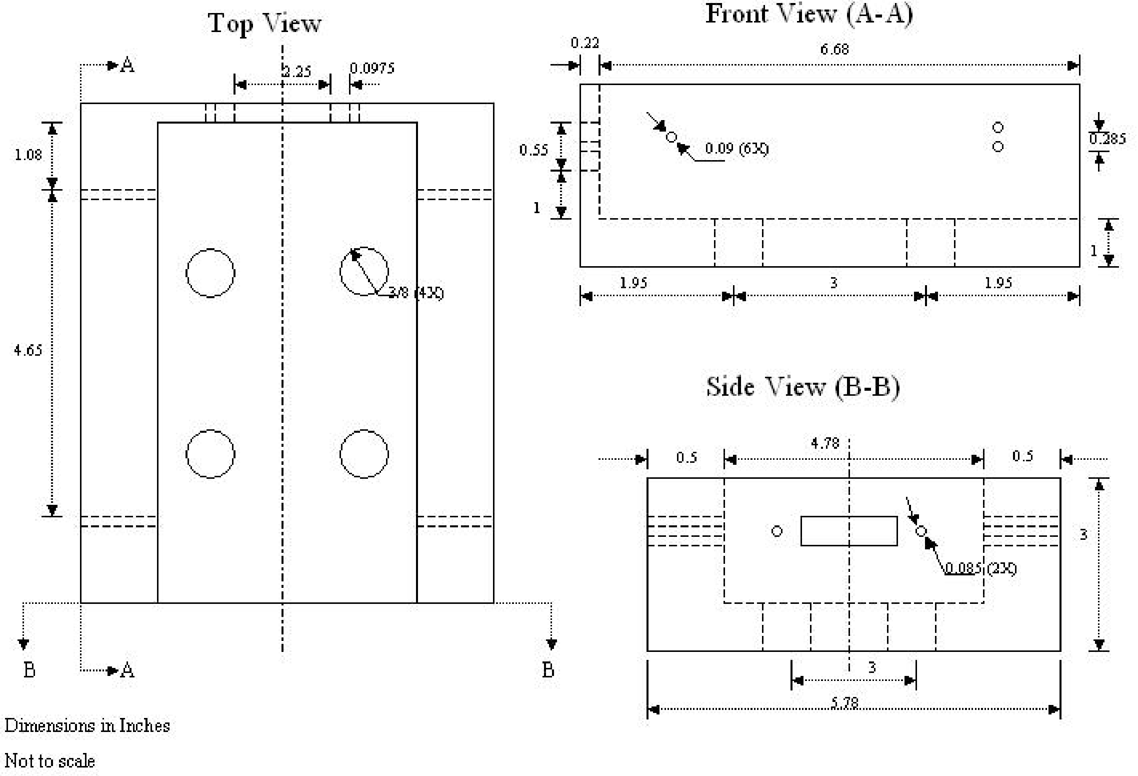

Figure 39: Fixture Design

Interface Plate

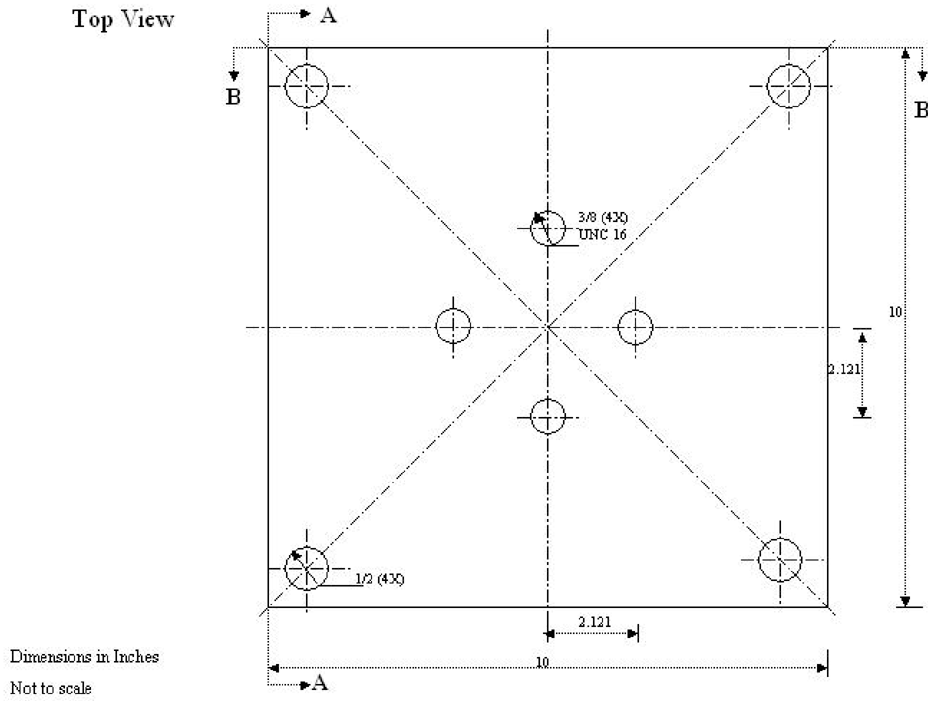

Figure 40: Top view of interface plate

Side View (A-A)

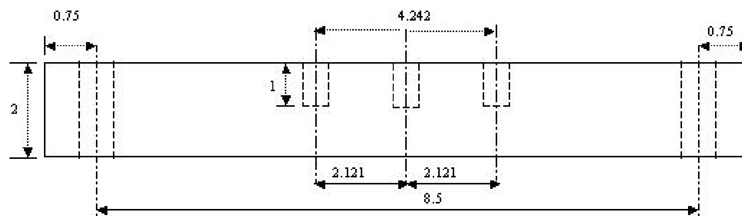

Side View (B-B)

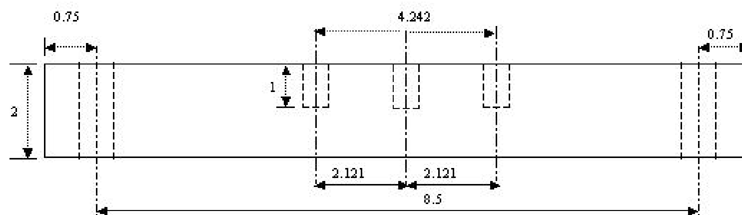

Dimensions in Inches

Not to scale

Figure 41: Side view of interface plate

APPENDIX E: Grouping of SRB flight events for developing life test loads.

Event	Event Description	Duration [sec]		Time [sec]		Grouping [sec]	
		*Flight 1	**Flight 2	Flight 1	Flight 2	Flight 1	Flight 2
01	Transition	7.5	7.0	0.0	0.0		
02	Liftoff	2.5	2.5	7.5	7.0		
03	Transition	1.5	1.0	10.0	9.5		
04	Liftoff Peak	2.5	3.5	11.5	10.5		
05	Transition	11.0	21.0	14.0	14.0		
06	Ascent	13.0	10.0	25.0	35.0		
07	Transition	16.0	15.0	38.0	45.0		
08	High Transition	9.0	10.0	54.0	60.0		
09	Transition	22.0	25.0	63.0	70.0	Low PSD	Low PSD
10	High Transition Peak	20.0	10.0	85.0	95.0	400.9	375.3
11	Transition	28.0	29.0	105.0	105.0		
12	Pre-separation	3.0	2.0	133.0	134.0		
13	Transition]	5.5	8.5	136.0	136.0		
14	Separation	2.0	0.5	141.5	144.5		
15	Transition	6.5	35.0	143.5	145.0		
16	Apogee	160.0	80.0	150.0	180.0		
17	Transition	17.7	45.0	310.0	260.0		
18	Re-entry 1	1.5	0.9	327.7	305.0		
19	Transition	2.7	6.3	329.2	305.9		
20	Re-entry 2	0.4	0.6	331.9	312.2	High PSD	High PSD
21	Transition	2.2	5.7	332.3	312.8	32.3	35.0
22	Re-entry 3	1.5	0.7	334.5	318.5		
23	Transition	9.0	4.8	336.0	319.2		
24	Re-entry 4	8.5	12.0	345.0	324.0		
25	Transition	6.5	4.0	353.5	336.0		
26	Re-entry 5	2.5	2.0	360.0	340.0		
27	Transition	4.5	5.0	362.5	342.0		
28	Re-entry 6	3.0	4.0	367.0	347.0		
29	Transition	4.0	27.0	370.0	351.0		
30	Parachute	8.0	12.0	374.0	378.0		
31	Transition	51.2	20.3	382.0	390.0		
32	Splashdown	0.1	0.3	433.2	410.3	Shock PSD	Shock PSD
-	Flight Ends			433.3	410.6	0.1	0.3

* Flight 1: Vibration isolated flight

** Flight 2: Vibration non isolated flight.

APPENDIX F: Life test loads data

Table 12: Life test X-axis acceptance profile

Sr. No	Hz	g^2/Hz
1	1.95E+01	1.32E-02
2	3.42E+01	2.35E-02
3	8.30E+01	4.83E-02
4	1.61E+02	6.67E-02
5	3.17E+02	3.17E-01
6	7.62E+02	5.17E-02
7	1.00E+03	2.50E-02

Table 13: Life test Y-axis acceptance profile

Sr. No	Hz	g^2/Hz
1	1.95E+01	1.18E-02
2	1.17E+02	8.67E-01
3	4.00E+02	5.00E-01
4	6.84E+02	1.93E+00
5	1.00E+03	9.00E-01

Table 14: Life test Z-axis acceptance profile

Sr. No	Hz	g^2/Hz
1	1.95E+01	1.22E-02
2	7.32E+01	3.60E-02
3	1.46E+02	9.50E-02
4	3.22E+02	5.79E-01
5	1.00E+03	5.00E-02

Table 15: Life test X-axis low PSD profile

Sr. No	Hz	g^2/Hz
1	4.88E+00	3.33E-03
2	9.77E+00	4.91E-03
3	1.95E+01	2.48E-03
4	2.93E+01	8.02E-04
5	1.42E+02	5.93E-03
6	4.79E+02	7.43E-04
7	6.30E+02	1.61E-03
8	1.00E+03	3.00E-04

Table 16: Life test Y-axis low PSD profile

Sr. No	Hz	g^2/Hz
1	4.88E+00	1.94E-04
2	1.03E+02	9.02E-01
3	6.84E+02	2.63E-02
4	1.00E+03	1.00E-02

Table 17: Life test Z-axis low PSD profile

Sr. No	Hz	g^2/Hz
1	4.88E+00	3.03E-04
2	9.77E+00	1.34E-03
3	1.46E+01	6.99E-04
4	4.88E+01	4.61E-03
5	9.77E+01	7.36E-03
6	3.22E+02	1.16E-02
7	1.00E+03	1.00E-03

Table 18: Life test X-axis high PSD profile

Sr. No	Hz	g^2/Hz
1	4.88E+00	1.55E-01
2	1.92E+01	2.17E-01
3	9.77E+01	2.24E-01
4	1.95E+02	3.14E-02
5	3.17E+02	8.75E-01
6	6.49E+02	1.58E-01
7	1.00E+03	5.00E-02

Table 19: Life test Y-axis high PSD profile

Sr. No	Hz	g^2/Hz
1	4.88E+00	3.38E-03
2	1.95E+01	1.30E-02
3	5.86E+01	4.78E-01
4	9.77E+01	8.26E+00
5	3.76E+02	8.82E-02
6	6.88E+02	4.66E+00
7	1.00E+03	1.00E+00

Table 20: Life test Z-axis high PSD profile

Sr. No	Hz	g^2/Hz
1	4.88E+00	1.43E-01

2	1.95E+01	2.02E-01
3	9.77E+01	1.71E-01
4	1.95E+02	2.43E-02
5	3.22E+02	1.76E+00
6	6.88E+02	6.69E-02
7	1.00E+03	3.00E-02

Table 21: X-axis shock profile

Sr. No	Hz	g^2/Hz
1	4.88E+00	1.04E-01
2	2.44E+01	3.39E+00
3	1.27E+02	1.22E-01
4	2.93E+02	2.84E-01
5	4.74E+02	1.14E-02
6	6.64E+02	1.58E-02
7	1.00E+03	5.00E-03

Table 22: Y-axis shock profile

Sr. No	Hz	g^2/Hz
1	4.88E+00	2.02E-01
2	3.91E+01	1.97E+00
3	1.27E+02	1.37E+00
4	3.71E+02	1.82E-02
5	6.79E+02	3.89E-01
6	1.00E+03	1.00E-02

Table 23: Z-axis shock profile

Sr. No	Hz	g^2/Hz
1	4.88E+00	9.46E-02
2	2.44E+01	3.56E+00
3	4.88E+01	5.41E-01
4	1.27E+02	7.55E-02
5	2.93E+02	3.17E-01
6	1.00E+03	1.00E-02

Table 24 X axis shock spectrum

Hz	Min gp	Max gp
50	25	80
100	25	80

200	45	75
300	55	125
400	55	125
500	60	125
600	50	90
700	55	90
800	50	85
900	60	100
1000	70	125

Table 25 Y axis shock spectrum

Hz	Min gp	Max gp
50	25	95
100	100	300
200	45	100
300	40	110
400	55	125
500	55	125
600	60	110
700	50	95
800	45	95
900	50	100
1000	55	110

Table 26 Z axis shock spectrum

Hz	Min gp	Max gp
50	32	90
100	50	110
200	50	75
300	60	150
400	45	70
500	32	60
600	28	50
700	25	48
800	23	45
900	23	45
1000	25	45

APPENDIX G: Life test procedure

The procedures followed during the four phases of testing mentioned in Chapter 5, Section 6 are detailed here.

1. Fixture characterization procedure

The following procedure was followed for conducting the fixture characterization test at University of Maryland:

1. Place the interface plate on the shaker table and match the hole pattern.
2. Secure the interface plate onto the shaker table with ½ inch bolts.
3. Fix the accelerometers on the interface plate.
4. Set up the connections from accelerometers to digital signal analyzer to collect data.
5. Program the shaker table to generate a low flat PSD level over frequency range of 0 Hz to 2400 Hz
6. Start the shaker table and shake the interface plate.
7. Record the output of the digital analyzer and note the resonant frequencies of the interface plate.
8. Stop the shaker table.
9. Secure the fixture onto the interface plate with 3/8 inch bolts.
10. Attach the aluminum guides to the fixture.
11. Attach the electrical connector to the fixture.
12. Fix the accelerometers on the fixture.
13. Set up the connections from accelerometers to digital signal analyzer to collect data.
14. Start the shaker table and shake the assembly (use the frequency range and PSD level programmed in step 5).
15. Record the output of the digital analyzer and note the resonant frequencies of the fixture assembly.
16. Stop the shaker table.
17. To test the assembly for ruggedness, reprogram the shaker table to generate a high flat PSD level over frequency range of 0 Hz to 1200 Hz.
18. Start the shaker table and shake the assembly.
19. Record the output of the digital analyzer and check for chattering.
20. Stop the shaker table.
21. Fix the accelerometers and strain gauges on the 3-amp combination switch card.
22. Insert the circuit card into the fixture by sliding it through the aluminum guides.
23. Set up the connections from accelerometers and strain gauges to digital signal analyzer to collect data

24. Program the shaker table to generate a low flat PSD level over frequency range of 0 Hz to 1000 Hz
25. Start the shaker table and shake the assembly and circuit card.
26. Record the output of the digital analyzer and note the resonant frequencies.
27. Stop the shaker table.
28. End of testing.

2. Initial test procedure

The following is the procedure to conduct the pilot test at MSFC:

1. Conduct a visual inspection of the engineering card.
2. Secure the adapter plate to the shaker table.
3. Secure the interface plate onto the shaker table adapter plate with ½ inch bolts in the Z-axis.
4. Secure the fixture onto the interface plate with 3/8 inch bolts.
5. Attach the aluminum guides to the fixture.
6. Attach the electrical connector to the fixture.
7. Fix the accelerometers on the fixture.
8. Fix the accelerometers and strain gauges on the engineering card.
9. Insert the circuit card into the fixture by sliding it through the aluminum guides.
10. Set up the connections from accelerometers and strain gauges to data loggers to collect data.
11. Set up the electrical connections and electrical monitoring system.
12. Program the shaker table to generate the PSD profile for the acceptance test section in the current axis.
13. Start the shaker table.
14. Shake the circuit card for the time duration specified for the current section.
15. Record the output of the data logger.
16. Stop the shaker.
17. Program the shaker table to generate the PSD profile for the low PSD section in the current axis.
18. Repeat steps 13, 14, 15 and 16.
19. Program the shaker table to generate the PSD profile for the high PSD section in the current axis.
20. Repeat steps 13, 14, 15 and 16.
21. Program the shaker table to generate the shock section profile in the current axis.
22. Repeat steps 13, 14, 15 and 16.
23. End of testing.

3. Life test procedure

The following is the procedure for conducting the life test of the 3-amp combination switch card at MSFC:

1. Conduct a visual inspection of the 3-amp combination switch card.
2. Secure the adapter plate to the shaker table.
3. Secure the interface plate onto the shaker table adapter plate with ½ inch bolts, in the Z-axis.
4. Secure the fixture onto the interface plate with 3/8 inch bolts.
5. Attach the aluminum guides to the fixture.
6. Attach the electrical connector to the fixture.
7. Fix the accelerometers on the fixture.
8. Fix the accelerometers and strain gauges on the 3-amp combination switch card.
9. Insert the circuit card into the fixture by sliding it through the aluminum guides.
10. Set up the connections from accelerometers and strain gauges to data loggers to collect data.
11. Set up the electrical connections and electrical monitoring system.
12. Program the shaker table to generate the PSD profile for the acceptance test section in the current axis.
13. Start the shaker table.
14. Shake the circuit card for the time duration specified for the current section.
15. Record the output of the data logger.
16. Stop the shaker.
17. Once the test section in this axis is completed, unbolt the interface plate.
18. Bolt the interface plate in the Y-axis direction.
19. Repeat steps 12, 13, 14, 15 and 16.
20. Once the test section in the Z and Y-axis is completed, unbolt the interface plate.
21. Bolt the interface plate in the X-axis direction.
22. Repeat steps 12, 13, 14, 15 and 16.
23. Once the test section is completed in the X, Y and Z-axis, repeat the procedure for the next test section.
24. One mission cycle is completed when all four test cycle sections are completed in all the three axes.
25. After every 20 such mission cycles the circuit card is removed from the fixture for optical inspection.

4. Optical inspection procedure

The following is the procedure for the optical inspection to be done at MSFC:

1. Conduct a visual inspection of the 3-amp combination switch card under a microscope, before the life test.
2. Record the physical condition of the circuit card.
3. After 20 mission cycles remove the 3-amp combination card from the fixture.
4. Disconnect the accelerometers and strain gauges form their respective data loggers if necessary.
5. Observe the circuit card under a microscope.
6. Record any visible anomalies.
7. Reconnect the accelerometers and strain gauges to the data loggers if disconnected in step 4.
8. Insert the circuit card into the fixture.
9. Repeat steps 3 to 8 after every 20 mission cycles.
10. After 60 mission cycles testing is stopped.

APPENDIX H: Schematic of aluminum frame

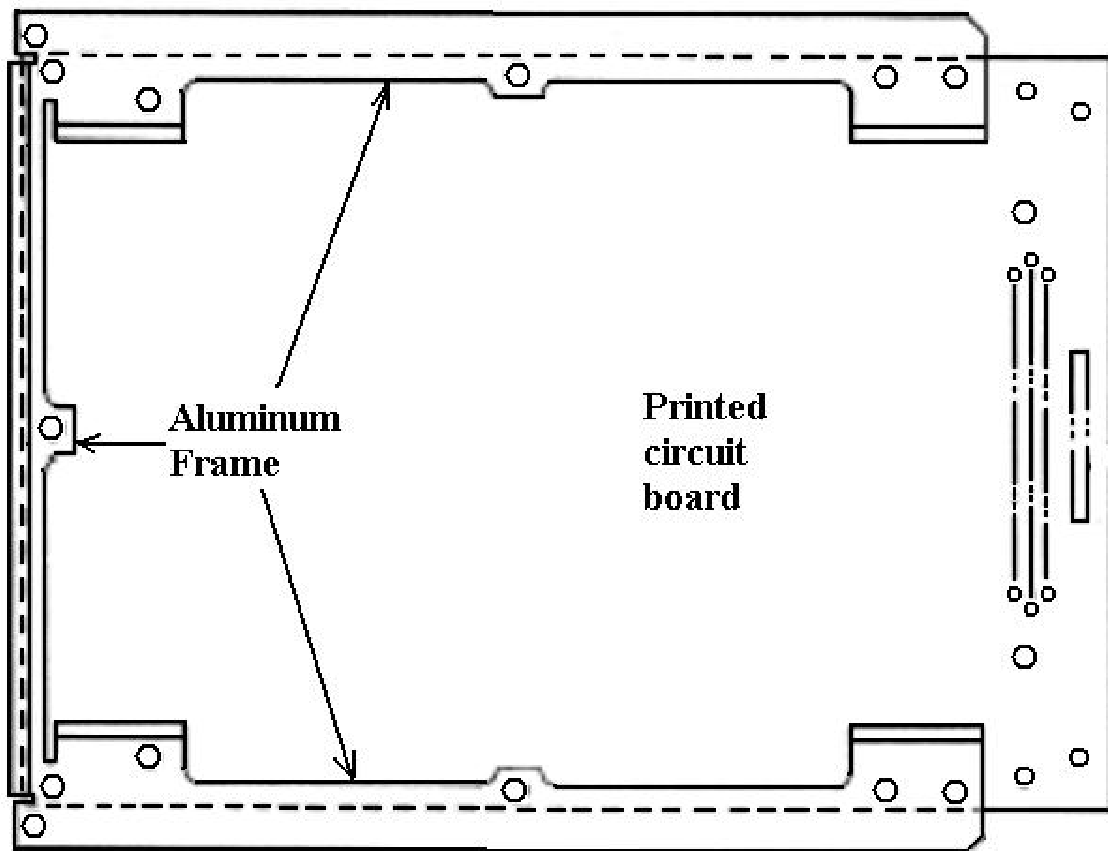

Figure 42: Aluminum frame top view

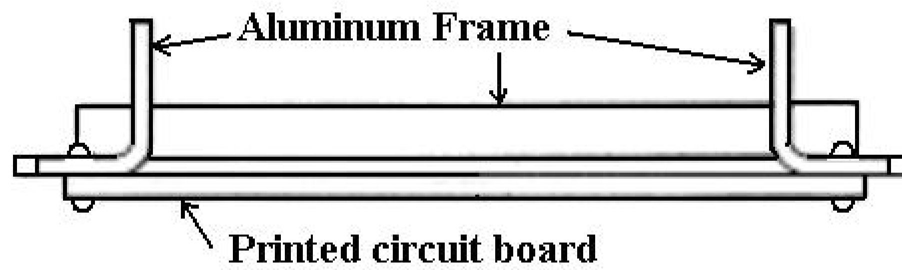

Figure 43: Aluminum frame front view

APPENDIX I: Matlab program for calculation of bracket damage

```
clear all
clc
% Material = 1100 H14 Aluminum
L=0.018338;                    % L=Length m
B =0.01905;                    % B=Breadth m
T=0.002286;                    % T=Thickness m
E =6.89E10;                    % E=Modulus of Elasticity Pa
d =2700;                       % d=Density Kg/m^3
w =0.013;                      % w=Weight of transistor kg
g =386;                        % g=Gravity remove this
m =L*B*T*d                     % m=Mass of Beam
I =(B*(T^3))/12                % I=Moment of inertia
W = w+m;                       % W= Total weight kg
l = L/2;                       % Length to the center of mass
c=T/2;                         % Distance from Neutral Axis (c) =T/2
b=6.4;
K=2;                           % Stress Factor
N2=1000;                           % cycles to fail
S2=1.24E8;                         % Pa
a=0.01633;                     % load distance (m)
fl=8;                          % Number of Flights
F=270;                         % Forcing frequency
Fn=950                         % Natural frequency
Time= 0.0091;                  % Duration of 1 harmonic cycle
cp= 1;                         % Harmonic cycles per flight

%*********************************************************************
% Response of the beam to Random Vibrations
Q=sqrt(Fn);                    % Transmissibility
%*********************************************************************

% For Life test at NASA

p1=Textread('C:\Documents and Settings\sonym\Desktop\NASA1\LT@952.txt');    % Input PSD
t1=Textread('C:\Documents and Settings\sonym\Desktop\NASA1\LT time.txt');        % Life test acceptance
section time

G=sqrt((3.142/2)*p1*Fn*Q)*9.81;         % G=RMS Acceleration Response newly multiplied by 9.81

%Dynamic 1 sigma RMS bending stress in the beam acting 68.3 % of the time

M=W*G*l;                       % RMS bending Moment (M)=W*G(RMS)*L
S1b=(M*c)/I;                   % Sb= RMS bending Stress=(Mc)/I lb/in^2

%Number of stress cycles required to produce fatigue failure using the 3 bend method

%N1=N2*(S2/Sb)^b

N11=N2*((S2/S1b)^b);                % RMS 1 sigma
N12=N2*((S2/(2*S1b))^b);            % RMS 2 sigma
N13=N2*((S2/(3*S1b))^b);            % RMS 3 sigma

%Actual number of stress cycles during vibration acceptance test section of life test in Y axis.
n1=Fn*t1*0.683;                     % 1 sigma
```

```
n2=Fn*t1*0.271;                    % 2 sigma n2
n3=Fn*t1*0.0433;                   % 3 sigma n3

%Damage ratio Rn
%ActualRn = (n1/N1)+(n2/N2)+(n3/N3)
R1n=(n1/N11)+(n2/N12)+(n3/N13);
R1nC=(R1n*6)
%*******************************************************************
% For A5

p2 =Textread('C:\Documents and Settings\sonym\Desktop\NASA1\A5@952.txt');
t2 =Textread('C:\Documents and Settings\sonym\Desktop\NASA1\A5 times.txt');
 for i=1:31
    G2(i)=sqrt((3.142/2)*p2(i)*Fn*Q);
 end
 for j=1:31
    M2(j)=W*G2(j)*l;
 end
 for k=1:31
    S2b(k)=(M2(k)*c)/I;
 end
 for x=1:31
   N21(x)=N2*((S2/S2b(x))^b);
   N22(x)=N2*((S2/(2*S2b(x)))^b);
   N23(x)=N2*((S2/(3*S2b(x)))^b);
 end
 for y=1:31
   n21(y)=Fn*t2(y)*0.683;
   n22(y)=Fn*t2(y)*0.271;
   n23(y)=Fn*t2(y)*0.0433;
 end
 for z=1:31
   R2n(z)=(n21(z)/N21(z))+(n22(z)/N22(z))+(n23(z)/N23(z));
 end

R2nB=0;
 for u=1:31
    s=R2n(u);
    R2nB=R2nB+s;
    s=0;
 end
R2nC=(R2nB*1);

i=1;j=1;k=1;x=1;y=1;z=1;u=1;
%*******************************************************************
% For 41d

p3 = Textread('C:\Documents and Settings\sonym\Desktop\NASA1\41d@952.txt');
t3 =Textread('C:\Documents and Settings\sonym\Desktop\NASA1\41d times.txt');
 for i=1:31
    G3(i)=sqrt((3.142/2)*p3(i)*Fn*Q);
 end
 for j=1:31
    M3(j)=W*G3(j)*l;
 end
 for k=1:31
```

```
   S3b(k)=(M3(k)*c)/I;
 end
 for x=1:31
   N31(x)=N2*((S2/S3b(x))^b);
   N32(x)=N2*((S2/(2*S3b(x)))^b);
   N33(x)=N2*((S2/(3*S3b(x)))^b);
 end
 for y=1:31
   n31(y)=Fn*t3(y)*0.683;
   n32(y)=Fn*t3(y)*0.271;
   n33(y)=Fn*t3(y)*0.0433;
 end
 for z=1:31
   R3n(z)=(n31(z)/N31(z))+(n32(z)/N32(z))+(n33(z)/N33(z));
 end

 R3nB=0;
 for u=1:31
    o=R3n(u);
    R3nB=R3nB+o;
    o=0;
 end
 R3nC=(R3nB*7);

 i=1;j=1;k=1;x=1;y=1;z=1;u=1;
%*******************************************************************
% For Acceptance test

p4 =Textread('C:\Documents and Settings\sonym\Desktop\NASA1\AT@952.txt');
t4 =Textread('C:\Documents and Settings\sonym\Desktop\NASA1\AT time.txt');
G4=sqrt((3.142/2)*p4*Fn*Q);

 M4=W*G4*l;
 S4b=(M4*c)/I;

 N41=N2*((S2/S4b)^b);
 N42=N2*((S2/(2*S4b))^b);
 N43=N2*((S2/(3*S4b))^b);

 n41=Fn*t4*15*0.683;
 n42=Fn*t4*15*0.271;
 n43=Fn*t4*15*0.0433;

 R4n=(n41/N41)+(n42/N42)+(n43/N43);
 R4nC=(R4n*15);
%*******************************************************************
%Calculate the total damage ratio
Note='Total damage ratio due to random vibrations'
 Rt=R1nC+R2nC+R3nC+R4nC

%*******************************************************************

% Response of the beam to sinusoidal vibration
Romega=(F/Fn);                    %Frequency Ratio
Qs= (1/(1-(Romega)^2));           % Transmisibility
%*******************************************************************
```

```
Gin=Textread('C:\Documents and Settings\sonym\Desktop\NASA1\Gin.txt');                    % Input G

% displacement Z =((9.8*Gin*Q)/(f)^2)
for i=1:22
Z(i) =((9.8*Gin(i)*Qs)/(4*(3.142)^2*(F)^2));  %%  check
end

% Considering the bracket as a cantilever beam with uniformly distributed
% load through a distance 'a' from the end of the beam
% deflection of beam given by 'd'
% d = ((w*(L)^4)/(8EI))-(((w*(L-a)^4)/(8EI))-(w*a*(L-a)^3)/(6EI))
% d= w*formula2
% formula2=((3*(L)^4)-(3*(L-a)^4)-(4*a*(L-a)^3))/(24EI)
% Equating the value of displacement to the equation for static deflection we can get the dynamic load
% dynamic load Wd= z/formula2

formula2=((3*(L)^4)-(3*(L-a)^4)-(4*a*(L-a)^3))/(24*E*I);

for j=1:22
   Wd(j)=Z(j)/formula2;
end

% Bending Moment M = Wd*a*(L-(a/2))

for k=1:22
  M (k)= Wd(k)*a*(L-(a/2));
end

% Stress Sb= (M*c)/I

for u=1:22
   Sb(u)= (M(u)*c)/I;
end

% Cycles to failure N1= N2*((S2/Sb)^b)

for v=1:22
   N1(v)=N2*((S2/Sb(v))^b);
end
% Actual number of cycles n = cp*fl

n = cp*fl;
% Damage ratio D= n/N2

for x=1:22
   D(x)= n/N1(x);
end
% Total damage due to shock Ds
Ds=0;
for y=1:22
   r= D(y);
   Ds=Ds+r;
   r=0;
end
Note='Total damage ratio due to harmonic vibrations'
```

```
Ds

%**********************************************************************
Note='Total damage ratio for the bracket '
Dt= Rt+Ds

%**********************************************************************
```

REFERENCE

[1] Caccialupi, A., Crudeli, R., Fazio, G.P., Porro, F., Santoro, M., and Zannoni, M., "Approach to residual life assessment of large steam turbine components", *International Journal of Pressure Vessels and Piping*, Vol. 59, pp. 241- 258, 1994.

[2] Jaske, Carl E., "Benefits of remaining life assessment", *Chemical Engineering Progress*, Vol. 83, No. 4, pp. 37-46, Apr, 1987.

[3] Swaminathan, V.P., Viswanathan, R.; Clark, C.P., "Material property studies of two high-pressure turbine rotors for remaining life assessment", *Journal of Engineering Materials and Technology, Transactions of the ASME*, Vol. 116, No. 1, pp. 19-26, Jan, 1994.

[4] Wu, Y.H., Wu, C.H., and Lai, H.C., "Life assessment activities of fossil fuel power plant in the Republic of China", *International Journal of Pressure Vessels and Piping*, Vol. 59, pp. 185-195, 1994.

[5] Vishwanathan, R., Paterson, S.R., Grunloh, H., and Gehl, S., "Life assessment of superheater / reheater tubes in fossil boilers", *Journal of Pressure Vessel Technology, Transactions of the ASME*, Vol. 116, No. 1, pp. 1-16, Feb, 1994.

[6] Dai, S.H., "A study of residual life prediction for pressurized tubes of an industrial furnace operated at elevated temperature by using the method of extrema of fuzzy functions", *International Journal of Pressure Vessels and Piping*, Vol. 63, pp. 199-204, 1995.

[7] Gigilio, M., and Vergani, L., "Life prediction of pressure vessel nozzles", *International Journal of Pressure Vessels and Piping*, Vol. 63, pp. 199-204, 1995.

[8] Nottingham, L.D. (EPRI); Alley, C.T. ,"Turbine rotor remaining life assessment", *American Society of Mechanical Engineers, Power Division (Publication) PWR*, Vol. 3, pp. 179-185, 1988.

[9] Byron, J.D., Paterson, S.R., Proctor, R.R., and Feiereisen T.J., "Assessment of remaining useful life of ships service turbine generator steam chests", *Naval Engineers Journal*, Vol. 98, No. 3, pp. 95-106, May 1986.

[10] Yee, R.K., "Fitness for service and remaining useful life assessment of a steam drum", *American Society of Mechanical Engineers, Pressure Vessels and Piping Division (Publication) PVP*, Vol. 459, pp. 41-46, 2003.

[11] May, I.L., Da Silveria, T.L., and Vianna, C.H., "Criteria for evaluation of damage and remaining life in reformer furnace tubes", *International Journal of Pressure Vessels and Piping*, Vol. 66, No. 1-3, pp. 233-241, 1996.

[12] Kim, D.S., and Mead, H.E., "Remaining Life assessment of refinery heater tubes", *American Society of Mechanical Engineers, Pressure Vessels and Piping Division (Publication) PVP*, Vol. 388, pp. 361-366, 1999.

[13] Ohtani, R., "Questions and solutions on the method of remaining life evaluation of structural materials in High temperature power plants", *Transactions of the Japan Society of Mechanical Engineers*, Part A, Vol. 59, No. 565, pp. 2019-2026, Sep, 1993.

[14] Cheruvu, N.S., and Malmfeldt, L.R., "Metallurgical characterization of high pressure rotor for remaining service life assessment after 26 years of service", *American Society of Mechanical Engineers, Joint ASME/IEEE Power Generation Conference*., Miami Beach, FL, 1987.

[15] Sivaprasad, S., Swaminathan, J., Tiwary, Y.N., Roy, P.K., and Singh, R., "Remaining life assessment of service exposed reactor and distillation column materials of a petrochemical plant", *Journal of Engineering Failure Analysis*, Vol. 10, No. 3, pp. 275-289, June, 2003.

[16] Liu, Z., Volovoi, V., and Marvis, D.N., "Probabilistic remaining creep life assessment for gas turbine components under varying operating conditions", *American Inst. Aeronautics and Astronautics, 43rd Structures, Structural, Dynamics and Materials Conference*, Vol. 1, pp. 587-597, Denver, CO, Apr 22-25 2002.

[17] Shor, S.W.W., Call, A.O., Loos, R.L., Bozo, M.R., and Vanvick, T.W., "Criteria for economical remaining life assessment", *American Society of Mechanical Engineers, Joint ASME/IEEE Power Generation Conference*., Miami Beach, FL, 1987.

[18] Duvenhage, G., and Wannenburg, J., "Remaining life analysis of a pressure vessel subjected to cyclic loads based on fracture mechanics", *International Journal of Fatigue*, Vol. 17, No. 7, pp. 477-483, Oct, 1995.

[19] Rao, B.K., Anoop, M.B., Lakshmanan, N., Gopalakrishnan, S. and Appa Rao, T.V.S.R., "Risk-based remaining life assessment of corrosion affected reinforced concrete structural members", *Journal of Structural Engineering*, Vol. 31, No. 1, pp.51-64, April/June, 2004.

[20] Grunloh, H.J., and Hellner, R., "Remaining life assessment of superheater tubing by post service creep rupture testing", American Society of Mechanical Engineers, Pressure Vessel and Piping Conference, San Diego, CA, PVP, Vol. 22, 1987.

[21] Taillin, A.G., Sukamto, X., and Bagnoli, D.L., "Remaining life- risk ranking study for an LNG plant", *American Society of Mechanical Engineers, Pressure Vessels and Piping Division (Publication) PVP*, Vol. 336, pp. 139-148, 1996.

[22] Swaminathan, V.P., Pennick, H.G., Jirinec, M.J., and Madia, J., "Remaining life assessment of the East River 7 high pressure rotor", *American Society of Mechanical Engineers, Power Division (Publication) PWR*, Vol. 15, Recent Innovations and Experience with Plant Monitoring and Utility Operations, pp. 69-78, 1991.

[23] Vishwanathan, R., "Estimation of remaining life of boiler parts", American Society of Mechanical Engineers, Pressure Vessels and Piping Division (Publication) PVP, Vol. 98-1, pp. 183, 1985.

[24] Schlottner, G., and Seeley, R.E., "Estimation of remaining life of high temperature steam turbine components", *American Society of Mechanical Engineers, Pressure Vessels and Piping Division (Publication) PVP*, Vol. 98-1, pp. 35-44, 1985.

[25] Moss, C. J., and Finlay, M.R., "Remaining life assessment of furnace heater tubes", *American Society of Mechanical Engineers, Pressure Vessels and Piping Division (Publication) PVP*, Vol. 332, pp. 23-33, 1996.

[26] Rosario, D.A., Riccardella, P.C., Bisbee, L.H., Luttrell, M.E., Nelson, S., Eastman, A.D., and Rogers, M.D., "Remaining life assessment of a secondary superheater outlet header", *American Society of Mechanical Engineers, Pressure Vessels and Piping Division (Publication) PVP*, Vol. 303, pp. 291-299, 1995.

[27] Matsubara, M., and Nitta, A., "Remaining life assessment of actual steam turbine rotors using the ultrasonic method", *American Society of Mechanical Engineers, Pressure Vessels and Piping Division (Publication) PVP*, Vol. 303, pp. 49-55, 1995.

[28] Yang, S.I., Frangopol, D.M., and Neves, L.C., "Service life prediction of structural systems using lifetime functions with emphasis on bridges", Journal of Reliability Engineering and System Safety, Vol. 86, pp. 39-51, 2004.

[29] Liang, M.T., Wang, K.L., and Liang, C.H., "Service life prediction of reinforced concrete structures", *Journal of Cement and Concrete Research*, Vol. 29, No. 9, pp. 1411-1418, Sep, 1999.

[30] Torres-Acosta, Andres A., and Martinez-Madrid, M., "Residual life of corroding reinforced concrete structures in marine environment", *Journal of Materials in Civil Engineering*, Vol. 15, No. 4, pp. 344-353, July/August, 2003.

[31] Hong, H.P., "Assessment of reliability of aging reinforced concrete structures", *Journal of Structural Engineering*, Vol. 126, No. 12, pp. 1458-1465, Dec, 2000.

[32] Valentin, R., Osterman, M., and Newman, B., "Remaining Life Assessment of Aging Electronics in Avionic Applications", *Proceedings of Annual Reliability and Maintainability Symposium*, pp. 313-318, Tampa Florida, January 27-30, 2003.

[33] Shetty, V., Das, D., Pecht, M., Hiemstra, D., and Martin, S., "Remaining Life Assessment of Shuttle Remote Manipulator System End Effector", *Proceedings of the 22nd Space Simulation Conference*, Ellicott City, MD, October 21-23, 2002.

[34] McCluskey, F.P., Kweon, Y.D., Lee, H.J., Kim, J.W., and Jeon, H.S, "Method for assessing remaining life in electronic assemblies", *Microelectronics Reliability*, Vol. 40, pp. 293-306, 2000.

[35] Ramakrishnan, A., and Pecht, M., "Implementing a Life Consumption Monitoring Process for Electronic Product, *IEEE Transactions on Components and Packaging Technologies*, Vol. 26, No. 3, pp. 625-634, September, 2003.

[36] Hu, J., Barker, D., Dasgupta, A., and Arora, A., "Role of Failure-mechanism Identification in Accelerated Testing"**,** *Proceedings of Annual Reliability and Maintainability Symposium*, pp. 181-188, January 1992.

[37] Upadhyayula, K., and Dasgupta, A., "Guidelines for Physics-of-Failure Based Accelerated Stress Testing", *Proceedings of Annual Reliability and Maintainability Symposium*, Anaheim, California, January 19-22, 1998.

[38] Vichare, N., Eveloy, V., Rodgers, P., and Pecht, M., "In situ temperature measurement of a notebook computer - A case study in health and usage monitoring of electronics", *IEEE transactions on device and materials reliability*, Vol. 4, No. 4, December 2004.

[39] Vichare, N., Rodgers, P., Azarian, M., and Pecht, M., "Application of health monitoring to product take-back decisions", *Proceedings of the Joint International Congress and Exhibition - Electronics Goes Green 2004*, pp. 945-951, 6-8 September, 2004, Berlin, Germany.

[40] Cunningham, J., Valentin, R., Hillman, C., Dasgupta, A., and Osterman, M., "A Demonstration of Virtual Qualification for the Design of Electronic Hardware", *ESTECH 2001, IEST,* Phoenix, AZ, April 2001.

[41] Mishra, S., Pecht, M., Smith, T., McNee, I., and Harris, R., "Remaining life prediction of electronic products using life consumption monitoring approach", *Proceedings of the European Microelectronics Packaging and Interconnection Symposium*, Cracow, Poland, June 2002.

[42] Ranakrishnan, A., Das, D., Pecht, M., "The IEEE standards on reliability program and reliability prediction methods for electronic equipment", *Microelectronics Reliability*, Vol.42, pp. 1259-1266, 2002.

[43] Lall, P., Pecht, M., Harkim, E., "Influence of temperature on microelectronics and system reliability", New York, CRC Press, 1997.

[44] NASA, Moritz, K., Human Space Flight: - Background and Status, Updated 06/13/2002, http://www.spaceflight.nasa.gov/shuttle/reference/shutref/, Kennedy Space Center NASA Florida, (09/26/2003).

[45] Sandia National Laboratories, Wolff, T., Human Space Flight: Solid Rocket Boosters, http://www.sandia.gov/ciim/ISA/1hsfsrb.html, (11/01/2003).

[46] Rowan, C., Educational Space Simulations Project: Useful Simulations, http://www.rice.edu/armadillo/Simulations/NEWEST/prf1.gif, (10/06/2003).

[47] Cornish J., "The Space Shuttle", Updated 10/03, http://www.stemnet.nf.ca/CITE/sts_ascent.htm, Newfoundland, Canada, (11/20/2003).

[48] BD Systems, McDonald, E., and Rooker, B., SRB IEA Box Shock Environment, November 04, 2003.

[49] Ramakrishnan, A., Syrus, T., and Pecht, M., "Electronic Hardware Reliability", *The Modern Microwave and RF Handbook*, pp.3-102 to 3-121. CRC Press, Boca Raton, 2000.

[50] Valentin, R., Cunningham, J., Osterman, M., Dasgupta, A., Pecht, M., and Tsagos, D., "Virtual Life Assessment of Electronic Hardware Used in the Advanced Amphibious Assault Vehicle (AAAV)", *Proceedings of the IEEE Winter Simulation Conference*, San Diego, California, December 8-11, 2002.

[51] Osterman, M., Stadterman, T., "Failure Assessment Software for Circuit Card Assemblies", *Proceedings for the Annual Reliability and Maintainability Symposium*, pp. 269-276, January 1999.

[52] L3Communications, http://www.l-3com.com/spacenav/, New Jersey, (10/06/2003).

[53] BD Systems, Technical staff (McDonald, E., and Rooker, B.), "Presentation: - SRB IEA Box Shock Environment", Alabama, November 04, 2003.

[54] IEEE Standards Board, "Standard 1413: IEEE Standard Methodology for Reliability Prediction and Assessment for Electronic Systems and Equipment", IEEE, New York, NY, 1998.

[55] IEEE Standards Board, "Standard 1413.1: IEEE Guide for Selecting and Using Reliability Predictions based on IEEE 1413™ ", IEEE, New York, NY, 2002.

[56] Dasgupta, A., "Failure mechanism models for cyclic fatigue", *IEEE Transactions on Reliability*, Vol. 42, No. 4, pp. 548-555, December, 1993.

[57] Lall, P., Pecht, M., "An Integrated Physics of Failure Approach to Reliability Assessment," *Advances in Electronic Packaging Conference*, Binghamton, NY, September 29- October2, 1993.

[58] Barker, D., Vodzak, J., Dasgupta, A., and Pecht, M., "Combined Vibration and Thermal solder joint fatigue – A generalized strain versus life approach", *Journal of Electronic Packaging*, Vol. 112, pp. 129-134, June 1990.

[59] Solomon, H.D., "Fatigue of 60/40 Solder", *IEEE transactions on Components, Hybrids and Manufacturing Technology*, Vol. 9, pp 423- 432, December 1986.

[60] Basaran, C., and Chandaroy, R., "Mechanics of Pb40/Sn60 near-eutectic solder alloys subjected to vibrations", *Applied Mathematical Modeling*, Vol. 22, pp. 601-627, Aug, 1998.

[61] Pecht, M., "Physics of Failure Approach to Design and Reliability Assessment of Microelectronic Packages," *Proceedings of the First International Symposium on Microelectronic Package and PCB Technology*, Beijing, China, pp. 175-180, September 19-23, 1994.

[62] Pecht, M., Dasgupta, A., "Physics of Failure: An Approach to Reliable Product Development", *Journal of the Institute of Environmental Sciences*, pp. 30-34, September/October, 1995.

[63] Pecht, M., Dasgupta, A., "Material Failure Mechanism and Damage Models", *IEEE Transactions on Reliability*, Vol. 40, pp. 531-536, December 1991.

[64] Pecht, M., Dasgupta, A., Barker, D., and Leonard, C. T., "The Reliability Physics Approach to Failure Prediction Modeling (sic)," *Quality and Reliability Engineering International*, Vol. 6, pp. 267–273, 1990.

[65] Upadhyayula, K. and Dasgupta, A., "An Incremental Damage Superposition Approach for Interconnect Reliability under Combined Accelerated Stresses," *ASME International Mechanical Engineering Congress & Exposition*, Dallas, TX, 1997.

[66] Upadhyayula, K. and Dasgupta, A., "Physics of Failure Guidelines for Accelerated Qualification of Electronic Systems", *Quality and Reliability Engineering International*, Vol. 14, pp. 433-447, 1998.

[67] Jones, J. and Hayes, J., "A Comparison of Electronic-Reliability Prediction Models," *IEEE Transactions on Reliability*, Vol. 48, No. 2, pp. 127–134, June 1999.

[68] Dasgupta, A., "Failure Mechanism Models For Cyclic Fatigue," *IEEE Transactions on Reliability*, Vol. 42, No. 4, pp. 548–555, December, 1993.

[69] Liguore, S., and Followell, D., "Vibration Fatigue of Surface Mount Technology (SMT) Solder Joints", *Proceedings of Annual Reliability and maintainability Symposium*, pp. 18-26, 16 – 19 January 1995.

[70] Wang, H., Zhao, M., and Guo, Q., "Vibration fatigue experiments of SMT solder joint", *Microelectronics Reliability*, Vol. 44, pp. 1143-1156, July 2004.

[71] Basaran, C., and Chandaroy, R., "Thermomechanical analysis of solder joints under thermal and vibrational loading", *Journal of Electronic Packaging*, Transactions of the ASME, Vol. 124, pp. 60-66, March, 2002.

[72] Li, R. S., "A methodology for fatigue prediction of electronic components under random vibration load", *Journal of Electronic Packaging*, Transactions of the ASME, Vol. 123, pp. 394-400, December, 2001.

[73] Stadterman, T., Connon, W., and Barker, D., "Accelerated Vibration Life Testing of Electronic Assemblies", *Proceedings of Institute of Environmental Sciences*, pp. 233-238, 1997.

[74] Krascih M, "Accelerated Testing for Demonstration of Product Lifetime Reliability", *Proceedings of Annual Reliability and Maintainability Symposium*, 2003.

[75] Barker, D., Dasgupta, A., Pecht, M., "PWB Solder Joint Life Calculations under Thermal and Vibrational Loading", *Proceedings of Annual Reliability and Maintainability Symposium,* Vol. 35, No.1, pp. 451-459, January 1991.

[76] Osterman, M., Stadterman, T., "Reliability and Performance of PWB Assemblies", Chapter 9, in High Performance Printed Circuit Boards, C. Harper (editor), McGraw-Hill, New York, 2000.

[77] Osterman, M., Dasgupta, A and Stadterman, T., "Virtual Qualification of Electronic Hardware", Case Studies in Reliability and Maintenance, ed. W.R. Bilschke and D. N. P. Murthy John Wiley, 2002.

[78] Hu, J., Dasgupta, A., and Rothman, T., "Test-Time Compression for Qualification Testing of Electronic Systems: A Case Study", *Proceedings of the Annual Reliability & Maintainability Symposium*, pp. 246-252, January 1995.

[79] Upadhyayula, K., and Dasgupta, A., "Accelerated Testing of CCA's under Combined Temperature–Vibration Loading", *2nd Annual Workshop on Accelerated Testing, IEEE CPMT Society, Ottawa*, Canada, Oct 16-18, 1996.

[80] Jawaid, S., Rogers, P., "Accelerated Reliability Test Results: Importance of Input Vibration Spectrum and Mechanical Response of Test Article", *Proceedings of Annual Reliability and Maintainability Symposium*, Pages: 248 – 253, 24-27 Jan. 2000.

[81] Nemeth, P., "Accelerated life time test methods for new package technologies", *Electronics Technology Concurrent Engineering in Electronic Packaging*, 2001. 24th International Spring Seminar, pp. 215 – 219, 5-9 May 2001.

[82] Steinberg. D.S, "Vibration Analysis for Electronic Equipment", John Wiley & Sons, New York, 1988.

[83] Thomson W.T., "Theory of Vibration with Applications", Prentice-Hall, Inc., NJ, 1972.

[84] Harris, C.M., and Crede, C.E., "Shock and Vibration Handbook", McGraw-Hill, Inc., NY, 1961.

[85] Ramamrutham, S., and Narayan, R., "Strength of Materials", Danpat Rai & Sons, New Delhi, India, 1992.

[86] Penton Publications, "Materials Engineering - Materials Selector 1987", December 1986, Cleveland, OH.

[87] Shetty, V., "Remaining life assessment process of electronic systems", *Masters Thesis,* University of Maryland, 2003.

[88] Edmonds, J., and Hickman, G.A., "Damage detection and identification in composite aircraft components", *Proceedings of IEEE Aerospace Conference*, Vol. 6, pp. 263-270, 2000.

[89] Suhir, E., "Is the maximum acceleration an adequate criterion of the dynamic strength of a structural element in an electronic product*?", IEEE transactions on Components , Packaging and Manufacturing Technology- Part A*, Vol.20, No. 4, pp. 513-517, December 1997.

[90] Suhir, E., "Could shock tests adequately replace drop tests?", *Proceedings of 8th International Symposium on Advanced Packaging Materials*, pp. 67 – 81, 3-6 March 2002.

[91] Wang, F.F., "Relating sinusoid to random vibration for electronic packaging testing", *The Eighth Intersociety Conference on Thermal and Thermomechanical Phenomena in Electronic Systems, ITHERM 2002*, pp. 892 – 895, 30 May-1 June 2002.

[92] Wong, T.E., Palmieri, F.W., and Fenger, H.S., "Under-filled BGA solder joint vibration fatigue damage", *The Eighth Intersociety Conference on Thermal and Thermomechanical Phenomena in Electronic Systems, ITHERM 2002*, pp. 961 – 966, 30 May-1 June 2002.

[93] Fluss, H.S., "Methodology for the vibration testing of connectors", *Proceedings of the 44th Electronic Components and Technology Conference*, 1994, pp. 839 – 844, 1-4 May 1994.

[94] Zhu, Z.Y., Lee, H.P., and Cheok, B. T., " Finite Element Analysis of Mechanical Shock Responses of RF Connectors", *Journal of Electronic Packaging, Transactions of the ASME*, Vol. 125, No. 1, pp. 144-152, 2003.

[95] Ong, J.H., and Lim, G.H., "A Simple Technique for Maximizing the Fundamental Frequency of Vibrating Structures" , *Journal of Electronic Packaging, Transactions of the ASME*, Vol. 122, No. 4, pp. 341-349, December, 2000.

[96] Suhir, E., "Predicted Fundamental Vibration Frequency of a Heavy Electronic Component Mounted on a Printed Circuit Board", *Journal of Electronic Packaging, Transactions of the ASME*, Vol. 122, No. 1, pp. 3-5, March, 2000.

[97] Tong, Y. T., Jing-en, L., Pek, E., Chwee, T. L., and Zhaowei, Z., "Novel numerical and experimental analysis of dynamic responses under board level drop test", *Proceedings of the 5th International Conference on Thermal and Mechanical Simulation and Experiments in Microelectronics and Microsystems, EuroSimE 2004*, pp. 133 – 140, 2004.

[98] Liu, J., "Digital Signal processing method of flight equipment shock test system", *Proceedings of the IEEE 1996 National Aerospace and Electronics Conference, 1996. NAECON 1996*, Vol. 1, pp. 336 – 338, 20-23 May 1996.

[99] Stolkarts, V., Moran, B., and Keer, L.M.., "Constitutive and damage model for solders", *48th IEEE Electronic Components and Technology Conference*, pp. 379 – 385, 25-28 May 1998.

[100] Chiang, A.C., Barker, D.B., Krolewski, J.G., and Cushing, M.J., "Electronic box-level reliability assessment using computer modelling and simulation", *Proceedings of Annual Reliability and Maintainability Symposium, 1995*, pp. 49 – 53, 16-19 Jan. 1995.